

SMC Bulletin

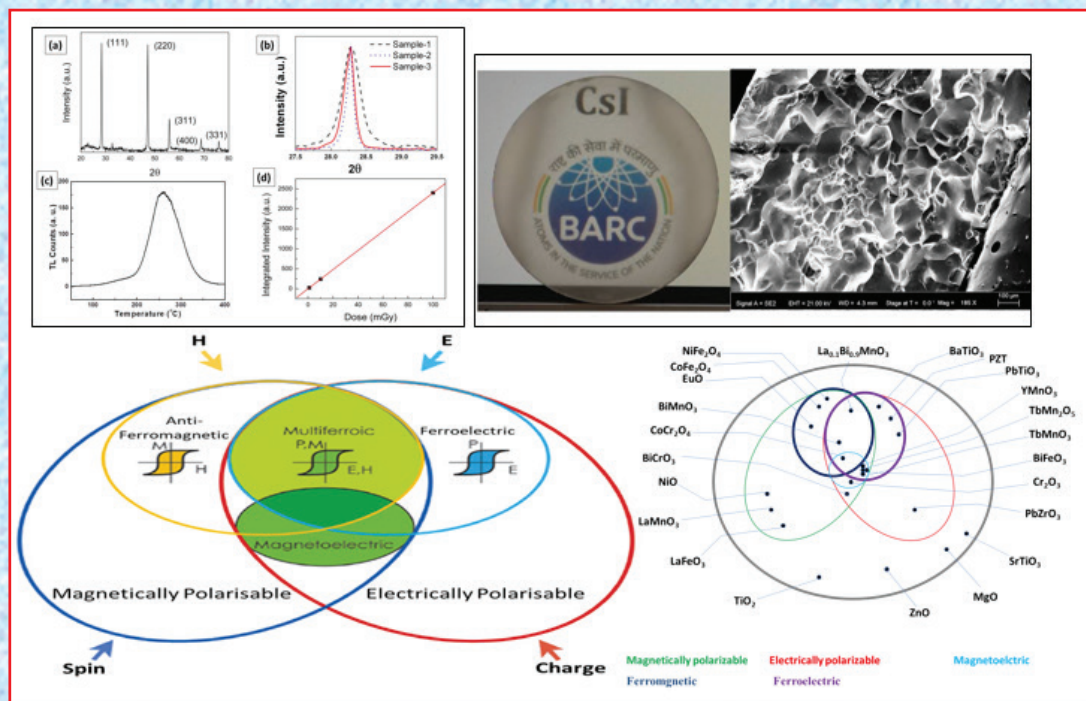
ISSN 2394-5087

A Publication of the Society for Materials Chemistry

Volume 12

No. 2

August 2021



Special Issue on
Ceramics for nuclear and other technological applications



Society for Materials Chemistry

Society for Materials Chemistry was mooted in 2007 with following aims and objectives:

- to help the advancement, dissemination and application of the knowledge in the field of materials chemistry,
- to promote active interaction among all material scientists, bodies, institutions and industries interested in achieving the advancement, dissemination and application of the knowledge of materials chemistry,
- to disseminate information in the field of materials chemistry by publication of bulletins, reports, newsletters, journals.
- to provide a common platform to young researchers and active scientists by arranging seminars, lectures, workshops, conferences on current research topics in the area of materials chemistry,
- to provide financial and other assistance to needy deserving researchers for participation to present their work in symposia, conference, etc.
- to provide an incentive by way of cash awards to researchers for best thesis, best paper published in journal/national/international conferences for the advancement of materials chemistry,
- to undertake and execute all other acts as mentioned in the constitution of SMC.

Executive Committee

President

Dr. A. K. Tyagi

Bhabha Atomic Research Centre
Trombay, Mumbai – 400 085
Email: aktyagi@barc.gov.in

Vice-Presidents

Prof. Kulamani Parida

Siksha 'O' Anusandhan University
Bhubaneswar – 751 030, Odisha
Email: kulamaniparida@soa.ac.in

Dr. P. A. Hassan

Bhabha Atomic Research Centre
Trombay, Mumbai – 400 085
Email: hassan@barc.gov.in

Secretary

Dr. Sandeep Nigam

Bhabha Atomic Research Centre
Trombay, Mumbai – 400 085
Email: snigam@barc.gov.in

Treasurer

Dr. K. C. Barick

Bhabha Atomic Research Centre
Trombay, Mumbai – 400 085
Email: kcbarick@barc.gov.in

Members

Prof. Amreesh Chandra

Indian Institute of Technology
Kharagpur Kharagpur – 721 302

Dr. Chandra N. Patra

Bhabha Atomic Research Centre
Trombay, Mumbai – 400 085

Dr. Deepak Tyagi

Bhabha Atomic Research Centre
Trombay, Mumbai – 400 085

Prof. (Smt.) Kanchana V.

Indian Institute of Technology
Hyderabad Kandi-502284, Sangareddy,
Telangana

Dr. (Smt.) Mrinal R. Pai

Bhabha Atomic Research Centre
Trombay, Mumbai – 400 085

Dr. Pranesh Senguta

Bhabha Atomic Research Centre
Trombay, Mumbai – 400 085

Dr. R. K. Vatsa

Department of Atomic Energy Mumbai
Mumbai – 400 001

Dr. Sukhendu Nath

Bhabha Atomic Research Centre
Trombay, Mumbai – 400 085

Prof. Tokeer Ahmad

Jamia Millia Islamia
Jamia Nagar, New Delhi – 110 025

Dr. V. K. Jain,

UM-DAE Centre for Excellence in Basic
Sciences, University of Mumbai
Kalina Campus, Mumbai – 400098

Dr. (Smt.) Vinita G. Gupta

Bhabha Atomic Research Centre
Trombay, Mumbai – 400 085

Prof. Vivek Polshettiwar

Tata Institute of Fundamental
Research Mumbai – 400 005

Dr. Y. K. Bhardwaj

Bhabha Atomic Research Centre
Trombay, Mumbai – 400 085

Co-opted Members

Dr. Adish Tyagi

Bhabha Atomic Research Centre
Trombay, Mumbai – 400 085

Prof. G. Mugesh

Indian Institute of Science Bangalore
Bangalore – 560 012

Dr. Pramod Sharma

Bhabha Atomic Research Centre
Trombay, Mumbai – 400 085

Prof. Sandeep Verma

Indian Institute of Technology Kanpur
Kanpur – 208 016

Contact address

Society for Materials Chemistry

C/o Chemistry Division

Bhabha Atomic Research Centre, Trombay, Mumbai, 400 085, India

Tel: +91-22-25592001, E-mail: socmatchem@gmail.com

SMC Bulletin

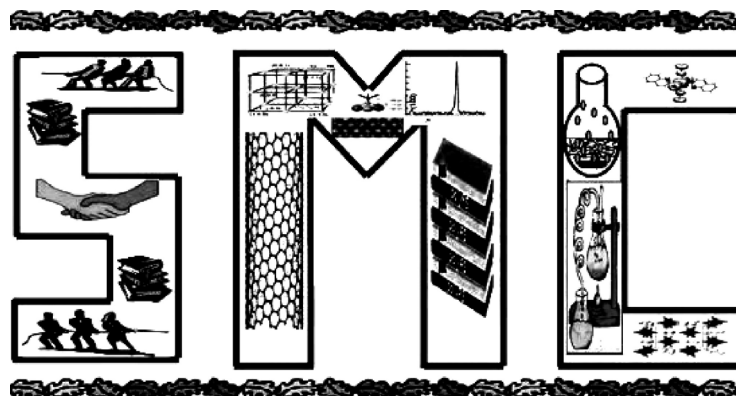
A Publication of the Society for Materials Chemistry

Volume 12

No.2

August 2021

Special Issue on
Ceramics for nuclear and other technological applications



SOCIETY FOR MATERIALS CHEMISTRY

SMC Bulletin

Vol. 12

No. 2

August 2021

Guest Editor

Mohsin Jafar

Chemistry Division
Bhabha Atomic Research centre
email: mohsinj@barc.gov.in

K Sandeep Rao

Chemistry Division
Bhabha Atomic Research Centre
email: sandeepkr@barc.gov.in

Editorial Board	
Dr. C. Majumder (Editor-in-Chief) Chemistry Division Bhabha Atomic Research Centre Trombay, Mumbai - 400 085 Email: chimaju@barc.gov.in	Dr. Arvind Kumar Tripathi Chemistry Division Bhabha Atomic Research Centre Trombay, Mumbai, 400 085 e-mail: catal@barc.gov.in
Dr. (Smt.) S. N. Sawant Chemistry Division Bhabha Atomic Research Centre Trombay, Mumbai - 400 085 Email: stawde@barc.gov.in	Dr. (Smt.) Mrinal Pai Chemistry Division Bhabha Atomic Research Centre Trombay, Mumbai - 400 085 Email: mrinalr@barc.gov.in
Dr. (Kum.) Manidipa Basu Chemistry Division Bhabha Atomic Research Centre Trombay, Mumbai, 400 085 e-mail: deepa@barc.gov.in	Prof. (Smt.) Kanchana V. Department of Physics Indian Institute of Technology Hyderabad Kandi-502284, Sangareddy, Telangana Email: kanchana@phy.iith.ac.in
Dr. Kaustava Bhattacharyya Chemistry Division Bhabha Atomic Research Centre Trombay, Mumbai - 400 085 Email: kaustava@barc.gov.in	Dr. (Smt.) Gunjan Verma Chemistry Division Bhabha Atomic Research Centre Trombay, Mumbai - 400 085 Email: gunjanv@barc.gov.in

Published by

Society for Materials Chemistry
C/o. Chemistry Division
Bhabha Atomic Research Centre, Trombay, Mumbai, 400 085
E-mail: socmatchem@gmail.com,
Tel: +91-22-25592001

Please note that the authors of the paper are alone responsible for the technical contents of papers and references cited therein. Front cover shows the salient figures of this Bulletin

Guest Editorial



Dr. Mohsin Jafar



Shri. K. Sandeep Rao

The present century witnessed a great advancement in ceramics for varieties of technologies. The thrust for facile, more efficient, economical and environment friendly production methodologies for advanced ceramics and their composites is a continuous endeavor from decades. Varieties of novel ceramic-based materials capable of operating under extreme conditions have emerged over the years. This includes both oxide and non-oxides, crystalline and amorphous, single phase and composites. These extremely versatile class of materials find applications in myriad fields ranging from nuclear to societal technologies. The non-oxide ceramics are promising candidates for application in next-generation nuclear reactors and fuel cycles with enhanced safety features. There has been an upsurge regarding the fabrication of transparent ceramics for potential technological applications as laser hosts, infrared (IR) windows/domes, lamp envelopes, radiation detectors and transparent armors. These materials offer dual advantages of transparency akin to glass/single crystal and mechanical hardness afforded by conventional ceramics. Alkaline earth and rare earth based ceramics materials with perovskite or pyrochlore structure have gained substantial importance due to their remarkable electronic and optical properties. Nano-ceramic materials are presently being touted as technologically important materials because of fascinating behavioral changes at nano-dimension. Band gap engineering of ceramic and ceramic-based materials for application in photocatalytic hydrogen generation and carbon dioxide conversion are important aspects of modern-day research. In addition to these, development of novel glasses and glass-ceramics materials for immobilization of nuclear waste is vital for nuclear program. Further, the research towards the development of new-age ceramics with lower corrosion, very high temperature stability, improved mechanical strength, varied porosity/density, etc. to meet the industrial and technological requirements are gaining importance

The thematic bulletin of SMC on “Ceramics for nuclear and other technological applications” is aimed to cover the current research and development in the in the above-mentioned area of ceramics. We sincerely hope that this thematic bulletin of SMC would present a wholesome view to the readers in this particular research area. We express our sincere thanks to all the contributors for sharing their research works and experiences. We are also thankful to SMC for giving us this opportunity which we have thoroughly enjoyed.

From the desks of the President and Secretary



Dr. A. K. Tyagi



Dr. Sandeep Nigam

Dear SMC Members, colleagues and Readers,

Warm greetings from the Executive Council of the Society for Materials Chemistry (SMC)!

The Editorial Board of SMC Bulletin has been consistently working to bring out thematic issues on cutting edge research. The thematic issues of SMC Bulletin have always been multidisciplinary landscape linking the researchers across different disciplines. The present issue of the SMC bulletin is also in the same direction and is based on “Ceramics for nuclear and other technological applications”.

The articles in this special issue deal with various aspects of novel ceramic-based materials capable of operating under extreme conditions and their technological applications. This special issue consists of five articles from distinguished scientists in the field. The topics covered in this issue are potential and challenges of non-oxide ceramics in nuclear technology, advances in iron phosphate glass as vitrification matrix for nuclear waste, transparent ceramics for radiation detection, influence of Gd³⁺ doping on the structural and luminescence properties of SrSnO₃ nano-rods, prospects of nanocrystalline multiferroic materials. Overall, this compilation provides an excellent collection of articles highlighting recent advances in Ceramics for nuclear and other technological applications.

We would like to thank Dr. Mohsin Jafar and Shri Sandeep Rao who agreed to guest-edit this issue and put in efforts to bring out this special issue in a timely manner. We are grateful to the Editorial Staff and Reviewers for their efforts. We thank all authors for their sincere efforts towards contributing to SMC Bulletin. We extend our sincere gratitude to all our members of the society for their continued cooperation and active participation in SMC activities.

CONTENTS

Sr. No	Feature Articles	Page No.
1	Non-oxide Ceramics in Nuclear Technology: Potential and Challenges <i>Sourav Majumder, Dheeraj Jain and V. Sudarsan</i>	63
2	Recent advances in iron phosphate glass as vitrification matrix for nuclear waste <i>Dimple P. Dutta</i>	73
3	Transparent ceramics for radiation detection <i>Shashwati Sen, S G Singh, G D Patra, S Pitale, M Ghosh</i>	79
4	Influence of Gd³⁺ doping on the structural and luminescence properties of SrSnO₃ nano-rods <i>Dinesh K. Patel, B. Rajeswari, R. M. Kadam and V. Sudarsan</i>	88
5	Chemistry and Prospects of Some Nanocrystalline Multiferroic Materials <i>Tokeer Ahmad and Irfan H. Lone</i>	96

Non-oxide Ceramics in Nuclear Technology: Potential and Challenges

Sourav Majumder^a, Dheeraj Jain^{a,*} and V. Sudarsan^{a,b}

^aChemistry Division, Bhabha Atomic Research Centre, Trombay, Mumbai – 400085, India.

^bHomi Bhabha National Institute, Anushaktinagar, Mumbai – 400094, India.

*jaind@barc.gov.in; Phone: +91 22 2559 0278; Fax: +91 22 2550 5151

Abstract

Although metals and oxide-based ceramics find wide applications in nuclear technology, non-oxide based ceramics are expected to play a pivotal role in next generation nuclear reactor technology and fuel cycles. A large number of non-oxide ceramics have been identified, which can be used for constructing nuclear reactors with advanced security features and improved energy efficiency. Such materials include Si_3N_4 , SiC, graphene, etc. Issues associated with currently existing nuclear materials and how the same can be addressed by possible utilization of non-oxide ceramics have been discussed in this review. Finally, a way forward in this area of research is suggested.

1. Introduction

Ceramics are non-metallic inorganic solids that usually have high melting point, good resistance towards atmospheric corrosion, durability and strength. As compared to metals, ceramics have poorer ductility, lesser malleability and lower electrical conductivity [1]. With respect to atomic arrangement, ceramics can be either crystalline or amorphous. Use of ceramics is all-pervading in our daily life ranging from cookware, pottery, brick, cement, floor / roof-tiles to components in electronic devices, capacitors, batteries, cars, etc. [2]. Ceramics are widely used in various industrial applications as well as high-end technologies, which include nuclear, space and aviation technologies. On the basis of chemical composition, ceramics can be categorized as (i) oxide ceramics, (ii) oxygen-bearing ceramics and (iii) non-oxide ceramics. In oxide ceramics (M_xO_y), metal-oxygen (M-O) bond primarily forms the structural architecture. Alumina (Al_2O_3), titania (TiO_2), silica (SiO_2), etc. are examples of widely used oxide ceramics. In oxygen-bearing ceramics, oxygen is usually present as covalently bonded distinct polyhedral such as silicate ($-\text{SiO}_4$), phosphate ($-\text{PO}_4$), borate ($-\text{BO}_3$), etc. The overall structure is formed by metal-polyhedra framework. Phosphates, silicates, borates, etc. are examples of oxygen-bearing ceramics. Non-oxide ceramics do not contain oxygen (other than impurity) and include carbides, nitrides, borides, sulfides, silicides, phosphides, etc. Elemental ceramics such as graphite can also be categorized as non-oxide ceramics. Apart from above three main categories, mixed ceramics (e.g., oxycarbides, oxynitrides, oxyborides, etc.) consist of both oxygen and non-oxygen element (C, N, S, B, etc.) in the structural framework of material. Composite

ceramics consist of more than one ceramic phases and their overall properties are governed by (i) relative fraction of different ceramic constituents, (ii) nature of microstructure formed by such multi-phase material(s) and (iii) nature of physico-chemical interaction at the interphase regions.

Ceramics are extensively used in nuclear energy technology also, encompassing both, the front end as well as the back end of nuclear fuel cycle. Starting from nuclear fuel, structural materials, shielding materials, reactor confinement materials to storage and disposal of radioactive waste, ceramics play a significant role [3–5]. Actinide dioxides (c.a., UO_2 , ThO_2 , PuO_2) and mixed oxides (MOX; $\text{U}_{1-x}\text{Pu}_x\text{O}_2$, $\text{Th}_{1-y}\text{U}_y\text{O}_2$, etc.) dominate the ceramic fuel forms used in most of the commercially operational nuclear power plants (NPPs). Along with oxides, carbide (UC_x , $\text{U}_{1-y}\text{Pu}_y\text{C}_x$, etc.) and nitride (UN_x , $\text{U}_{1-y}\text{Pu}_y\text{N}_x$, etc.) fuels are also being developed as they exhibit superior performance potential over metallic nuclear fuels [6–9]. Borosilicate glass forms are used as host matrices for long-term immobilization of high-level nuclear waste (HLW) [10, 11]. Specially engineered concrete and cement-based ceramics are used for radiation shielding and safe confinement of nuclear facilities. Ceramics are also used in fusion energy technology. For example, low neutron activation carbides (SiC) and nitrides (Si_3N_4) of silicon are potential candidate for structural and blanket materials in fusion reactors / Tokamaks [12, 13]. Apart from oxide-based ceramics and glasses, various non-oxide ceramics are also used / useful in nuclear energy technologies. While vast literature is available on use of oxide ceramics and glasses in nuclear technologies, discussion on non-oxide ceramics from a similar perspective is relatively limited. This article attempts an introductory overview of non-oxide ceramics

that are potentially useful in nuclear energy technologies covering the front and back end of fission-based systems as well as fusion reactors.

2. Non-oxide ceramics in nuclear fission technology

Since the inception of fission-based nuclear energy technology in early 1950s, oxide-based ceramic nuclear fuels are being used industrially on a large scale. On the contrary, in spite of possessing suitable / superior physico-chemical properties (c.a., higher thermal conductivity, heavy metal fraction, refractory behavior, *etc.*), non-oxide fuel forms such as carbides, nitrides, silicides, fluorides, *etc.* have been utilized on smaller scales; predominantly in research reactors / neutron irradiation facilities. Evolution of fission-based technologies towards safer and efficient NPPs is stimulating the discussion on large-scale use of non-oxide ceramic nuclear fuels. For example, Generation-IV nuclear reactor concepts that include fast breeder reactors (FBRs), advanced light water reactors (ALWRs), molten salt reactors (MSRs) and gas-cooled reactors (AGRs) increasingly advocate for accelerated research and development (R&D) on non-oxide fuels [5, 9, 14].

Among non-oxide ceramics, graphite has been used as neutron moderator on large scale in gas cooled reactors (GCRs) [15]. Use of graphitic carbonaceous coatings as well as silicon carbide ceramics is gaining momentum in advanced TRISO-coated fuels, which are envisaged to be used in high temperature reactors (HTRs). Coating the reactor structural materials (c.a., clad, pressure vessels, coolant tubes, *etc.*) by non-oxide ceramics is being explored to enhance safety margins under both, normal and transient operation conditions [16]. A few examples of utilization potential of non-oxide ceramics in fission-based nuclear energy technologies; in comparison to oxide-ceramics, are briefly discussed below.

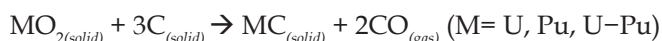
2.1. Actinide carbides as fast breeder reactor (FBR) fuels

Development of nuclear fuels all began with metals and alloys; owing to their high fissile atom density, high thermal conductivity and well known fabrication methodologies. Earliest metal fuels included uranium, Uranium-fissium (U-Fs) alloys, U-Zr alloys, *etc.* Irradiation performance of these alloy fuels affirmed their advantages such as compact core, high breeding ratios, electrometallurgical reprocessing, lower operating temperatures, *etc.* At the same time, their limitations in terms of lower melting / solidus temperatures, high fuel swelling, temperature dependent phase transformations, *etc.* were also realized. For utilization in large-scale nuclear power reactors, this

led to development of oxide nuclear fuels (UO_2 , $\text{U}_{1-x}\text{Pu}_x\text{O}_2$, *etc.*), which offer high temperature operation, high burn-up potential (up to 20 atom % in mixed oxide (MOX)-fuelled FBRs), isotropic structural stability, reasonable thermal stability and low swelling with better fission gas retention. A major drawback although was poor thermal conductivity, which deteriorated faster with both, increasing burn-up as well as temperature. Relative to oxides, notably higher thermal conductivity of non-oxide ceramics; along with the inherent advantages offered by ceramic fuel form were among the key factors, which drove global efforts to develop carbide, nitride, silicide-based novel fast reactor fuel forms during 1960-70s.

During early 1960s, actinide carbides were among the primary candidate high burn-up fuels for FBRs. Compared to actinide oxides, corresponding carbides (c.a., UC_x , PuC_y , $\text{U}_{1-z}\text{Pu}_z\text{C}_x$, $\text{Th}_{1-y}\text{Pu}_y\text{C}_x$, *etc.*) offer several advantages. These include higher fuel density, superior heat transport behaviour and better neutron economy. Utilization of high thermal conductivity carbide fuels offers enhanced thermal efficiency. Further, carbide fuels offer higher breeding capacity (breeding ratio) as compared to MOX fuels in fast reactors.

Preparation methods available for large-scale synthesis of actinide carbides include carbothermic reduction of oxide-carbon mixture under inert / reducing atmosphere [17, 18] and carburization of pulverized actinides (metal) produced by hydride-dehydride cycle. Dense carbide ceramics (pellets, tubes) are fabricated by high temperature powder metallurgy under controlled environment. Using air-stable actinide dioxides (UO_2 , PuO_2 , $\text{U}_{1-x}\text{Pu}_x\text{O}_2$, *etc.*) as starting materials, monocarbides are synthesized as follows:



Although above reaction scheme seems a simple solid-state reaction, careful control of reaction parameters is crucial to obtain phase-pure monocarbides. These parameters include (i) oxide to carbon ratio, (ii) reactants' powder properties, (iii) extent of homogeneity in reactants' mixing, (iv) purity of reaction atmosphere and (v) temperature. Deviation from optimized conditions results into formation of higher carbides (sesquicarbides ($\text{MC}_{1.5}$), dicarbides (MC_2)) and oxycarbides as well as presence of residual oxides and / or carbon. Such impurities affect fuels' physico-chemical properties as well as their in-pile performance. India is among the very few countries that have developed carbide-fuel technology. At present, India is the only nation successfully operating the 40 MW_{el} Fast Breeder Test Reactor (FBTR) fuelled by hybrid core of high plutonium content U-Pu mixed carbides, namely $\text{U}_{0.3}\text{Pu}_{0.7}\text{C}$

(Mark-I fuel) and $U_{0.45}Pu_{0.55}C$ (Mark II fuel) [19]. Notably, FBTR is also the, first carbide fuelled fast neutron spectrum reactor in Asia.

Although carbide fuels have advantages as mentioned above, several technical challenges are encountered in carbide-nuclear fuel cycle that have impeded its large-scale deployment; especially in commercial nuclear power reactors. These challenges are faced during fuel fabrication, in-reactor fuel handling and reprocessing of spent carbide fuels. Pyrophoric nature of powdered carbides makes it necessary to fabricate / handle these fuels under inert atmosphere glove boxes [20, 21]. During neutron irradiation [22], various fission products (FPs) are formed and chemical state of fission products dynamically evolves as mixture of carbides (FPC_x), metals (noble metals), gases (Xe and Kr), etc. As a result, carbon-to-metal (C/M) ratio also varies continuously with burn-up. Carbon potential of the fuel therefore depends upon C/M ratio of starting fuel and the burn-up. Excess increase in carbon potential may initiate clad carburization by solid-state reaction of free carbon with metallic (mostly stainless steel) clad surface, thereby rendering it brittleness. On the other hand, drop in carbon potential (from its value for fresh fuel) beyond a certain threshold may initiate formation of low melting eutectics, both within the fuel as well as at fuel-clad interface. The latter becomes a fuel failure concern and must therefore be minimized / avoided. Reprocessing of spent carbide fuels by PUREX-based approach also brings in additional challenges. For example, during spent fuel dissolution in nitric acid, various organic compounds are produced, which pose difficulties during solvent extraction (partitioning and separation) process. Destruction of such organic phases is required prior to solvent extraction stage, thereby making carbide fuel reprocessing further challenging [23].

With more than four decades of operational experience in FBTR, achieving high burn-up (~165 GWd / Te) in Pu-rich mixed carbide fuels and successfully demonstrating the closure of carbide fuel cycle, India is among very few countries to have developed / practiced carbide fuel technology. However, development of large-scale carbide-fuelled reactors for powder production is still awaited and offers opportunities for future innovations in carbide fuel cycle.

2.2. Nitride fuels for advanced nuclear reactors

Like carbides, actinide nitride (AnN_x) ceramic nuclear fuels also offer unique attributes. These nitrides have high heavy metal density; crystallize in isotropic cubic structure and show comparable melting points along with notably higher thermal conductivity as compared to corresponding

oxides. Therefore, nitride fuels offer larger safety margins to melting during operation. Due to inherently higher safety features, nitrides are being advocated among preferred fuel choice for Generation-IV (Gen IV) nuclear reactors [14]. Actinide nitrides can be synthesized from different methods such as, direct nitridation of oxide / hydroxide precursors under N_2 or NH_3 atmosphere, nitridation of actinide metal / alloy powders obtained by hydriding-dehydriding cycle(s), carbothermic reduction of oxides under nitrogen-rich environment, etc. [9, 14]. Fig. 1 shows a schematic representation of these preparation methods.

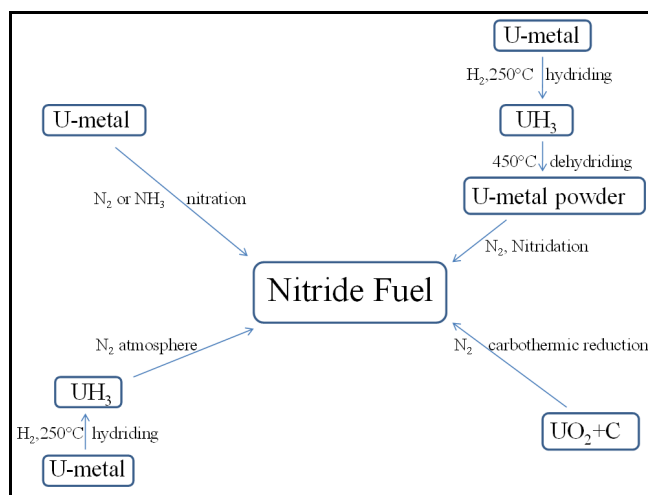
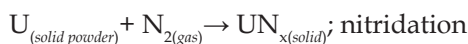
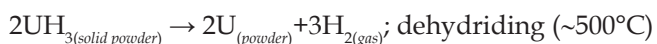


Fig. 1. Schematic description of synthesis methods for uranium nitrides

Preparation of nitrides using high purity uranium metal as starting material under highly inert environments minimizes the ingress of non-metallic impurities (C, O, F, etc.) in nitride product. However, direct nitridation of bulk uranium metal by gaseous N_2 is quite sluggish due to formation of passive uranium nitride layer on metal surface, which impedes complete nitridation of bulk metal unless carried out at elevated temperatures. On the other hand, carbothermic reduction of powdered actinide oxides (UO_2 , PuO_2 , $U_{1-x}Pu_xO_2$, etc.) mixed with carbon under nitrogenous atmosphere results into complete formation of nitride powders. The method however is associated with invariable presence of impurities such as oxynitrides, oxycarbides and oxides; all of which deleteriously affect nitride fuel performance.

An alternative route to overcome the limitations associated with either direct nitridation of bulk actinides or carbothermic reduction of actinide oxides is direct nitridation of actinide hydrides (UH_3 , PuH_3 , $(U-Pu)H_x$, etc.) or fine metallic powders (U, Pu, etc.); both of which can be obtained by hydriding bulk metals / alloys at relatively

lower temperatures (< 500°C). Hydriding-dehydriding cycles pulverize the metal powder thereby increasing the reactive surface of metal towards nitridation, which in turn facilitates the completion of reaction. The process is explained in the following reaction steps:



While the hydride-mediate method offers advantages of completion of nitridation with minimum impurities, care must be taken to carry out hydriding reaction under hydrogen atmosphere and subsequent handling of highly pyrophoric hydride / metal powders.

Although many other methods are available for synthesis of actinide nitrides, carbothermic reduction of oxides (MO_x ; $M = U, Pu, \text{etc.}$) carried out under N_2 or N_2/Ar atmosphere; as depicted by following reaction scheme, is routinely practiced.



In carbothermic reduction method, N_2 gas acts both as nitriding agent and carrier for removal of gaseous by-product (CO). This method can be used to prepare nitrides of various individual as well as mixed actinides starting from U to Cm, which are potential fuels options for Gen IV nuclear reactors. Dense nitride fuel pellets are produced by high temperature powder metallurgical process under strictly controlled nitrogenous environment.

Apart from inherent advantages of nitride nuclear fuels, they show better dissolution performance in nitric acid medium, which is in contrast to carbide fuels (organic compounds formation) as discussed in previous section. Irradiated nitride fuels comprising of even carbon / oxygen impurities can be reprocessed by PUREX process established for oxide fuels [14]. Better dissolution rate of irradiated nitride fuels in nitric acid makes them even more advantageous over oxides. For utilization in liquid metal cooled FBRs, nitride fuels show excellent compatibility with liquid sodium (Na) coolant as well as steel-based cladding material(s). Furthermore, probability of clad nitridation due to burn-up driven variation in nitrogen potential (analogous to clad carburization due to increased carbon potential in carbide fuels) is relatively lower in nitride fuels. This makes nitride fuel even a better choice than mixed carbide fuel for FBRs. Uranium Nitride (UN) can also be used in compact, light-weight space reactors, which require higher power-to-mass ratio.

In spite of the advantages nitride fuels offer over oxides and carbides, nitride-based fuel cycle is yet to be implemented for large-scale power reactor application(s). Following challenges are associated with nitride nuclear fuels: (i) Actinide nitrides show chemical instability in presence of water / moisture / steam and undergo complete oxidation under superheated steam at relatively lower temperatures ($\sim 500^{\circ}C$). (ii) Fabrication of nitride fuels; particularly mixed nitrides ($U_{1-x}Pu_xN_y$, $U_{1-x}MA_xN_y$, etc.; MA = minor actinides) is rather complex. Due to high hardness of nitride crystals, sintering of nitride fuels is challenging at elevated temperatures and may even lead to dissociation of nitrides (UN, PuN) into metal and nitrogen. (iii) as-prepared nitride powders are pyrophoric and must be handled in controlled atmosphere glove boxes and (iv) use of natural nitrogen ($\sim 99.64\%$ ^{14}N and $\sim 0.36\%$ ^{15}N) in nitride fuels leads to production of long-lived beta emitter ^{14}C by $^{14}N(n, p)^{14}C$ reaction, since ^{14}N has notable cross-section for (n, p) reaction. This not only affects neutron economy within the reactor core but also adds to long-term radiological challenges by undesirably increasing the net radioactive inventory in spent nuclear fuel (^{14}C half life ~ 5700 years). The only way to overcome the issue of ^{14}C formation via ^{14}N activation is use of enriched nitrogen (^{15}N) for fuel fabrication. Enrichment at such large scale invokes significant escalation in fuel fabrication cost apart from challenging implementation of enrichment technology starting from lean source of ^{15}N ($\sim 0.36\%$) in naturally available feed. Alternatively, from the perspective of once-through high burn-up nitride fuel utilization in FBRs, issue of $^{14}N(n, p)^{14}C$ transformation may rather be discussed in terms of additional safety attribute; which minimizes prospects of fuel reprocessing for proliferation purpose(s). It can therefore be asserted that ample opportunities await material researchers to innovate novel nitride fuel forms and their fabrication methodologies that can be implemented in a scalable and economically viable manner.

2.3. Non-oxide ceramics as accident tolerance fuels (ATF): case of Uranium Silicide

Core damage accident at Nuclear power plants in Fukushima Daiichi (Japan), which were caused by follow-up events of the Great East Japan Earthquake and resulting tsunami on 11 March 2011, led to serious discussion on development of accident tolerant fuels (ATFs). ATF concepts envisage development of improved / newer fuel forms and clad materials that have greater tolerance to transient situations such as loss of coolant accident (LOCA) or station black out (SBO). Hence a relook at replacement / improvement of UO_2 -zircaloy system; currently used on most of commercial power reactors, is

essential. Attributes desirable for ATF include (i) reduced H_2 generation resulting from clad-oxidation, (ii) enhanced retention of fission products under severe transients, (iii) enhanced resistance towards coolant-clad and fuel-clad interaction, (iv) reactor design improvements, *etc.* In this context, newer fuel types are being designed / developed to withstand coolant loss in reactor core for longer duration (also referred as 'fuel coping time' so that increased safety margins are available for plant operation [24]. Fuel's physico-chemical properties that meet accident tolerance attributes include higher melting point, larger heavy metal density, high thermal conductivity, *etc.* Uranium silicide ceramics meet most of the above criterion and are being contemplated as non-oxide accident tolerant fuel [25] along with carbides and nitrides. Table 1 compares few important properties of U_3Si_2 and UO_2 [26].

Table 1: Important physico-chemical properties of U_3Si_2 in comparison to UO_2

Properties	Uranium Silicide (U_3Si_2)	Uranium dioxide (UO_2)
Crystal structure	Tetragonal (Space group: P4/mbm)	Cubic fluorite (Space group: Fm3m)
Melting point (K)	1938 K	3138 K
Theoretical density ($g\ cm^{-3}$)	12.2	10.97
Thermal conductivity ($Wm^{-1}K^{-1}$)	13 to 22.3 (673 to 1473 K)	6 to 2.5 (673 to 1473 K)

Preparation of uranium silicides by arc-melting uranium metal with silicon is reported [26, 27]. Taking uranium in powder form is reported to yield better phase homogeneity of U_3Si_2 . Uranium powder prepared by hydriding-dehydriding of bulk metal is mixed with Si powder; pre-compacted and subjected to arc-melting with / without pre-sintering. Arc-melted ingot (U_3Si_2) is pulverized to make fine powder, which is further pelletized, sintered and machined in desired fuel-shape. Limited information is available on in-pile irradiation behaviour of U_3Si_2 -based nuclear fuels under experimental transient conditions and ample scope is available to explore the ATF potential of these silicide fuels.

2.4. Use of non-oxide ceramics in TRISO nuclear fuels

TRISO Nuclear fuels are a type of advanced fuel systems; especially engineered for use in high temperature

reactors (HTRs). The term 'TRISO' means 'Tri-structural ISotropic', which indicates multiple-coating(s) over the near-spherical tiny fuel particle such that individual fuel particle (also known as fuel kernel) is completely enclosed by multiple physical barriers (coating) to enable efficient and fast transport of fission heat but restrict the migration of most of the fission products outside the TRISO particles up to high burn-ups. In this way, each TRISO particle satisfies the 'defence-in-depth' principle of nuclear fuel system.

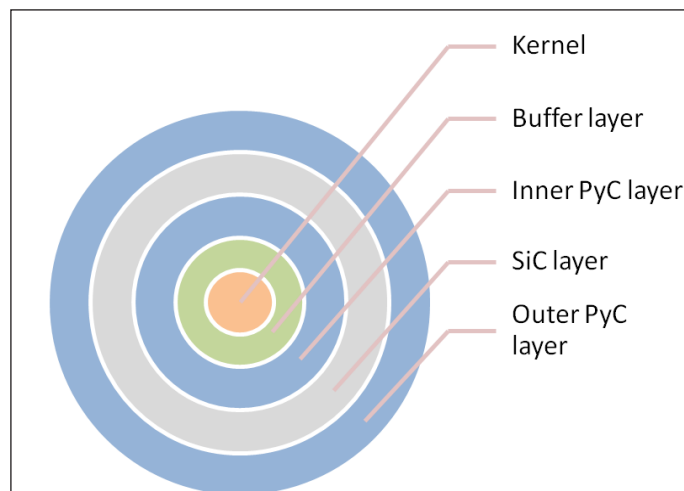


Fig. 2. Schematic illustration of TRISO fuel particle

Use of non-oxide ceramics is integral to TRISO fuel particles that were originally proposed in 1950s. A TRISO particle consists of fuel 'kernel' in the form of sub-millimetre sized near-spherical pebble or cylindrical particle; usually synthesized by sol-gel technique [28]. The kernel consists of fissile inventory in the form of oxides (UO_2 , $(U,Pu)O_2$), carbides (UC, $(U-Pu)C$) or oxycarbides. Each kernel is encapsulated by multiple layers of heat conducting and radiation resistant ceramic coatings namely silicon carbide (SiC) and Pyrolytic carbon (PyC). Fig. 2 shows schematic of a typical TRISO fuel particle.

Typically, the kernel ($\sim 100-800\ \mu m$ diameter) is encapsulated by carbon buffer layer followed by inner pyrolytic carbon (i-PyC) layer. This is followed by silicon carbide (SiC) layer and outer pyrolytic carbon (o-PyC) layer [5]. Carbon buffer layer must be thick enough ($\sim 30-60\ \mu m$) to sustain damages occurring due to fission products recoil. Fission gases can be accumulated within i-PyC layer ($\sim 30-50\ \mu m$), which also protects interaction of outer SiC layer with fuel. Retaining certain fission products like Ba, Sr and Cs is the main purpose of SiC layer ($\sim 25-30\ \mu m$). The high density o-PyC layer ($\sim 30-60\ \mu m$) minimizes Si loss from SiC layer at high temperature(s) and makes the system compact by compressing the SiC layer.

Advantages of TRISO fuels over traditional ceramic nuclear fuels include (i) capability to withstand high temperature (up to $\sim 1600^\circ\text{C}$) and (ii) superior resistance to corrosion, oxidation and neutron irradiation, all of which degrade fuel performance. TRISO particle can retain radioactive fission products (FPs) within its environment and thereby acts as 'its own primary containment for FPs', thanks to its triple coated layer [29]. Due to these superior qualities, TRISO fuels can be used in high temperature reactors (HTRs), molten salt cooled reactors (MSRs), micro-reactors, portable reactors as well as accident tolerance fuels (ATFs) in LWRs. During neutron irradiation in a reactor, oxygen potential goes up in UO_2 -based fuels [30]. Excess oxygen, which is not stabilized within fuel's crystal structure, releases from the fuel kernel of TRISO particle and may react with PyC layers to form carbon monoxide (CO). Excess CO pressure at high temperatures may cause failure of TRISO fuel structure [29]. If oxy-carbides (UCO , $\text{U}_{1-x}\text{Pu}_x\text{CO}$, etc.) are used in place of oxide fuels (UO_2 , $\text{U}_{1-x}\text{Pu}_x\text{O}_2$, etc.), then overall oxygen content in fuel kernel is reduced. This leads to enhanced safety margins with respect to burn-up dependent rise in fuel's oxygen potential. As a result, such fuels can be safely irradiated to higher burn-ups. For utilization in high temperature reactors (HTRs), neutron irradiation behaviour of UCO-based TRISO fuel has been investigated and very high burn-up ($\sim 19\%$) has been reported [31]. This is three times higher than that of current LWR fuels.

Use of TRISO fuels has been reported in few reactors worldwide including HTR-10 (China) and HT-engineering test reactor (Japan) [31]. HTRs are best options to extract the maximum energy from TRISO fuels. In a typical TRISO fuel-based HTR, $\sim 200,000$ fuel pebbles are irradiated with continuous rotation within the reactor core which allows reactor's operational life up to 60 years. Each such pebble is embedded with $\sim 18,000$ TRISO particles [28]. The coolant circulating through the reactor core absorbs fission heat energy, which boils water to produce steam. The steam then rotates turbine and produces large amount of clean energy. It is evident that significant advantages offered by TRISO fuels in comparison to conventional UO_2 -based bulk ceramic fuels stem from the multilayer coating of non-oxide ceramics (pyrolytic graphite & silicon carbide) over the fuel kernel. Performance attributes of this core (fuel kernel) - shell (buffer-PyC-SiC-PyC coatings) type composite structure depends on the efficacy of coating methodologies. Future efforts to develop commercial HTRs for both, electricity generation and large-scale hydrogen production (by waste heat utilization) would witness further evolution of TRISO fuels and increasing role of carbon-based non-oxide ceramics in nuclear technology.

2.5. Non-oxide ceramics in inert matrix fuels (IMFs)

With over 426 fission-based commercial nuclear power reactors having more than 19340 reactor years (cumulative) of operation, thousands of tonnes of nuclear fuel has already been irradiated for energy production [32]. The spent nuclear fuel (SNF) thus far generated is either stored in specially engineered facilities (like in USA) or is chemically reprocessed to retrieve un-burnt uranium, as-bred plutonium and valuable radioisotopes (like in India). A large inventory of plutonium along with long-lived minor actinides (MA = Np, Am, Cm, etc.) is thus stockpiled in the form of either stored SNF or reprocessed Pu and MAs. Additional large inventory of plutonium; produced mainly in research reactors during the global proliferation regime [33] is also stockpiled. Incineration of stockpiled Pu and MAs by nuclear fission for clean electricity production is the most attractive way forward to global efforts towards non-proliferation. The objective of utilizing the stockpiled fissile inventory (Pu & MA) with minimum further proliferation threat can be met by either utilizing MOX fuels ($\text{U}_{1-x}\text{M}_x\text{O}_2$, $\text{Th}_{1-y}\text{M}_y\text{O}_2$; M = Pu, MA) in FBRs or by using inert matrix fuels (IMFs) that incorporate Pu and / or MAs. Given that widespread commercial deployment of FBRs is delayed globally and they can further breed Pu, MAs and ^{233}U (although not weapon-grade), IMFs becomes preferred option wherein Pu / MAs embedded in a non-fertile (inert) matrix not only virtually eliminates opportunities for further proliferation but also reduces the radiotoxicity of long-lived MAs. Non-oxide ceramics can play an important role in development of future IMFs, which is briefly discussed below.

Conceptualized in early 60's; inert matrix fuels (IMFs) essentially consist of fissile material (c.a., Pu, MAs, $^{235}\text{U}/^{233}\text{U}$, etc.) uniformly dispersed in a neutron transparent matrix. Stabilized cubic zirconia is a well studied matrix for IMF development. Dispersion of fissile nuclei can be in the form of atomic incorporation in crystal structure of inert matrix (c.a., $\text{Zr}_{1-x-y}\text{Y}_x\text{M}_y\text{O}_{2\pm\delta}$; M = Pu / MA / ^{235}U / ^{233}U) so that the IMF fuel form is similar to typical MOX fuel (c.a., $\text{U}_{1-x}\text{Pu}_x\text{O}_2$, $\text{Th}_{1-y}\text{Pu}_y\text{O}_2$) except that no fertile nuclei (c.a., ^{238}U , ^{232}Th) is present. Such systems are categorized as homogenous IMFs. Alternatively, fissile material (Pu, MA, etc.) can also be dispersed in inert matrices as macroscopic inclusions (c.a., MO_x particles / crystallites; M = Pu / MA / ^{235}U / ^{233}U) giving rise to multi-phase IMFs. The multi-phase IMFs can be designed in various ways such as (i) ceramic fuel form dispersed in ceramic matrix (cer-cer; e.g., $\text{MgAl}_2\text{O}_4\text{-Y}_x\text{Pu}_y\text{Zr}_{1-x}\text{O}_{2-x/2}$), (ii) metallic fuel form dispersed in a metallic matrix (met-met; e.g., $\text{PuAl}_4\text{-Al}$) and (iii) ceramic fuel form dispersed in metallic matrix (cer-met; e.g., Zr-PuO_2) [33].

For inert matrix fuels, desirable characteristics of matrix include high density, high thermal conductivity, structural / dispersion stability of fissile inventory in matrix, compatibility with cladding, coolant and other structural components, mechanical stability, high melting points, *etc.* Potential matrices, which meet most of the above criterion include (i) oxides (yttria stabilized zirconia, calcia stabilized zirconia, CaO, MgO-ZrO₂ composites, ZrSiO₄, *etc.*), (ii) metallic alloys (stainless steel, zirconium-based alloys, *etc.*), (iii) intermetallics (AlSi, ZrSi, *etc.*); and (iv) non-oxide ceramics such as nitrides (AlN, TiN, ZrN, *etc.*) and carbides (SiC, TiC, ZrC, *etc.*) [33]. Due to their excellent high temperature stability, oxides are primary choice as IMF matrices and are most researched so far. However, carbides and nitrides too have immense potential as they possess significantly higher thermal conductivity and high density. Been used only in specific cases, non-oxide ceramics-based IMFs require further development.

To improve the performance of IMFs, neutron absorbing additives like B, Gd, Ho, Dy, Eu are added as burnable poison to stabilize core reactivity as a function of burn-up. Additives like Al₂O₃ in SiC, Y₂O₃ in ZrO₂, *etc.* are incorporated for thermodynamic phase stabilization of solid solution matrices. Current development efforts are focused on performance evaluation of IMFs loaded in research / power reactors without significant alteration in reactor core geometry. IMF rods can be loaded either in homogeneous (all fuel rods made of IMFs) or heterogeneous (IMF rods partially occupying the core) [33]. By optimizing the core loading pattern, upto 90% of fissile inventory (Pu, MAs) present in IMFs can be burnt to produce useful energy.

From the perspective of SNF management, IMFs are categorized as recyclable and non-recyclable. For recyclable IMFs, easier chemical reprocessing of SNF is preferred criterion over the need of high burn-ups. On the other hand, deep burn-up capability as well as long-term stability of matrix in irradiated SNF is essential for non-recyclable IMFs. IMF strategy thus has immense potential to safely utilize stock-piled plutonium and minor actinides for energy production along with nearing total non-proliferation.

3. Non-oxide ceramics-based clad materials for improved safety and performance

Development of accident tolerant fuels (ATFs) gained momentum after the Fukushima accident in 2011. Apart from safer fuel forms, as discussed earlier (section 2.3), development of superior cladding materials that can provide enhanced safety margins during LOCA or SBO scenario were also conceptualized. These included (i)

use of SiC-based ceramic composite clad in place of conventional zircaloy [25] and (ii) coating of zircaloy clad with metals (Cr, Nb, Ti, *etc.*), alloys (FeCrAl and CrZr) or ceramics (SiC, TiN, TiAlN, CrN, *etc.*) [34]. Development of alternative / superior cladding materials in ATF regime aims both, increased safety margins during transients as well as improved clad performance during normal reactor operation. Among various non-oxide ceramics, development of SiC-based cladding materials is given notable attention due to its high temperature compatibility, high melting point, superior heat transport behavior and significantly lower rate of oxidation (by 2-3 orders of magnitude) as compared to conventional zircaloy clad [35]. Due to its brittleness, monolithic SiC cannot be used as cladding. Therefore, its composites such as SiC-CMC (CMC = ceramic matrix composite), which can be fabricated by chemical vapor deposition (CVD) or polymer infiltration pyrolysis (PIP) techniques, are also being explored [35]. Coating of zircaloy-based clad by heat conducting stable nitrides (SiN, TiN, TiAlN, CrN, *etc.*) as well as nanocrystalline diamond (NCD) is yet another approach to develop accident tolerant cladding materials.

4. Non-oxide ceramics for back end of nuclear fuel cycle:

Safe management of SNF obtained after the attainment of discharge burn-up in a nuclear reactor constitutes the back end of nuclear fuel cycle. Countries following open (once-through) fuel cycle store SNF in engineered facilities while those practicing closed fuel cycle chemically reprocess it to retrieve uranium, plutonium and valuable radioisotope fission products. The liquid nuclear waste left behind is categorized as low, medium and high level waste depending upon its specific radioactivity. These wastes are managed through basic principles of dilute, disperse, decay and disposal. Chemically treated low level waste (LLW) is usually managed through decay, dilute and disperse strategy. Intermediate level waste (ILW) is pre-concentrated and mostly immobilized in cement / concrete. The high level liquid waste (HLLW), which contains most of the radioactivity from SNF, comprises of long-lived fission products and minor actinides. HLLW is immobilized in borosilicate-based solid glass wasteform by process known as vitrification [36]. Vitrified wasteform is produced by homogenously melting together the glass constituents and HLW followed by pouring the molten glass into steel canisters kept near ambient temperature (melt-quenching). 'SYNROC' or 'synthetic rock' is an alternative wasteform being developed for management of HLW. It is a crystalline composite primarily consisting of laboratory synthesized waste loaded analogues of three oxide minerals namely, zirconolite, hollandite and perovskite [37]. For 'SYNROC'

wasteform, powdered mineral constituents are mixed with HLLW to form a slurry, which is dried, calcined and finally compressed within stainless steel containers by hot isostatic pressing (HIP; ~1423 - 1473 K) to form dark colored, hard and dense ceramic. HLW immobilized either in 'vitrified glass' or 'SYNROC' form inside stainless steel canisters, is to be stored in interim storage facilities for a few decades before their permanent storage in deep geological repository (DGR). Challenges associated with storage of immobilized HLW include (i) long-term efficient heat removal from waste-loaded canister, (ii) crystalline phase evolution in glass wasteform(s) due to de-vitrification, (iii) temperature dependent chemical interactions at waste-canister and canister-atmosphere (air, moisture, chloride, *etc.*) interfaces, *etc.* Non-oxide ceramics can play a significant role in alleviating these challenges. For example, coating of canister's inner surface with heat conducting and chemically resistant (towards glass-steel or SYNROC-steel interaction) ceramics such as metal carbides / nitrides (CrN, TiC, *etc.*), nanocrystalline diamond (NCD), diamond-like carbon (DLC), *etc.* are being contemplated for attaining higher safety margins. Similarly, providing a well adhered coating (ceramic / polymer-based coating) over the outer surface of waste-loaded canister can avoid / delay its corrosion. Potential polymer-based coating materials include polyetherketoneketone, polyimide / polyurea, phenolic resins, silane-based polyurethane, *etc.* [38]. Similarly, sol-gel derived ceramic-polyurethane hybrid coatings are also being explored [38]. Silicon oxycarbonitride (SiOCN(H)) coating over SS-304 / SS 304L / SS 304H canisters has also been proposed to address the issue of corrosion-induced canister failure.

Use of glass-ceramic composites for nuclear waste management is a recent development wherein chemical flexibility of glass is combined with better durability of sintered ceramics so that higher loading of nuclear waste is possible [37]. Both, oxide and non-oxide-based glass-ceramics are being developed for this purpose. Borates, silicates, phosphates usually are chosen as oxygen-bearing glass-ceramics while halides and chalcogenides are being explored as non-oxide glass-ceramics.

5. Non-oxide-based ceramics in nuclear fusion technology:

Use of nuclear fusion for controlled release of energy to generate electricity or process heat is a much awaited scientific leap in energy technology since 1950s. With rapidly advancing construction of the International Thermonuclear Experimental Reactor (ITER) at France, which is a multi-nation collaborative experiment, the nuclear fraternity is poised to see if controlled fusion

reaction with net energy output can be accomplished [39]. Similar to fission-based energy technologies, ceramics are widely used in fusion technology also. In nuclear fusion reaction, a large amount of energy is released when two (or more) lighter nuclei fuse together to form a heavier nucleus along with release of fast neutron(s). Fusion of lighter nuclear requires that the short-range nuclear attractive forces between them are stronger than the long-range electrostatic repulsive forces. Heavier isotopes of hydrogen i.e., deuterium (^2H) and tritium (^3H) are commonly used fuels for fusion reaction and almost 80% of fusion energy is carried by fast moving neutrons.



A major challenge in fusion reactor technology is damage of structural materials by high energy neutrons (via (n, α) and (n, p) reactions) at very high temperatures. Radiation-resistant high temperature ceramics therefore play important role in fusion-based systems and are used as structural materials, electromagnetic wave windows and electrical insulators [12]. Neutron transparent (i.e., low-activation cross section) ceramics are used in the first wall and blanket region of fusion reactor to reduce radio-toxicity levels [12, 40].

Several oxide-based ceramics are used in experimental fusion-devices. These include Lithium-based oxides as breeding materials and those based on MgO, Al₂O₃ and BeO as radiofrequency heating windows. Non-oxide ceramics such as SiC, Si₃N₄ and carbon-based materials are also potential candidates for fusion technology [12, 40]. Inside a fusion reactor, high energy plasma loses some of its energy due to the presence of impurities at plasma interface area. Extent of such energy loss is proportional to atomic number of impurity element. As a result, ceramics based on lighter elements such as carbon, SiC, B₄C, Si₃N₄, *etc.* are favoured than heavier iron-based materials [12, 40].

Silicon carbide (SiC); a low activation ceramic is primarily used as the first wall (which covers the magnetic field) and blanket (which completely surrounds the plasma region) material [41]. Among various polymorphs of SiC, cubic phase (β -SiC) is preferred due to its high thermal and radiation stability as well as high thermal conductivity [12]. As structural materials for fusion reactor, graphite, SiC and lighter (low-Z) oxides are preferred over transition metal (Ni and Fe-based) alloys since the former lowers the neutron activation by 5-6 order of magnitudes. High strength silicon nitride (Si₃N₄) ceramics are generally used in diesel engines and gas turbines sections of fusion devices. Al, Mg, Be, Li-based ceramics are also alternate choices for structural materials in fusion reactor [12, 40].

Such low activation ceramics not only reduce radioactive wastes but also facilitate easier handling of equipments during maintenance.

Moreover, electrical insulators exposed to intense radiation field must be made from radiation hard and thermally stable ceramics. Support structures for winding of large magnets, which are used to confine the plasma within fusion reactor core, are usually made from SiC and graphite-based ceramic fibres. With further evolution of fusion technology, enhanced use of non-oxide ceramics is envisaged.

Summary

Applications of non-oxide ceramics in both, nuclear fission and fusion technologies with reference to their advantages have been outlined in this review article. Carbide and nitride fuels exhibit superior performance potential in fast breeder reactors and development of innovative methods for their preparation in phase-pure forms is desirable. Potential of actinide silicides like U_3Si_2 as an accident tolerant fuel (ATF) is indicative to bring in enhanced safety margins of fission-based reactor under transient conditions. Discussion on TRISO fuel systems has clearly indicated the role of non-oxide ceramic coatings in imparting high temperature performance potential to such fuels for HTRs. For proliferation-resistant utilization of stockpiled Pu and MAs, development of future inert matrix fuels beyond oxide-based systems calls for research on non-oxide ceramics and composites. For enhanced compliance towards safer accident tolerant fuel systems, future cladding materials are likely to be based on SiC-composites or non-oxide coated metallic alloys. Challenges associated with management of high level nuclear waste; either based on 'vitrified wasteform' or ceramic 'SYNROC', indicate the potential role; non-oxide ceramics can play in advanced waste management practices. At the end, potential role of non-oxide ceramics in nuclear fusion technology has been outlined.

Way forward

Extensive research is an absolute essential for overall evaluation of performance characteristic of non-oxide based nuclear materials. This includes innovation in their synthesis and processing methodologies and evaluation of their physico-chemical properties as a function of temperature, radiation fields, mechanical and chemical stress encountered / anticipated under normal as well as transient reactor operation conditions. Such an approach would contribute in a major way towards development of clean and sustainable nuclear energy systems.

References:

1. "Material science and engineering: ceramics", University of Maryland. (Web-link: <https://mse.umd.edu/about/what-is-mse/ceramics>; last accessed on 10.10.2022)
2. D. E-Quesada, L. P-Villarejo, P.J. S-Soto, "Ceramic materials - synthesis, characterization, applications and recycling", *IntechOpen Publications* (2019) (DOI: 10.5772/intechopen.75375).
3. T.O. Mason, "Nuclear ceramics", (Web-link: <https://www.britannica.com/technology/nuclear-ceramics>; last accessed on 10.10.2022).
4. S.J. Zinkle, J.T. Busby, "Structural materials for fission & fusion energy", *Mater. Today*12(11) (2009) 12-19.
5. J. Marra, "Advanced ceramic materials for next-generation nuclear applications", *IOP Conf. Ser.: Mater. Sci. Engg.* 18 (2011) 162001.
6. K.D. Reeve, "Ceramics as nuclear reactor fuels", *Ceramurg. Int.* 1(2) (1975) 59-71.
7. Y. Zhang, X-M. Bai, "Ceramic Materials for Nuclear Energy Applications", *JOM: J. Minerals, Metals Mater. Soc.* 71 (12) (2019) 4806-4807.
8. H. Suzuki, T. Iseki, T. Maruyama, "Ceramics for nuclear reactors", *Bull. Res. Lab. Nucl. Reactors (Tokyo Institute of Technology)* 7 (1982) 239-255.
9. H.J. Matzke, "Fabrication and testing of non-oxide nuclear fuels for fast breeders", *Ceram. Int.* 17 (1991) 315-323.
10. W.E. Lee, M.I. Ojovan, C.M. Jantzen, "Radioactive waste management and contaminated site clean-up: Processes, technologies and international experience", *Woodhead, Cambridge, UK* (2013) 924.
11. M.I. Ojovan, W.E. Lee, S.N. Kalmykov, "An introduction to nuclear waste Immobilisation. 3rd Edition", *Elsevier; Amsterdam, The Netherlands* (2019) 497.
12. G.R. Hopkins, R.J. Price, "Fusion reactor design with ceramics", *Nucl. Engg. Design/Fusion* 2 (1985) 111-143.
13. G.P. Pells, "Ceramic materials for fusion reactor applications", *J. Nucl. Mater.* 123 (1-3) (1984) 1338-1351.
14. C. Ekberg, D.R. Costa, M. Hedberg, M. Jolkkonen, "Nitride fuel for Gen IV nuclear power systems", *J. Radioanal. Nucl. Chem.* 318 (2018) 1713-1725.
15. B.J. Marsden, S.D. Preston, A.J. Wickham, A. Tyson, "Evaluation of graphite safety issues for the British production piles at Windscale: Graphite sampling in preparation for the dismantling of pile 1 and the further safe storage of pile 2" *IAEA-TECDOC-1043* (1997) 213-234.
16. C.P. Deck, G.M. Jacobsen, J. Sheeder, O. Gutierrez, J. Zhang, J. Stone, H.E. Khalifa, C.A. Back, "Characterization of SiC-SiC composites for accident tolerant fuel cladding", *J. Nucl. Mater.* 466 (2015) 667-681.
17. P. Rodriguez, "Mixed plutonium-uranium carbide fuel in fast breeder test reactor", *Bull. Mater. Sci.* 22 (3) (1999) 215-220.
18. C. Duguay, G. Pelloquin, "Fabrication of mixed uranium-plutonium carbide fuel pellets with a low oxygen content and an open-pore microstructure", *J. Eur. Ceram. Soc.* 35 (2015) 3977-3984.
19. U. Basak, "Fabrication, properties and irradiation behaviour of MOX, carbide and nitride fuels, inert matrix fuels with and

- without minor actinides”, School on physics and technology on fast reactor systems, ICTP, Trieste, Italy (2009).
20. C.N. Venkiteswaran, N Raghun, V. Karthik, A. Vijayaraghavan, V. Anandraj, T. Ulaganathan, T. Saravanan, V.V. Jayaraj, S. Kurien, J. Philip, T. Johny, N.G. Muralidharan, J. Joseph, K.V. Kasiviswanathan, “Irradiation Behavior of FBTR Mixed Carbide Fuel at Various Burn-ups”, *Energy Procedia* 7 (2011) 227-233.
 21. A.S. Kudinov, B.Ya. Zilberman, N.D. Goletskii, “Status of and Prospects for Using Carbide Fuel”, *Atomic Energy* 117 (6) (2015) 388-393.
 22. S. Clement, R. Chandar, C.N. Venkiteswaran, R. Divakar, D.N. Sivayya, A.K. Sengupta, R. Agarwal, H.S. Kamath, “Carbide fuel”, in *Comprehensive Nuclear Materials (2nd Edition) Vol. 5*, (Eds.: R. Konings and R. Stoller) (2020) 102-138.
 23. K. Ananthasivan, S. Anthonysamy, V. Chandramouli, I. Kaliappan, P.R. Vasudeva Rao, “Reprocessing of carbide fuels: Conversion of carbide to nitride as a head end step”, *J. Nucl. Mater.* 228 (1996) 18-23.
 24. B. Zhang, P. Gao, T. Xu, M. Gui, J. Shan, “Performance evaluation of Accident Tolerant Fuel under station blackout accident in PWR nuclear power plant by improved ISAA code”, *Nucl. Engg. Tech.* 54 (7) (2022) 2475-2490.
 25. T.L. Wilson, E.E. Moore, D.A. Lopes, V. Kocovski, E.S. Wood, J.T. White, A.T. Nelson, J.W. McMurray, S.C. Middleburg, P. Xu, T.M. Besmann, “Uranium nitride-silicide advanced nuclear fuel: higher efficiency and greater safety”, *Adv. Appl. Ceram.* 117 (2018) 76-81.
 26. J.M. Harp, P.A. Lessing, R.E. Hoggan, “Uranium silicide pellet fabrication by powder metallurgy for accident tolerant fuel evaluation and irradiation”, *J. Nucl. Mater.* 466 (2015) 728-738.
 27. A.R. Wagner, J.M. Harp, K.E. Archibald, S.C. Ashby, J.K. Watkins, K.R. Tolman, “Fabrication of stoichiometric U_3Si_2 fuel pellets”, *MethodsX* 6 (2019) 1252-1260.
 28. “TRISO particles: The most robust nuclear fuel on earth”, *US Office of Nuclear Energy* (2019) (Web-link: <https://www.energy.gov/ne/articles/triso-particles-most-robust-nuclear-fuel-earth>; last accessed on 10.10.2022).
 29. S. Patel, “The Allure of TRISO Nuclear Fuel Explained”, (2021) (Web-link: <https://www.powermag.com/the-allure-of-triso-nuclear-fuel-explained>, last accessed on 10.10.2022).
 30. K. Une, M. Oguma, “Oxygen potential of UO_2 fuel simulating high burnup”, *J. Nucl. Sci. Tech.*, 20 (1983) 844-851.
 31. M. Andrei, “Why TRISO particles could open a new age for nuclear power”, (2022) (Web-link: <https://www.zmescience.com/other/feature-post/triso-particles-nuclear-04062020/>, last accessed on 10.10.2022).
 32. “IAEA Power Reactor Information System, PRIS (Web-link: <https://pris.iaea.org/pris/home.aspx>, last accessed on 10.10.2022).
 33. “Viability of inert matrix fuel in reducing plutonium amounts in reactors”, *IAEA-TECDOC-1516*, (2006) (Web-link: https://www-pub.iaea.org/MTCD/Publications/PDF/te_1516_web.pdf).
 34. M.I.A. Sagiroun, C. Xinrong, “Zirconium-based cladding coating technique for oxidation, corrosion and embrittlement reduction at high-temperature: An overview”, *IOP Conf. Series: Mater. Sci. Engg.*, 649 (2019) 012008.
 35. S. Bragg-Sitton, K. Barrett, I.J.V. Rooyen, D. Harley, M. Khafizov “Studying silicon carbide for nuclear fuel cladding”, *Nucl. Engg. Int.* (2013) (Web-link: <https://www.neimagazine.com/features/featurestudying-silicon-carbide-for-nuclear-fuel-cladding/>, accessed on 10.10.2022).
 36. Wm. L. Lennemann, “The Management of High-Level Radioactive Wastes”, *IAEA Bulletin* 21 (4) (1979) 2-16.
 37. “SYNROC Wasteform”, World Nuclear Association (2019) (Web-link: <https://www.world-nuclear.org/information-library/nuclear-fuel-cycle/nuclear-wastes/synroc.aspx>, last accessed on 10.10.2022).
 38. “Spent fuel and waste disposition, FY21 status report: SNF canister coatings for corrosion prevention and mitigation”, *Sandia National Laboratory Report SAND2021-10810R* (2021) 1-53.
 39. “International Thermonuclear Experimental Reactor (Web-link: <https://www.iter.org/proj/inafewlines>; last accessed on 10.10.2022).
 40. F.W. Clinard, Jr, “Ceramics for fusion applications”, *Ceram. Int.* 13 (1987) 69-75.
 41. F. Porz, G. Grathwohl, F. Thümmel, “SiC as a structural material in the plasma chamber of nuclear fusion reactors”, *Mater. Sci. Engg.* 71 (1985) 273-282.

Recent advances in iron phosphate glass as vitrification matrix for nuclear waste

Dimple P. Dutta*

Chemistry Division, Bhabha Atomic Research Centre, Mumbai 400085, India

E-mail: dimpled@barc.gov.in

Abstract

Nuclear energy technology is critically linked with safe disposal of radioactive waste. Various fission products including noble metals as well as minor actinides are present in the nuclear waste in high concentration. The commonly used borosilicate glass is not an efficient matrix to vitrify all these different components present in nuclear waste. In this context, Iron phosphate glass (IPG) is gaining predominance as nuclear waste vitrification matrix due to its capability to load higher concentration of several problematic components of nuclear waste. For certain wastes, the use of iron phosphate glass reduces the vitrified waste volume by almost 50% compared to a borosilicate glass wasteform. The chemical durability of IPG vitrified wasteforms is comparable to borosilicate glass based wasteforms. However, the available literature lacks thorough analysis of the structural and radiation stability of IPG which necessitates a detailed study on the effect of loading of various nuclear fission waste materials in it. In this article, an overview of the work done with iron phosphate glass matrix has been compiled and the course of future research directions has been identified.

Introduction:

Proper disposal of radioactive waste generated from nuclear reactors is of paramount importance in proliferation of utilization of clean energy available through nuclear technology. Particularly, reprocessing of spent nuclear fuel from nuclear power plants for various applications have necessitated research on suitable matrix for safe storage and disposal of fission products and actinides. For immobilization of nuclear waste, vitrification has been established as one of the most suitable techniques. In vitrification process, the waste material is concentrated and added into a glass matrix melt at high temperature in which it gets bonded and is thus immobilized. Borosilicate glass is the most commonly used matrix for vitrification of nuclear waste.¹ However, the composition of nuclear waste is extremely diverse and generally consists of radionuclides with long half-life like ³⁶Cl, ⁴¹Ca, ⁵⁹Ni, ⁷⁹Se, ⁹³Zr, ⁹³Mo, ⁹⁴Nb, ¹⁰⁷Pd, ¹²⁶Sn, ¹²⁹I, ¹³⁵Cs, ²³⁹Pu, ²³⁷Np, ²³⁸U, ²⁴¹Am, etc. Elements from almost all groups of the periodic table including stable as well as radioactive isotopes are present in the waste. Reprocessing of spent nuclear fuel further adds phosphates, chlorides, fluorides and sulfates to this mixture. However, borosilicate glass exhibits very limited solubility for phosphates, chlorides, fluorides, rare earths, noble metals, and oxides of heavy metals such like Cs, Sr, Zn, Zr, Cr, Mo, and Bi.²⁻⁴ To circumvent this problem, either the waste needs to be diluted or some pretreatment of the waste for the removal of these components needs to

be performed. The former process leads to generation of voluminous quantity of waste glass while latter adds on to the cost. Hence, it is imperative to look for alternative host matrices with better solubility for these components. In this context, iron phosphate glass (IPG) has been identified as suitable host for nuclear waste vitrification.⁵ It is important to note that the properties of IPG is quite different compared to conventional phosphate glass but are more similar to that of silicate glass. The factors which contribute to the use of IPG in nuclear waste vitrification is its remarkable chemical durability even when it is loaded with excess alkali oxides and its compatibility with wastes that contain phosphate, fluorides, sulfates and components such as heavy metals (e.g., Zr, Bi, Cr, Ag, and Mo) which results in enhanced solubility. This final outcome is reduction of the waste glass volume and overall cost of the process.

Ordinary phosphate glass lacks chemical durability due to the moisture sensitive nature of the P-O-P bonds.¹ In phosphate glass, the phosphate anions are joined via their nonbridging oxygens and also forms bond with metal cations which are added as modifier. The PO₄⁻ (P) tetrahedra which are linked on either side to two neighboring similar P-tetrahedra is denoted as Q² tetrahedra. In case it is linked to one unit then the anion is terminated, and it is denoted as Q¹ tetrahedra. Other highly cross-linked connections like Q³ tetrahedra are relatively scarce due to their susceptibility to moisture. The oxygen to phosphorous (O/P) ratio plays

a crucial role in determining the length of the P-tetrahedra chains. On increasing the metal oxide concentration in phosphate glass, the O/P ratio increases which decreases the length of P-tetrahedra chains. Glass with O/P ratio ≈ 3 have relatively long chain of Q^2 type tetrahedra (> 20) and are called metaphosphates. When O/P ratio ≈ 3.5 , it is mostly diphosphate anion with two Q^1 units and termed as pyrophosphate. The glasses with O/P ratio ranging between 3 and 4 are also classified as polyphosphates.⁶ Phosphate glass can be considered as an inorganic polymer with combination of PO_4 monomers, dimers, trimers, etc. which are joined by other metal cations. The property of any glass is dependent on the different linkages of the constituent phosphate anions and the metal cations that are bonded to it.

The addition of iron to phosphate glass results in formation of Fe-O-P bonds which has relatively better moisture stability than P-O-P linkages.^{7,8} There is a shortening of the extent of P-O-P linkages with Fe addition which improves the strength of the glass network via Fe-O-P bond creation. It also affects the glass transition temperature and thermal expansion coefficient of IPG and enhances its chemical durability. For Fe_2O_3 - P_2O_5 combination, the glass formation region extends from 15 to 45 mol% of Fe_2O_3 . It has been established that IPG with a composition of 40 mol% Fe_2O_3 -60 mol% P_2O_5 has optimum chemical durability. Glass with higher content of Fe_2O_3 tends to form crystallites and those with lower content lack adequate chemical durability. The melting temperature needed for IPG is < 1273 K which is lower than that in case borosilicate glass (1423K). Another important factor is the higher fluidity of IPG which reduces the time needed for homogenization to 1.5-3h. The borosilicate glass synthesis requires a much longer period of homogenization (> 24 h). In IPG, iron exists in both +2 and +3 oxidation states and generally the proportion of the latter increases with increased iron content. The structure of the iron phosphate glass gradually evolves from meta- to pyro- to orthophosphate linkages.

Synthesis:

Glass can be synthesized using various techniques, for e.g., melt quenching, melt spinning, thermal evaporation, sputtering, chemical vapour deposition, high energy neutral or charged particles bombardment of crystalline material and sol-gel method.⁹⁻¹⁵ However, melt quench is the preferred route since it is an easy, fast and commercially viable method. Synthesis method of the glass matrix is an important parameter which needs to be standardized before loading of nuclear waste commences. For the synthesis of IPG, it has been established that a wide variety

of precursors can be used. IPG synthesis using $FePO_4$, $Fe_4(P_2O_7)_3$, Fe_3O_4 , Fe_2O_3 , ammonium phosphate, P_2O_5 , and phosphoric acid have been reported.^{16,17} A typical melt quench synthesis in the laboratory scale, involves grinding of the precursors in their respective stoichiometric quantities and heating of the resultant mixture in dense silica, alumina or alumino-silicate refractory crucibles till it forms a homogenous melt. The furnace temperature ranges between 900 - 1350°C and the heating period varies between 2-4h. Compared to other phosphate glasses, the extent of corrosion of refractory crucibles is less in case of IPG. This is extremely advantageous when nuclear waste loaded glass melt is heated in joule heater with refractory lining as it improves the cost effectiveness of the process.

The presence of Fe^{2+} ions in IPG has a critical role to play in its resultant viscosity and crystallization tendency.¹⁸ Excess of Fe^{2+} ions increase the viscosity and crystallite formation in the melt. The Fe^{2+}/Fe^{3+} ratio in IPG is dependent on composition and condition in which the melt is formed. The temperature, time and atmosphere used for the furnace heating plays a critical role. It has been established that the melting temperature affects the Fe^{2+}/Fe^{3+} ratio more compared to the melting time. Heating at higher temperature in air leads to oxidation of Fe^{2+} to Fe^{3+} in the melt. If the melt is heated in N_2 atmosphere, the oxidation process does not occur and the Fe^{2+}/Fe^{3+} ratio is unchanged. However, if the melt is heated in a mixture of N_2/H_2 , there is an increase in the Fe^{2+}/Fe^{3+} ratio. The composition of the glass also determines the fraction of Fe^{2+} and Fe^{3+} ions that are present in the final as-prepared glass. The metal cation/s added apart from Fe in IPG leads to a variation in the Fe/P as well as O/P ratio which affects the Fe^{2+} concentration.

To eliminate the formation of Fe^{2+} , the synthesis of IPG has been performed by furnace heating of crystalline $Fe_4(P_2O_7)_3$ at 1323K followed by quenching of the melt in air.¹⁹ The resultant IPG has all Fe ions in +3 oxidation state. The method results in the reduction of pouring temperature by 100K and the absence of NH_3 as by-product during glass formation improves the scalability of the process.

Characterization:

Since there is a direct correlation between the structural groups present in IPG and its properties, proper characterization of IPG is essential to gauge its suitability for loading of nuclear waste which generally has a complex composition. The commonly used techniques are Mössbauer spectroscopy, X-ray absorption fine structure (XAFS) and X-ray absorption near-edge (XANES) spectroscopy, Raman and infra-red spectroscopy, X-ray and neutron diffraction, nuclear magnetic resonance

(NMR) and electron paramagnetic resonance (EPR) studies. The short-range structure of IPG is mostly identified by analyzing a combination of these results.

For crystalline materials, interpretation of the Mössbauer spectrum is quite straightforward. However, for glasses which have disordered structure, the absence of long-range order results in analysis of complex sets of hyperfine interaction parameters in order to establish the coordination around the metal ions and their oxidation numbers.²⁰ In case of IPG with 40% Fe₂O₃-60% P₂O₅ composition, the fitted Mössbauer spectrum exhibits three distinct doublets attributed Fe²⁺ in octahedral site and Fe³⁺ in both octahedral and tetrahedral sites.²¹⁻²³ As shown in Figure 1, the three distinct isomer shifts (IS) have been observed at 0.252±0.005, 0.458±0.005, and 1.124±0.005 mm s⁻¹. They are attributed to Fe³⁺ in tetrahedral coordination, Fe³⁺ in distorted octahedral and/ or trigonal bipyramidal (TBP) co-ordination and Fe²⁺ in distorted octahedral and/ or TBP co-ordination, respectively. The areas under the respective components in the spectrum is an indication of the Fe²⁺/Fe³⁺ ratio in the IPG formed. When the melting temperature is 1273K and the homogenization time is 1h, the IPG has been reported to have ~6.9% of Fe²⁺.²⁴ When temperature and time of furnace heating is increased to 1323K and 3h, respectively, the concentration of Fe²⁺ increased to 13.3%.

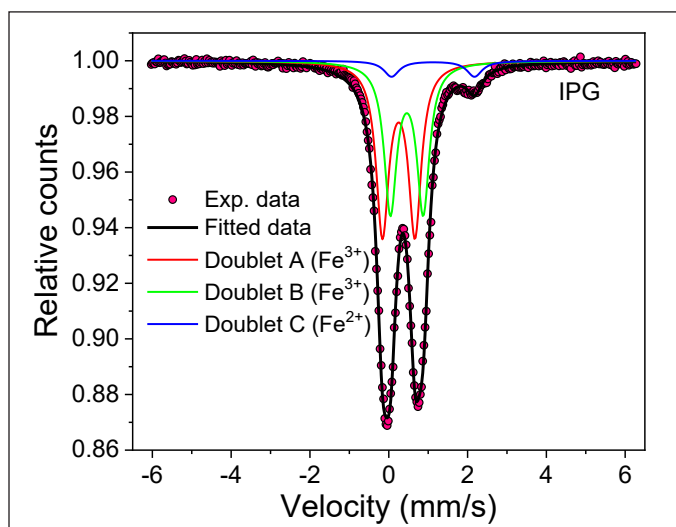


Figure 1. Fitted Mössbauer spectrum of IPG.

FTIR spectrum of IPG mostly exhibit a broad region of overlapping peaks extending from ~700-2000 cm⁻¹ and some weaker intensity peaks at lower wavenumber region (Figure 2). The high intensity feature observed between 1050-1250cm⁻¹ are attributed to various stretching vibrations in the Q¹ and Q² tetrahedra, signifying the presence of both the units in IPG. The peak at ~1160cm⁻¹ and ~1070cm⁻¹ is

due (P-O_{nb}) symmetric bond stretch in metaphosphate (PO₃)⁻¹ or Q₂ units and in the pyrophosphate (P₂O₇)⁴⁻ or Q¹ units, respectively. The peaks at 760cm⁻¹ are due to the symmetric stretching vibrations of bridging (P-O-P) oxygen in pyrophosphate (P₂O₇)⁴⁻ or Q¹ unit. The peak at 930cm⁻¹ is tentatively assigned to the (PO₄)_{asymm} vibration in Q⁰ unit. Presence of some phosphate in the glass is indicated by the hump at ~1280cm⁻¹ due to P=O stretching mode, and the kink at ~1200cm⁻¹ is due to the non-bridging (PO₂)_{asymm} units in Q² tetrahedra.²⁵⁻²⁸ Thus, FTIR spectrum indicates presence of Q², Q¹ and Q⁰ units in IPG.

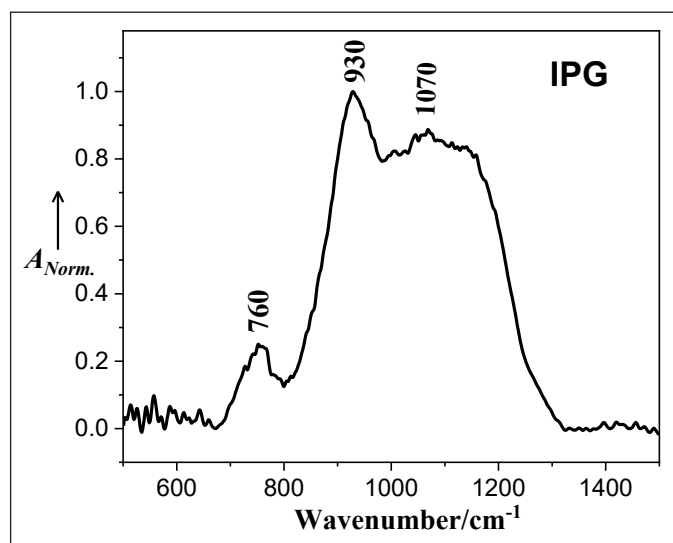


Figure 2. FTIR spectrum of IPG.

Raman spectrum of IPG also corroborates with FTIR and indicate the presence of Q², Q¹ and Q⁰ units with Q¹ being the most prominent as indicated by the highest intensity band at 1070 cm⁻¹ pertaining to symmetric stretching of (P-O)_{nb} in pyrophosphates (Figure 3). The

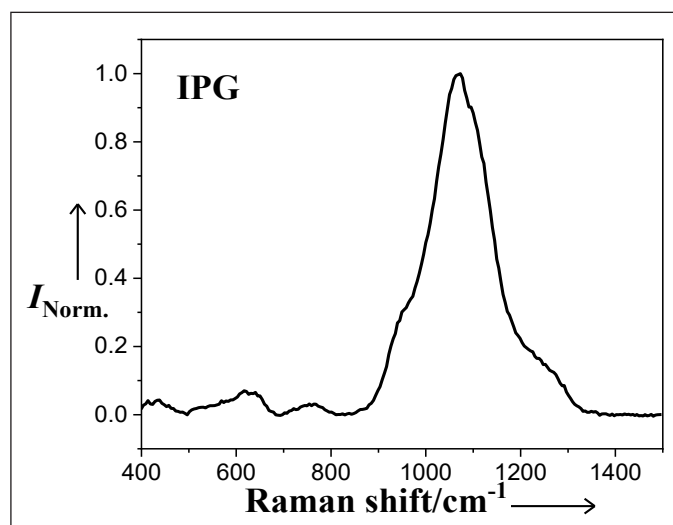


Figure 3. Raman spectrum of IPG.

shoulder peaks at $\sim 1220\text{cm}^{-1}$ and 1250cm^{-1} are due to asymmetric stretching modes in Q_1 and Q_2 tetrahedra. Presence of Q^0 unit is indicated by the peak at $\sim 1010\text{cm}^{-1}$ which is due to symmetric stretch of $(\text{P-O})_{\text{nb}}$ in phosphates.²⁴

The normalised XANES spectra at Fe K edge of IPG on comparison with Fe metal (Fe^0), FeS_2 (Fe^{2+}), and Fe_2O_3 (Fe^{3+}) indicate that iron is mostly present in +3 oxidation states. The centroid position of the pre-edge peak and its area indicates that some Fe^{2+} is also present in IPG. The average coordination number obtained from Fe K-edge EXAFS analysis is 4.74 for the Fe-O units.²⁴

Loading of nuclear waste (simulated):

IPG structure is made of $[\text{FeO}_4]^-$ and $[\text{PO}_4]^-$ tetrahedra which are corner shared and has some areas where Fe^{2+} is in octahedral coordination and Fe^{3+} in both octahedral and tetrahedral coordination. The Fe^{2+} concentration varies with loading of other metal ions as it can act as glass modifiers or glass former which alters the Q^n network of IPG. For the practical use of iron phosphate glass as a host matrix for vitrifying nuclear waste, it is imperative to study the structural changes which occurs in IPG with loading of various waste components. Nuclear waste generally has high concentration of alkali metal oxides (Na_2O , K_2O), alkaline earth metal oxides (CaO , SrO), other oxides like Al_2O_3 , Bi_2O_3 , Cr_2O_3 , and UO_2 , and volatile species such as sulfates, halides, and technetium. Addition of Na_2O in IPG does not result in drastic change in the Mossbauer spectrum and hardly affects the $\text{Fe}^{2+}/\text{Fe}^{3+}$ ratio. The waste loading of Na_2O was achieved upto 20 mol% which is also known as the solubility limit of the loaded material. Solubility limit is defined as the maximum amount of a component that can be fused before crystallization or phase separation occurred in the melt. However, simulated sodium bearing waste could be loaded in IPG up to 40 wt% using conventional and cold crucible induction melting techniques.³ The loading of any waste material substitutes either Fe_2O_3 or P_2O_5 or both constituents in the melt.²⁴ The solubility limit for Bi_2O_3 , Cs_2O , K_2O , MoO_3 , UO_2 in IPG is ~ 20 mol%, 30 mol%, 20 mol%, 30 mol%, and 15 mol%, respectively. These results indicate that a waste containing significant amounts MoO_3 or Cs_2O can be vitrified in iron phosphate glass.²⁴ Mo has high fission yield and forms a significant part of high level waste (HLW). However, it has relatively low solubility in borosilicate glass (≤ 3 mol%) and hence alternative glassforms like IPG are beneficial for the purpose of vitrification. With Cs_2O addition, the structure of IPG remains unchanged upto 22 mol% loading. When loading is between ~ 22 -30 mol%, some structural changes are observed. If loading of Cs_2O is increased

beyond 30mol%, precipitation of crystallites occur. Similarly, 25 wt% of BaO could be loaded in IPG without phase separation or crystallization. Improvement in glass network connectivity with Cs_2O or BaO loading in IPG is indicated by an increase in glass transition temperature due to higher concentration of metaphosphate linkage.²⁴ The thermal expansion behavior for Cs/Ba loaded IPG are similar and hence there will not be any structural change when radioactive Cs converts to Ba in the IPG matrix with time. IPG structure exhibits enhanced stability with Na_2SO_4 loading upto 30mol% which creates enabling conditions for further loading of waste into it. 0-0.5 mol% (in increments of 0.1) of metal sulphates of the type R_ySO_4 , where $\text{R} = \text{Li}, \text{Na}, \text{K}, \text{Mg}, \text{Ca}, \text{Ba},$ or Pb and $y = 1$ or 2 have been loaded in IPG and their effect on the structure and stability have been investigated.²³ The sulfates volatilize and result in the formation of corresponding metal oxides in the melt. Increasing the metal oxide concentration results in depolymerization of the phosphate network in IPG. Alkali metal oxides do not alter the density and show slight increase in glass transition temperature (T_g). It also promotes bulk crystallization at 600-700°C temperature. Increase in density, T_g and bulk crystallization at 700-800°C is observed with increase in concentration of divalent metal oxides in IPG. The leach rate is increased with increase in concentration of alkali oxide (30-40 mol% R_2O) to the base glass. Addition of divalent cations decrease the aqueous leach rates in IPG which are much lower than that observed in borosilicate glass.

It has been established that IPG can vitrify wastes containing phosphates and heavy metal oxides like Bi_2O_3 , UO_2 , ZrO_2 almost thrice more than is possible in borosilicate glass matrix. Detail thermal studies has also been reported for IPG loaded with 20 wt.% of simulated nuclear waste and it indicates almost unaltered thermal expansion, glass forming ability and glass stability characteristics. Also simulated high level waste (HLW) containing 4 wt% chrome oxides, could be vitrified in IPG to yield glassforms with excellent chemical durability.²⁹ The temperature of homogenization was 1150°C and 1250°C for waste loadings of ~ 55 and 75 wt%, respectively.

Radiation effects:

Since the glass matrix hosts radionuclides (RN), their consequent decay emitting α , β and γ rays can precipitate physical and chemical changes in it.³⁰ This can be detrimental for its application for long term storage. Hence, it is necessary to study the impact of radiation on such matrices to check its ability to withstand such effects. In high level waste, fission products like ^{137}Cs and ^{90}Sr are the β emitters while minor actinides like ^{241}Am ,

^{243}Am and ^{244}Cm are long lived α emitters. β particles emit energy in range of 100keV -1MeV and causes electronic excitation and ionization in the glass matrix but atomic dislocations are scarce. In α -decay, apart from α particle emission there is also motion due to the recoil nucleus. The energy of α particles range between 4-5MeV and cause electronic excitation as well as atomic displacement in the glass matrix. The atomic displacements are considerably enhanced by the elastic collisions of the recoil nuclei (energy varies between 80–120 keV). β emitters are short lived and are the main source of absorbed dose and heating of the matrix during first 500 years of storage. Later, the electronic collisions by α emission becomes the primary source of absorbed dose and can continue for a million year of storage. The nuclear collisions produce absorbed dose which are almost two orders of magnitude lower than that of electronic collisions. However, in case of certain host matrix like oxide glass, nuclear collisions exhibit much higher damaging effects and hence it is imperative to study the radiation tolerance level in any host matrix. The cumulative numbers of alpha decay events and the associated nuclear damage is expressed in dpa (displacements per atom of the glass).

To simulate and hasten the radiation induced damage in glass, ion beam irradiation studies are generally performed. When glass samples are exposed to ion beams of $\sim 100\text{keV}$ energy, they deposit energy via elastic nuclear collisions/stopping (Sn) creating ballistic damage. When the ion beam energy is higher, the damage is induced by inelastic electronic collisions/stopping. Theoretical studies on IPG with 4% and 17% Fe^{2+} ions irradiated with 4keV energy yielded interesting results.³¹ The Fe/P ratio plays an important role in the final number of displacements observed with irradiation. Also, IPG with lower Fe^{2+} content shows better radiation stability. Radiation tolerance of IPG ($\text{Fe}^{2+}/\Sigma\text{Fe}^{3+} = 0.15$) has been tested using Au ion beam at different energy: 750 keV to study nuclear loss and 5 MeV, 10 MeV and 20 MeV where both electronic and nuclear loss are active.³² It has been ascertained that though the total deposited energy in the IPG sample for all radiation energy is essentially the same, peak damage is located at different depth for different energies. The reduction of Fe leading to formation of Fe^{2+} in the sample was negligible in 750keV energy range but increased considerably during 5-20MeV irradiation. The nuclear and electronic losses in higher energy range leads to the reduction of Fe^{3+} in IPG. Precipitation of crystallites is also observed in IPG with high energy Au ion beam irradiation. Approximately 26% decrease in hardness in IPG is observed for both low and high energy irradiation which is attributed to the formation of non-bonding oxygen and precipitation of crystallites

as confirmed from Raman spectroscopy and electron microscopy techniques, respectively.

Future directions:

Compared to the exhaustive studies on borosilicate glass as host matrix for nuclear waste vitrification, there are much fewer reports in iron phosphate glass. The reason is that IPG is industrially used for immobilization of HLW in Russia whereas most of the other countries use borosilicate matrix. However, the $40\text{Fe}_2\text{O}_3\text{-}60\text{P}_2\text{O}_5$ stoichiometry of IPG has been optimized based on its chemical stability for nuclear waste loading. It has a low melting temperature of $\sim 945^\circ\text{C}$ and causes lower extent of corrosion in the Inconel alloys and oxide refractory materials used in the vitrification process which improves the lifetime of the melter. IPG has Fe-O-P linkages which are less susceptible to hydration and hence renders chemical durability to the phosphate glass. The composition of nuclear waste includes actinides like U, Pu, Am, Cm, fission elements (mainly Cs, Xe, I, Ru) and various other α -/ β -/ γ - ray emitting radionuclides. Therefore, any potential application of IPG as a host for these nuclear wastes demands a detailed investigation on the stability of the matrix on being loaded with these metal ions. Recently, the effect of loading oxides of Mo, Cs, Ba, Sb and Te in IPG has been reported but various other combinations of nuclear waste loading need to be studied in detail to generate a data bank for industrial application of IPG as host matrix for vitrification.^{24,33} Also, since IPG loading will be with radioactive waste, it is imperative to study the effect of radiation on the structure and stability of both pristine and waste loaded IPG. However, reports on radiation tolerance studies in IPG is quite scarce. Future endeavours should be also directed in filling up the knowledge gap in these areas.

References:

1. P. Stoch, W. Szczerba, W. Bodnar, M. Ciecinska, A. Stoch, E. Burkel, *Phys. Chem. Chem. Phys.*, **2014**,16, 19917.
2. J. M. Perez Jr., D. F. Bickford, D. E. Day, D.S. Kim, S. L. Lambert, S. L. Marra, D. K. Peeler, D. M. Strachan, M. B. Triplett, J. D. Vienna, R. S. Wittman, *Pacific northwest national laboratory report, PNNL*, **2001**, 13582.
3. C. W. Kim, C. S. Ray, D. Zhu, D. E. Day, D. Gombert, A. Aloy, A. Mogus-Milankovic, M. Karabulut, *J. Nucl. Mater.*, **2003**, 322, 152.
4. J. V. Crum, L. Turo, B. Riley, M. Tang, A. Kossoy, *J. Am. Ceram. Soc.*, **2012**, 95 (4), 1297.
5. K. Joseph, K. V. Govindan Kutty, P. Chandramohan, P. R. Vasudeva Rao, *J. Nucl. Mater.*, **2009**, 384, 262.
6. R. K. Brow, *J. Non-Cryst. Solids*, **2000**, 263–264, 1.
7. D. E. Day, C. S. Ray, C. W. Kim, *Final Report: Iron Phosphate Glasses: an Alternative for Vitrifying Certain Nuclear Wastes, Project No. DEFG07e96ER45618*, **2004**.

8. L. Pavic, M. P. F. Graca, Z. Skoko, A. M. Milankovic, M. A. Valente, *J. Am. Ceram. Soc.*, **2014**, 97, 2517.
9. D. Carta, D. M. Pickup, J. C. Knowles, I. Ahmed, Mark E. Smith, Robert J. Newport, *J. Non-Cryst. Solids*, **2007**, 353, 1759.
10. X. Cui, Q. D. Zhang, X. Y. Li, F. Q. Zu, *J. Non-Cryst. Solids*, **2016**, 452, 336–341.
11. R. M. Almeida, L. F. Santos, A. Simens, A. Ganjoo, H. Jain, *J. Non-Cryst. Solids*, **2007**, 353, 2066.
12. W. R. Sinclair, F.G. Peters, *J. Am. Ceram. Soc.*, **1963**, 46, 20.
13. L. A. Mochalov, A. S. Lobanov, A. V. Nezhdandov, A. V. Kostrov, V. M. Vorotyntsev, *J. Non-Cryst. Solids*, **2015**, 423-424, 76–80.
14. B. C. Sales, J.O. Ramey, J. C. McCallum, L. A. Boatner, *J. Non-Cryst. Solids*, **1990**, 126, 179.
15. S. Ahmadi, B. E. Yekta, H. Sarpoolaky, A. Aghaei, *J. Non-Cryst. Solids*, **2014**, 404, 61.
16. T. Li, Z. Tang, J. Weiwei, X. Gong, *Key Eng. Mater.*, **2008**, 368-372, 1446.
17. Y. M. Lai, X. F. Liang, S. Y. Yang, J. X. Wang, L. H. Cao, B. Dai, *J. Mol. Struct.*, **2011**, 992, 84.
18. K. Joseph, K. V. Govindan Kutty, M. C. Goswami, P. R. Vasudeva Rao, *Thermochim. Acta*, **2014**, 587, 42.
19. K. Joseph, V. Yuvaraj, R. Govindaraj, A. Senapati, S. Ghosh, R. Venkata Krishnan, T.R. Ravindran, *J. Non-Cryst. Solids*, **2019**, 520, 119327.
20. P. Stoch, A. Stoch, *Nucleonika*, **2015**, 60, 133.
21. K. Joseph, M.C. Stennett, N.C. Hyatt, R. Asuvathraman, C.L. Dube, A.S. Gandy, K.V. Govindan Kutty, K. Jolley, P.R. Vasudeva Rao, R. Smith, *J. Nucl. Mater.*, **2017**, 494, 342.
22. J. Bai, J. Hsu, P. Sandineni, C.-W. Kim, R.K. Brow, *J. Non-Cryst. Solids*, **2019**, 510, 121.
23. P.A. Bingham, R.J. Hand, O.M. Hannant, S.D. Forder, S.H. Kilcoyne, *J. Non-Cryst. Solids*, **2009**, 355, 1526.
24. D. P. Dutta, M. Roy, R. K. Mishra, S. S. Meena, A. Yadav, C.P. Kaushik, A.K. Tyagi, *J. Alloys and Compds*, **2021**, 850, 156715.
25. Y.M. Lai, X.F. Liang, S.Y. Yang, J.X. Wang, L.H. Cao, B. Dai, *J. Mol. Struct.*, **2011**, 992, 84.
26. M. Shi, Y. Liang, L. Chai, X. Min, Z. Zhao, S. Yang, *J. Mol. Struct.*, **2015**, 1081, 389.
27. L. Boroica, B.A. Sava, M. Sava, M. Elisa, *J. Optoelectron. Adv. Mater.*, **2013**, 15, 187.
28. X. Fang, C.S. Ray, A. Mogus-Milankovic, D.E. Day, *J. Non-Cryst. Solids*, **2001**, 283, 162.
29. W. Huang, D. E. Day, C. S. Ray, C. W. Kim, *J. Nuclear Mater.*, **2005**, 346, 298.
30. S. Gin, P. Jollivet, M. Tribet, S. Peugeot, S. Schuller, *Radiochim. Acta*, **2017**, 105(11), 927.
31. K. Jolley, R. Smith, *Nucl. Instruments Methods Phys. Research B*, **2016**, 374, 8.
32. C. L. Dube, M.C. Stennett, S. Akhmadaliev, N.C. Hyatt, *J. Non-Cryst. Solids: X*, **2020**, 8, 100055.
33. A. C. Joshi, M. Roy, D. P. Dutta, R. K. Mishra, S. S. Meena, R. Kumar, D. Bhattacharyya, R. Alexander, C. P. Kaushik, A. K. Tyagi, *J. Non-Cryst. Solids*, **2021**, 570, 121016.



Dr. Dimple P. Dutta joined Bhabha Atomic Research Centre (BARC), Mumbai in 1996 after obtaining her MS in Chemistry from IIT Kanpur, India. She was a Postdoctoral Fellow at University of Heidelberg, Germany, during the period 2001-2002. Her major area of research includes development of functional materials for energy storage, nuclear vitrification and environmental remediation applications. Dr. Dutta has an impressive list of research publications to her credit, written several book chapters and has presented her research work at several international forums. She received the prestigious Bronze medal from CRSI (Chemical Research Society of India) in 2021 and DAE Scientific & Technical Excellence Award (2020) for her seminal contribution in the field of chemical science. She is a Fellow of the Maharashtra Academy of Sciences since 2016. She has been awarded membership of National Academy of Sciences, India and is also the recipient of "DAE-SSPS Young Achiever Award". She has received the "ACS Award" from the American Chemical Society in 2015. Dr. Dutta also serves as reviewer for more than 30 journals of international repute and is an Associate Editor for International Journal of Applied Ceramic Technology.

Transparent ceramics for radiation detection

Shashwati Sen¹, S G Singh¹, G D Patra¹, S Pitale¹, M Ghosh¹

¹Technical Physics Division, BARC, Mumbai

E-mail: shash@barc.gov.in

Abstract

A transparent ceramic is similar in its transparency to a single crystal or a glass system. But it is different from both these systems as its polycrystalline in nature. Thus they have the mechanical properties of ceramic materials like hardness along with transparency. Because of this combination this class of material has many technological applications like in laser hosts, infrared (IR) windows/domes, lamp envelopes and transparent armors. The challenge in the fabrication of transparent ceramics is controlling the elements which lead to scattering of light in the bulk material and thus making it opaque to visible light. Synthesis strategies are required to eliminate pores and secondary phases at the grain boundary which are the source of light scattering. This article gives brief description on the techniques and challenges involved in the preparation of transparent ceramics. Few examples of fabrication of transparent ceramics with application in radiation detection are discussed in the end. The effect of sintering, vacuum sintering and sintering under pressure on pores and grain growth is analyzed using small angle neutron scattering technique to understand the process of formation of transparent ceramics.

1. Introduction:

Transparency of a solid material is the ability to allow light to pass through them without scattering. Transparent materials usually have a clear appearance, either in one color or any combination leading to a spectrum of multiple colors. Conventionally, materials that are optically transparent can be categorized into glasses, polymers, and single crystals. All these materials have various applications in industries and daily life. Among these applications single crystals are mostly used in the fields of laser and radiation detectors because of their superior properties and homogeneous nature¹. However, these single crystals are growth by melt growth techniques and are very expensive as their growth requires sophisticated facilities and are time-consuming techniques limiting their productivity. They are brittle in nature which makes their machining very difficult and adds to the cost of the final product. Furthermore, as-grown single crystals have shapes and sizes limited by their lattice structures². Another disadvantage of single crystals is the limitation in homogeneity of doping concentration due to segregation coefficient of dopants in melt. Also, the quality of the grown crystals depends on many parameters including, size of the crucible, thermal field distribution, mechanical stability, and so on. These drawbacks can be circumvented by using transparent ceramics³.

In general ceramic or polycrystalline bulk materials are opaque in nature. The presence of grain boundaries, secondary phases, birefringence and pores in a ceramic

material leads to its opacity. Figure 1 pictorially depicts the different scattering elements present in an ceramic sample⁴. The light photon gets reflected or scattered on these sites thus making them opaque. Among all these elements, the presence of a large number of residual pores within the grains and at the grain boundaries is the main factor which makes a ceramic material opaque. The surface of a pore acts as a boundary between two phases with different optical characteristics, which therefore intensely reflects and refracts light. Secondly, the difference in optical properties of grains and grain boundaries due to segregation of secondary phase also leads to scattering of light.

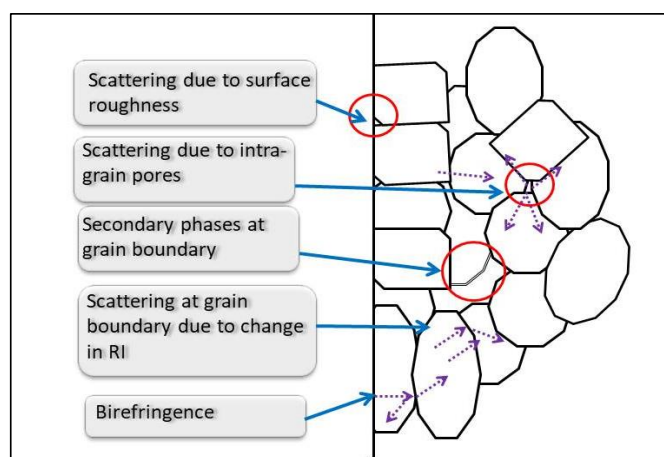


Figure 1. Different sites at which a light photon gets scattered inside a polycrystalline bulk sample

Thus to develop a transparent ceramic bulk material we have to eliminate all possible scattering sites of light. This includes achieving high density (>99.9% of theoretical density), removal of pores from the intergrain and intragrain region, reducing the pores size much less than the wavelength of light, eliminate any second phase or impurity at grain boundaries and maintain a uniform grain size which is comparable to the wavelength of visible light. In addition to these points it is beneficial to have an isotropic lattice structure and high surface finish to achieve high transparency in a ceramic material⁵.

This report aims to provide an overview on the recent progress in fabrication and characterization of transparent ceramics for various applications. The techniques used to develop transparent ceramics will be introduced first. After that few materials which have been made into transparent ceramics and their applications in various areas will be described and discussed.

2. Preparation technique for transparent ceramics

As discussed in the earlier section a ceramic material can be made transparent by reducing the concentration of defects, which include secondary or grain boundary phases and residual pores. In order to fulfill these requirements specific experimental conditions must be combined together. Foremost it is necessary to use raw material of high purity and to avoid any possible contamination during processing. This will avoid the formation of secondary phases and eliminate impurities in the bulk. Also, the concentration of any additive should be minimized to avoid any change in the refractive index of the bulk material. In addition the grain size of the constituent powder should be in nanometers (preferably less than 100nm) which avoids scattering of visible light having wavelength of the order of few hundreds of nanometers⁶.

Taking the above point into consideration the preparation of transparent polycrystalline bulk ceramic can be divided into the following steps. First is synthesis of precursor powder,

followed by calcination/sintering along with compacting, and finally post-treatment procedure like annealing, machining and polishing of the final bulk sample⁷. The sintering temperature in this process is much below the melting point of the material thus making it economical as compared to single crystal growth technique in which the material is melted which required high energy consumption. The schematic for the formation of transparent ceramic is shown in Figure 2.

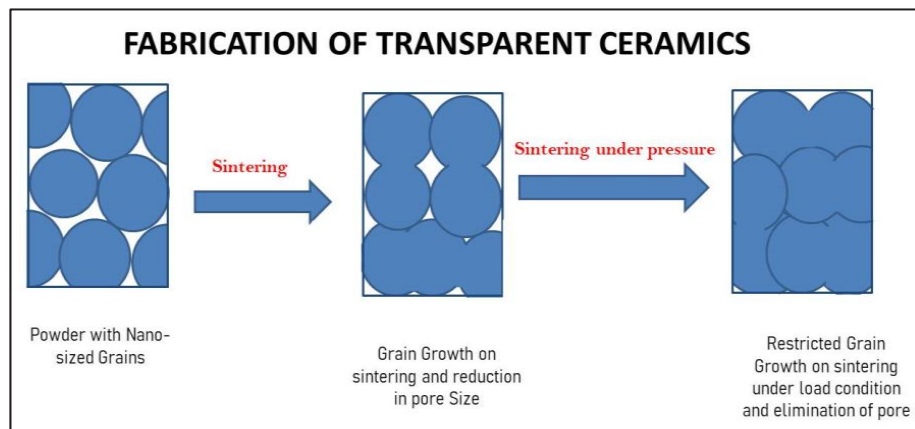


Figure 2. Schematic showing the formation of transparent ceramics from nano-powders by compaction and sintering

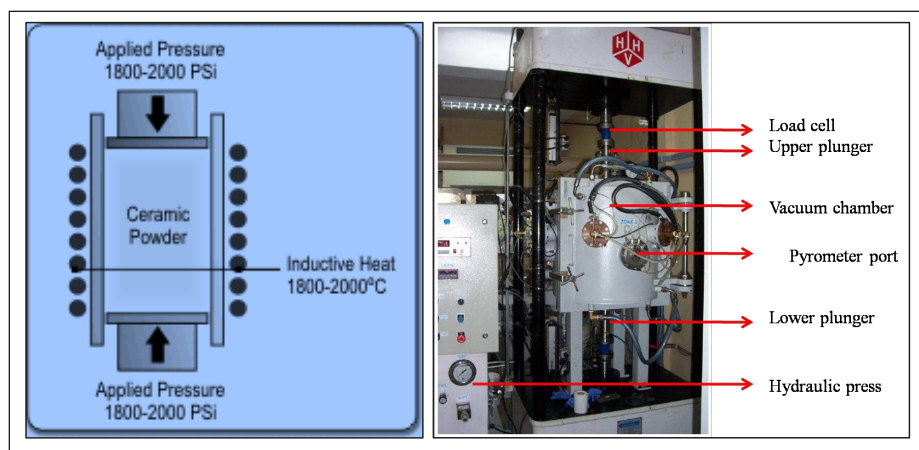


Figure 3. Schematic of a Hot Press system (left). Actual photograph of a Hot Press System showing the various parts.

The precursor powder can be synthesized by any nano-powder synthesis techniques which includes co-precipitation, sol-gel synthesis, ball milling etc. The main thing to consider during the material synthesis is to maintain the high purity and to have monotonic size distribution along with similar shaped grains with minimum agglomeration. The presence of agglomerates in the nano-powder makes the densification process very difficult due to the difficulty in the removal of nano-pores present between the individual

nanoparticles (intra-grain pores) and the large macro-pores (inter-grain pores) present between the agglomerates⁸.

The compaction along with sintering techniques commonly used for the formation of transparent ceramics are hot pressing (HP), hot isostatic pressing (HIP), vacuum sintering, spark plasma sintering (SPS) and microwave sintering.

2.1 Hot Pressing:

High pressure sintering or commonly known as Hot Pressing (HP) is a high-pressure high temperature process for compaction of a powder sample⁹. The temperature in this process is high enough to induce sintering as well as creep processes. This is achieved by the simultaneous application of heat and pressure. The pressure applied in this process is uni-axial i.e. from top and bottom. The material to be compacted is loaded in a die made either of graphite or molybdenum depending on the process temperature and nature of the processed material. The system is initially evacuated and temperature is increased before the application of pressure. The pressure of the order of 150-200MPa is applied through top and bottom plunger. However reports are also available of HP system with very high pressure of the order of 100GPa. A schematic of a HP system and actual photograph is shown in Figure 3. The system comprises of a vacuum chamber along with vacuum pumps. The vacuum pumps are generally a combination of rotary and diffusion pump to achieve a working pressure of 10^{-5} mbar. The high temperature furnace comprises of either inductive or resistive heating elements to achieve a temperature up to 2000°C. The temperature is controlled using thermocouple as well as pyrometer. The pressure is applied using a load cell with top and bottom plungers. The whole chamber is water cooled due to high operating temperature.

The sintering mechanism at high pressures is entirely different from that at ambient pressure. High pressure can restrain grain growth and initiate plastic deformation to eliminate pores and/or additional phases existing in triple junctions of the grains. The densification process at high pressure works through particle rearrangement and plastic flow at the point of contact between the particles¹⁰. As a consequence of presence of both high temperature and high pressure, formation of the necks between adjacent particles takes place leading to grain growth and compaction of the powder (as shown in Fig 2). Sometimes additives are mixed with the initial powder which flows into the pores at the processing temperature to increase the density of the compacted powder as well as the transparency to the ceramic. However the additive should not form any secondary phase and its refractive index should match

with that of the material to minimize light scattering at the interface.

Due to the ease of operation, HP has become an important technique to produce transparent ceramics. HP process was used to fabricate $MgAl_2O_4$ transparent ceramics, with a nearly 100 % densification¹¹. Also stepwise process has been reported to fabricate $Eu:Y_2O_3$ transparent ceramics using HP technique¹².

2.2 Hot isostatic (HIP) sintering:

Hot isostatic pressing (HIP) is a manufacturing process used to reduce the porosity and increase the density of various ceramic materials. The HIP process subjects the material to both elevated temperature and isostatic gas pressure in a high-pressure containment vessel¹³. This process has been found very effective in fabrication of transparent ceramic because of the uniform application of pressure on the sample from all side. This is the best way to reduce the number of pores; both inter grain and intra-grain. Other advantages of this process above HP are as the pressure is applied by heated gas molecules (mostly argon) there is minimum chance of contamination arising due to the process. Secondly the pressure applied on the ceramic sample is in the order of 300MPa as compared to 150MPa in case of HP which help in better compaction.

Schematic of a hot isostatic press system is shown in figure 4. The system consists of a high pressure chamber and a high temperature furnace. The powder sample which is to be compacted is first made into a green pellet by the application of cold isostatic compression (CIP). This is a crucial step before sintering the pellet to ensure high density of the pre-sintered object. This process forms a pellet of density greater than 95% of theoretical limit. The green pellet is loaded in the HIP system and the chamber is heated, causing the pressure inside the vessel to increase. Before the temperature is increased the system is generally evacuated and filled with process gas. The system is initially filled with an inert gas like Ar and then heated to elevated temperature. During the heating cycle the gas molecules exert very high pressure of the order of 300MPa on the green pellet from all the sides. The exerted pressure is equal from all sides and the pores are filled by coalescing of grains of the polycrystalline disc. Many systems use associated gas pumping to achieve the desired pressure levels. The heater comprises of tungsten mesh filaments so that the environment inside the furnace remains contamination free.

This process when used in combination with HP or vacuum sintering technique leads to formation of 100% dense ceramics. Hot pressing followed by hot isostatic

pressing (HIP) has been used to fabricate transparent $MgAl_2O_4$ ceramics¹⁴. Vacuum sintering with a subsequent HIP step was usually employed to synthesize cubic ceramics, including Y_2O_3 ¹⁵, Sc_2O_3 ¹⁶, and Lu_2O_3 ¹⁷. The vacuum sintering process is employed to remove closed pores and the HIP technique leads to the fabrication of fully dense sesquioxide ceramics with less possibility for contamination and reduction than hot pressing.

The main drawback of the HIP technique is the high safety features which have to be ensured in its operation. As the system is filled with gas at elevated pressure and temperature proper controls should be used so that there is no damage to any instrument.

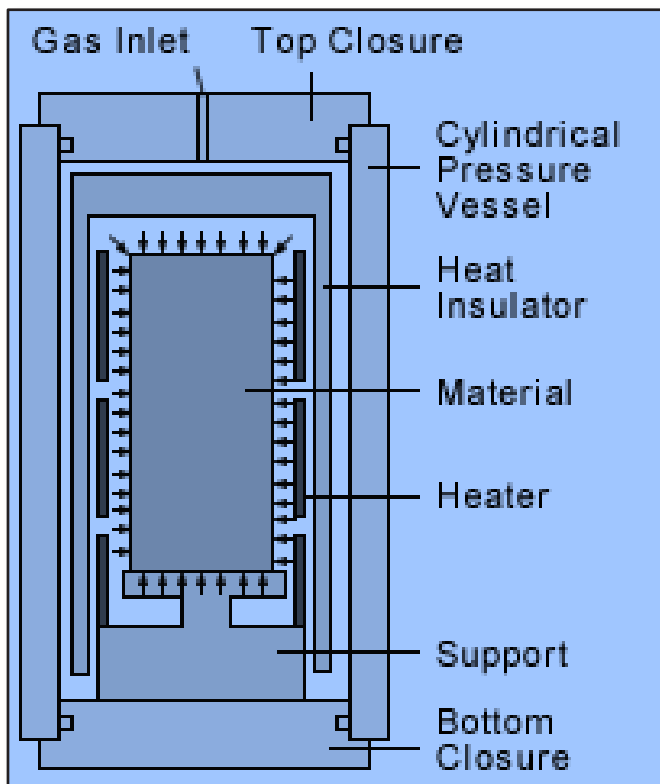


Figure 4. Schematic of a Hot Isostatic Press system

2.3 Vacuum sintering:

Vacuum sintering refers to a high temperature sintering processes of a compacted powder carried out in a vacuum equipment to achieve better results than those run at atmospheric pressure. As a first step, before vacuum sintering the green pellet of the material is formed by cold isotatic pressing (CIP) to achieve better density which is then loaded in a vacuum chamber and heated to elevated temperatures to form transparent ceramics. For example, the first transparent polycrystalline Nd:YAG ceramics was synthesized by using solid-state reactive sintering the mixture of Al_2O_3 , Y_2O_3 and Nd_2O_3 in a tungsten mesh heated to at 1800°C vacuum furnace at 5 x

10^6 Torr⁴. The densification in vacuum sintering happens as the air trapped in the pores is released in vacuum and the polycrystalline grains merge to make high density ceramic. Rapid heating cycle is generally employed to restrict grain growth. Many additives like SiO_2 is added to the powder to achieve high density and transparency in vacuum sintering. Vacuum sintering has been widely used to fabricate various transparent ceramics, including garnet, spinel, alumina, and rare earth sesquioxides ceramics

2.4 Spark plasma sintering (SPS):

Spark plasma sintering (SPS) is a newly developed method for obtaining fully dense and fine-grained transparent ceramics at low temperatures within short time durations¹⁸. It is also known as field-assisted sintering or pulsed electric current sintering. In HP and HIP technique the material is heated externally using a heating coil either by induction or resistive heating technique. In the SPS technique a high density current flux flows through the sample and the die to cause Joule heating within the sample. As very high current passes through the sample and the die, the temperature of the sample increases very fast the grain growth is restricted in this technique. This leads to better compaction and because of small grain size better transparency is achieved. The applied pressure in this technique is uni-axial as in hot press though top and bottom

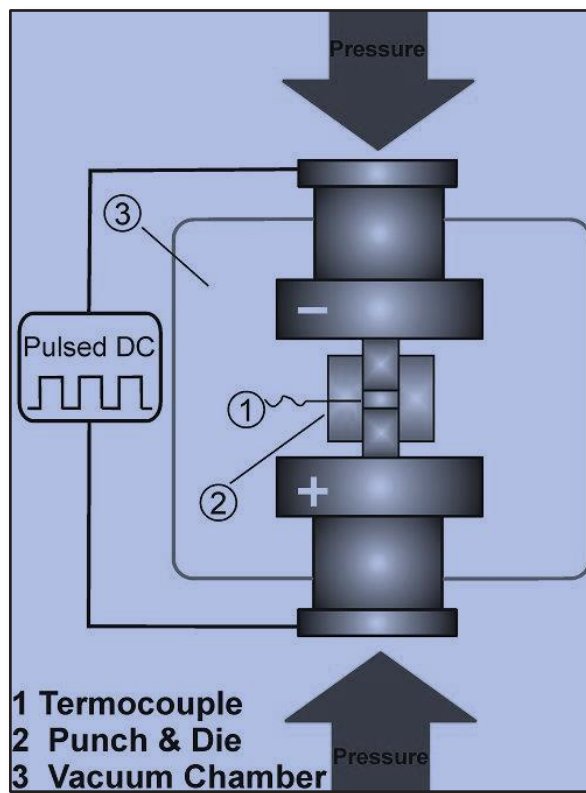


Figure 5. Schematic of a Spark Plasma Sintering System

plunger. A schematic diagram of a typical SPS system is shown in Fig. 5. The system has a vacuum chamber to protect the graphite plunger from oxidation. Pulsed DC current sources are used to pass very high current through the die. SPS technique even can be used to fabricate samples with special shapes, such as hemispherical domes. For instance, transparent polycrystalline alumina domes have been obtained by combining sintering and forming into one step in minutes.

3. Transparent ceramics for radiation detection:

In 1995 Nd:YAG laser based on transparent ceramic was fabricated by Ikesue *et al* using SiO₂ to sinter 0.9 at% Nd:YAG ceramics⁴ to sufficient transparency to achieve a laser slope efficiency similar to Czochralski grown single crystals. This started the commercial application of this class of materials. Use of transparent ceramics in the field of lasers is now well established.

The transparent ceramics used in the field of radiation detection are the ceramic scintillators like LuAlO₃, YAlO₃(LuAP and YAP:Ce)¹⁹, and the dosimeter crystals like LiF, CaF₂:Mn and Al₂O₃:C²⁰. Ceramic scintillators have some advantages compared with single crystal scintillators. They are mechanically strong, easy to obtain large size at low cost. New chemical compositions, which are impossible to grow in single crystal form, can be fabricated in ceramic form. Also ceramic scintillator ensures uniform doping at higher concentrations which is helpful to increase light yield in application for radiation detection. The first polycrystalline ceramic scintillator was the rare-earth ceramic scintillator Y_{1.34}Gd_{0.60}Eu_{0.06}O₃ which has been developed, by combining carefully controlled phosphor composition and doping technology with innovative technology on transparent, polycrystalline ceramics and used specifically for high-performance medical detectors and commercial X-ray CT²¹.

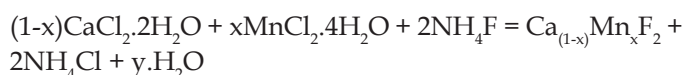
In the next section we discuss two examples of transparent ceramics prepared by our group. These are prepared by vacuum hot pressing technique and have application for radiation detection in the field of dosimetry and radiography.

3.1 CaF₂:Ce transparent ceramics:

The CaF₂:Mn is an important material for the thermoluminescence (TL) dosimetry also known as TL-400. The difficulty in growing doped single crystal of this material arises from the high vapour pressure of MnF₂ that prohibits its incorporation in the CaF₂ crystal lattice during the growth. Hence, most of the reports on this material are either on polycrystalline powder samples or pellets. Also, in the single crystal form it is very difficult to increase the

doping percentage in the matrix due to segregation of dopants in the melt. This hinders preparation of crystal samples with higher Mn concentration which is beneficial for dosimetric applications. The difficulty in the growth of CaF₂:Mn single crystals can be circumvented by using optically transparent ceramics of this compound. Optically transparent ceramic of CaF₂:Mn has been prepared by hot pressing of nano-phase powders under vacuum conditions.

CaF₂ nano particles containing Mn 2.5 mol% was prepared by the co-precipitation method.



Solution NH₄F and CaCl₂ (mixed with MnCl₂) was prepared in DI water separately and the two solutions were mixed under constant stirring at room temperature. White coloured precipitate was observed on mixing the two solutions. This precipitate was separated by centrifugation and washed several times using DM water to remove all residual chemical. The precipitates were dried at 100°C in air for 24 h and at 400°C for 2 hrs to remove all moisture and form powder of CaF₂:Mn²². The morphology of the as synthesized powder is shown in Figure 6(a). The phase purity and the crystallite size of the synthesized material was checked using XRD. SEM image along with XRD confirms that the as synthesized CaF₂ consists of ~200 nm size agglomerates of nano-crystalline grains with crystallite size ~40 nm Fig 7(a). The crystalline size of the as-grown sample was calculated from the full width at half maximum (FWHM) technique using the Scherer's formula $D = K \lambda / (\beta \cos \theta)$ where K is constant (0.99), λ is the wavelength of Cu K $_{\alpha}$ (1.54 Å) line, β is the FWHM and θ is the diffraction angle. The crystalline size of as prepared nanoparticles was in the range of 40 nm.

For synthesis of transparent ceramics the powder was loaded in a graphite die and hot pressed under vacuum conditions (10⁻⁵ mbar) at 1000°C and 20M Pascal pressure. The vacuum hot press system has been described in section 2.1. For hot pressing, first the system is evacuated to 10⁻⁵ mbar vacuum and then the temperature is slowly raised. Once the temperature reaches 1000°C the load is increased. The powder is hot pressed at the set temperature and pressure for 2 h duration and then cooled to room temperature. The load is removed when the cooling cycle starts to avoid cracking of the pellet. Once the pressed pellet is removed from the die it is lapped and polished before further characterization is carried out.

The microstructure of the polycrystalline CaF₂:Mn pellet was recorded at various steps of preparation using

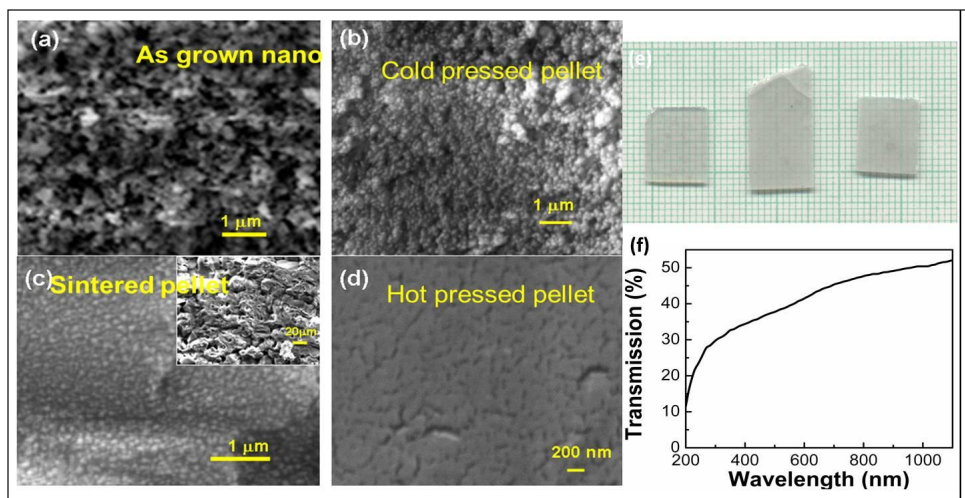


Fig 6. SEM image of (a) as synthesized $\text{CaF}_2:\text{Mn}$ nano particles (b) cold pressed pellet of CaF_2 (c) CaF_2 pellet vacuum sintered at 1000°C for 2 hrs, (d) transparent ceramic of CaF_2 prepared by vacuum hot pressing at 1000°C for 2 hrs, (e) photograph of prepared transparent ceramic samples of $\text{CaF}_2:\text{Mn}$ and (f) transmission spectra of CaF_2 transparent ceramic.

The change of crystallite size from as-grown powder (sample-1) to vacuum sintered pellet (sample-2) and optically transparent specimen (sample-3) is clearly visible in Fig 7(b). From the change in the peak width it is clear that the grain size increases from nm to μm region on hot pressing. It is to be noted that the asymmetric broadening of the peak in the sample-3 (transparent sample, hot pressed for 2 h) may be due to crystal defects (dislocation, slip planes etc) generated because of the pressure applied at high temperatures as reported (and not due to grain size) [28]. This confirms the grain growth during hot pressing to obtain the optically transparent ceramic. Same change in grain size from as synthesized powder to vacuum sintered ceramic and transparent ceramic is visible in SEM micrographs as discussed in Fig 6(a-d).

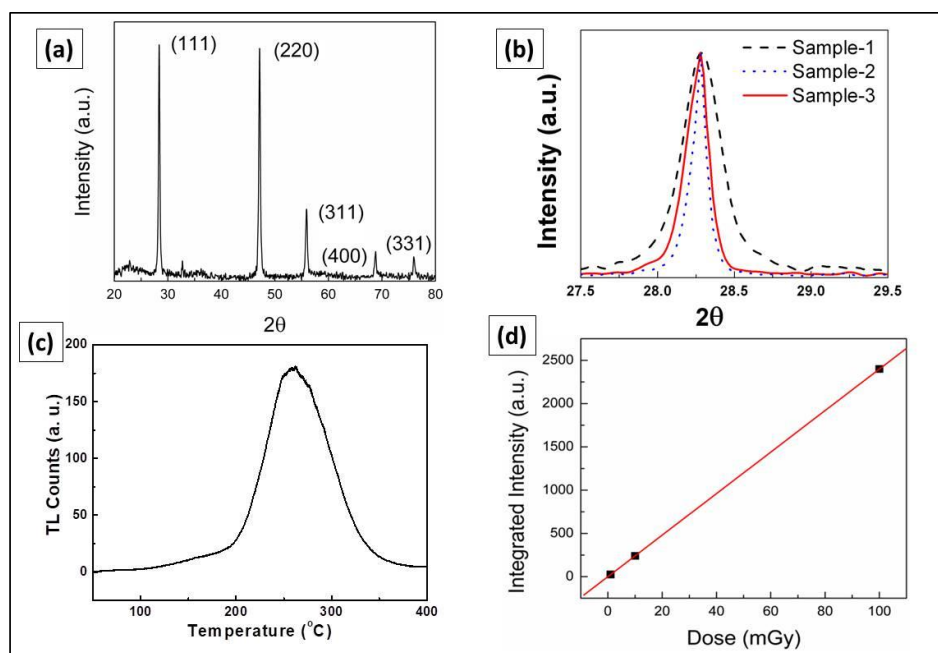


Fig 7. (a) XRD of as synthesized $\text{CaF}_2:\text{Mn}$ nano particles (b) Comparison of (111) XRD peak of cold pressed pellet of CaF_2 (sample 1), vacuum sintered pellet (sample 2) and Hot pressed transparent ceramic of CaF_2 (sample 3), (c) Glow curve of $\text{CaF}_2:\text{Mn}$ OTC after irradiated with a dose of 100 mGy gamma ray, (d) Integrated intensity of $\text{CaF}_2:\text{Mn}$ TL glow curve after irradiation with gamma radiation of different dose.

SEM. The SEM image of the as-prepared powder cold pressed at 5 kg/cm^2 pressure (in the form of 3 mm thick pellets of 25 mm diameter) is shown in Fig 5(b). SEM of the vacuum sintered CaF_2 pellet at 1000°C is shown in Fig 6(c) and Fig 6(d) shows the SEM image of the hot pressed transparent CaF_2 ceramic pellet.

For dosimetric application the ceramic pellet was cut into small pieces of $\sim 10 \text{ mg}$ weight and exposed to ^{60}Co gamma radiation to carry out TL dosimetric studies. After irradiation the dose was measured in a TL unit. The $\text{CaF}_2:\text{Mn}$ pieces were heated to 500°C at a heating rate of 5°C/s . A single glow peak was observed located at 260°C shown in Fig 7(c). The minimum dose that could be measured was about 3 mGy with a linear behaviour up to 100 mGy. These experiments confirmed that transparent

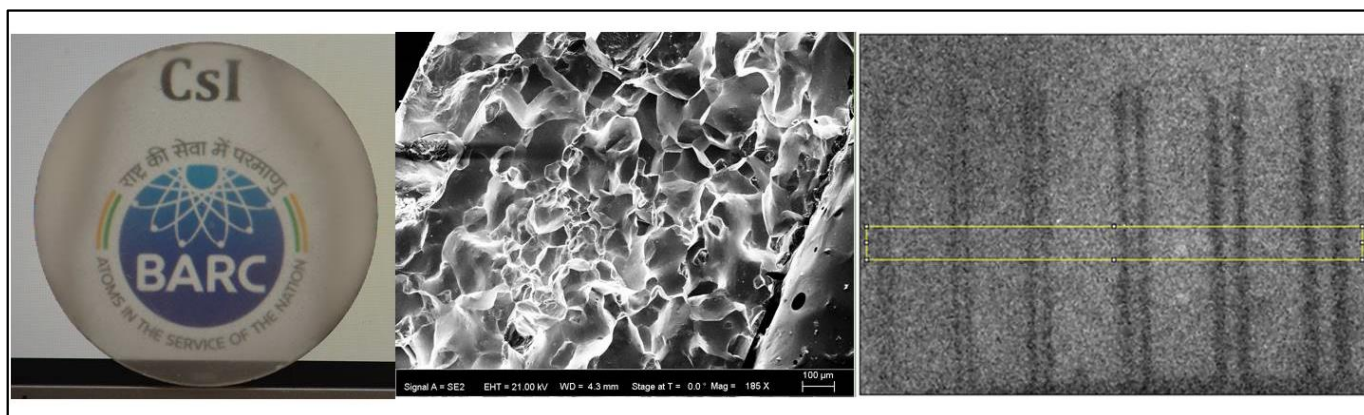


Fig 8. (a) Photograph of transparent ceramic of CsI prepared by Vacuum Hot Press at 300C (b) SEM micrograph of the fractured surface of CsI transparent ceramic showing grain size (c) Duplex type wire pattern image formed by the transparent CsI transparent ceramic and captured using CCD camera

ceramics of $\text{CaF}_2:\text{Mn}$ prepared by vacuum hot pressing can be used for gamma ray detection in the dosimetric mode. This material can be used for the safety of radiation worker as personal dosimeter.

3.2 CSI transparent Ceramics:

CsI:Tl is a conventional scintillators single crystal which has wide application in radiation detection. The thin film of this material has also been widely used in X-ray imaging detectors for medical and industrial applications. But to deposit these thin films on very large area with uniformity is a challenge and requires sophisticated instruments²³. An alternate to these films is the use of transparent ceramics.

To prepare the transparent plate of CsI, 50 g of commercially available CsI powder of 99% purity was taken in a high-density graphite die of ID 75 mm diameter and OD 100 mm. To avoid carbon contamination into CsI pellet during the processing both the face of the graphite punch was covered with aluminium foil. The commercially available CsI powder was initially dehydrated in a quartz crucible at 200°C under rotary vacuum of 10^{-3} mbar to remove all moisture content. It is important to ensure that the loaded powder for hot pressing is moisture free. If there is any moisture left in the powder, during heating cycle the release of moisture from the matrix leads to cracking or formation of voids in the pellet which makes it opaque. The dehydrated powder was then loaded into the graphite die. A Stainless Steel or Mild Steel die can also be used for the formation of transparent ceramics of CsI as the working temperature is very low. Maximum load of 10 ton is applied on the sample using top and bottom graphite RAM. The hot pressing was carried out at a base pressure of $<10^{-5}$ mbar at temperature around 300°C for 4 hrs and the pressure on the CsI powder is ~ 70 MPa. A highly compact translucent disc of CsI was obtained with

40% transmission at 1000nm (Fig 8(a)). The size of the disc is 75 mm and thickness 3 mm. This experiment showcases the advantage of fabrication of transparent ceramic over single crystal. A similar single crystal of CsI of 75 mm diameter can be grown in a minimum time of 15 days and at a process temperature of 700°C or above. On the other hand the transparent ceramic was fabricated in a single day and at a process temperature of 300°C²⁴.

The micro structure of the transparent CsI ceramic was probed using SEM technique. A typical micrograph is shown in Fig 8(b) showing absence of any void, secondary phase or pores. The grain size after hot pressing was around 50 μm . The disc was tested for X-ray imaging. In this experiment the object to be viewed was shined with X-ray. The scintillator plate of CsI was kept after the object and the light generated from the CsI plate was captured using a CCD. For testing a duplex type wire pattern was imaged using this plate. The minimum resolution the scintillator was able to achieve was a duplex wire pattern of 250 micron separation as observed in Fig 8(c). Our experiments proved that this kind of CsI ceramic plates can be used in industrial application for imaging using X-ray or other high energy sources. Further experiments can be carried out to increase light output, transparency and size of the CsI transparent ceramic.

4. Conclusion

Transparent ceramics have advantage over single crystal in terms of synthesis process, mechanical properties like hardness and size. Fabrication of transparent ceramics is a challenging process and utmost care has to be taken to ensure purity of the material. Many techniques are available to make ceramics pellets with minimum pores and voids. These materials have been found promising in many applications including radiation detection.


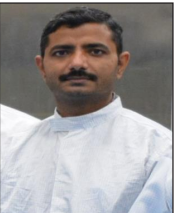



Transparent ceramic of $\text{CaF}_2:\text{Mn}$ has been found a good dosimetric material and transparent ceramic plates of CsI was found to have application in industrial radiography using X rays.

Acknowledgement:

Authors like to acknowledge the contribution of Mr A N Patil, CTS, TPD for the fabrication of CsI transparent ceramic and Mrs. C. More, CTS, TPD for the operation and maintenance of Vacuum Hot Press system.

References:

1. Changshuai Ding, Hanyu Jia, Qingqing Sun, Zhiqiang Yao, Huige Yang, Wentao Liu, Xinchang Pang, Shisheng Li, Chuan Liu, Takeo Minari, Jinzhou Chen, Xuying Liu and Yanlin Song, *J. Mater. Chem. C*, **2021**, 9, 7829–7851.
2. Z. Zhang, X. Xu, L. Qiu, S. Wang, T. Wu, F. Ding, H. Peng and K. Liu, *Adv. Sci.*, **2017**, 4, 1700087.
3. S.F. Wang a, J. Zhang b, D.W. Luo a, F. Gua, D.Y. Tang c, Z.L. Dong a, G.E.B. Tan a, W.X. Que d, T.S. Zhang S. Li e, L.B. Kong, *Progress in Solid State Chemistry*, **2013**, 41, 20.
4. A. Ikesue, T. Kinoshita, K. Kamata, K. Yoshida, *J Am Ceram Soc*, **1995**, 78, 1033–1040.
5. J. Sanghera, W. Kim, G. Villalobos, B. Shaw, C. Baker, J Frantz, *Materials*, **2012**, 5, 258–277.
6. A. Krell, T. Hutzler, J. Klimke, *J Eur Ceram Soc*, **2009**, 29, 207–221.
7. R. Apetz, M. P. B. van Bruggen, *J Am Ceram Soc*, **2003**, 86, 480–486.
8. M. Haruta, B. Delmon, *Journal de Chimie Physique et de Physico-Chimie Biologique*, **1986**, 83, 859–868.
9. S. R. Podowitz, R. Gaume, R. S. Feigelson *Journal of the American Ceramic Society*, **2010**, 93(1), 82.
10. R. L. Coble, *J Appl Phys*, **1970**, 41, 4798–4807.
11. Y. T. Zou, D. W. He, X. K. Wei, R. C. Yu, T. C. Lu, X. H. Chang, *Mater Chem Phys*, **2010**, 123, 529–533.
12. S. R. Podowitz, R. Gaume, R. S. Feigelson, *J Am Ceram Soc*, **2010**, 93, 82–88.
13. F. B. Swinkels, D. S. Wilkinson, E. Arzt, M. F. Ashby, *Acta Metall*, **1983**, 31, 1829–1840.
14. A. C. Sutorik, G. Gilde, J. J. Swab, C. Cooper, R. Gamble, J. Shanholtz, *J Am Ceram Soc*, **2012**, 95, 636–643.
15. J. Mouzon, A. Maitre, L. Frisk, N. Lehto, M. Oden, *J Eur Ceram Soc*, **2009**, 29, 311–316.
16. K. Serivalsatit, J. Ballato *J Am Ceram Soc*, **2010**, 93, 3657–3662.
17. Z. M. Seeley, J. D. Kuntz, N. J. Cherepy, S. A. Payne, *Opt Mater*, **2011**, 3, 1721–1726.
18. R. Chaim, R. Marder, C. Estournes, *Scripta Materialia*, **2010**, 63(2), 211.
19. L. Nadaraian, N. Jalabadze, R. Chedia, L. Khundadze, *Ceramics International*, **2013**, 39, 2207–2214.
20. S.G. Singh, Shashwati Sen, G.D. Patra, S. Bhattacharya, A.K. Singh, Seema Shinde, S.C. Gadkari, *Nuclear Instruments and Methods in Physics Research B*, **2012**, 287, 51–55.
21. W. Kostler, A. Winnacker, W. Rossner, B. C. Grabmaier. *J Phys Chem Solids*, **1995**, 56, 907–913.
22. S. G. Singh, Shashwati Sen, G. D. Patra, S. C. Gadkari, *Journal of Luminescence*, **2015**, 166, 222–226.
23. L. Cosentino, P. Finocchiaro, *IEEE Trans. Nucl. Sci.* **2001**, 48, 1132–1136.
24. Shashwati Sen, P. S. Sarkar, G. D. Patra, S. G. Singh, M. Ghosh, S. Pitale, A. N. Patil, Manoj K. Pal, *Ceramics International*, **2021**, 47, 2187–2193.

	<p>Dr. Shahswati Sen joined BARC in 1996 through 40th batch of training school and currently working at Crystal Technology Section of Technical Physics Division, BARC. She is working on the growth of various single crystals for application in radiation detection. Her research area spans both scintillator material as well as dosimetric materials. Beside single crystals she has also worked on transparent ceramics for dosimetric and radiography application using gamma rays and X-rays respectively.</p>
	<p>Dr. Shiv Govind Singh joined Crystal Technology Section, TPD, and BARC in 2006 after graduating from training school 49th batch. He is working in the field of single crystal growth of oxides, halides and semiconductor materials, their characterization and development of devices for radiation detection. His main research interests are development of technologies for single crystal growth and application and fabrication of ceramics/composites of scintillators for radiation detection.</p>
	<p>Dr. Giri Dhari Patra joined the Technical Physics Division, BARC after graduating from the 53th Batch of BARC Training School. He obtained his doctorate from HBNI, Mumbai. He is currently working on the growth of single crystal of halides, oxides and semiconductor materials and subsequent fabrication of radiation detectors. His research interests are single crystals growth, luminescence/scintillation studies of advanced scintillators and development of novel inorganic radiation detectors for various applications.</p>
	<p>Dr Pitale joined BARC as a Scientific officer in the year 2012 and currently working in the Crystal Technology Laboratory of Technical Physics Division, BARC. Prior to this, he was working as a Postdoctoral researcher at University of the Free State, South Africa and as a K.S. Krishnan Research Associate at this center. He is currently working on fabrication of high purity germanium detectors. His active interests also include synthesis of luminescent materials through various chemical routes.</p>
	<p>Dr. Manoranjan Ghosh joined BARC in 2010 as KSKRA after completion of his PhD from S. N. Bose National Centre for Basic Science on Optical properties of semiconductor nanomaterials. In the initial years he studied structural and gas sensing properties of wide band gap semiconductor nanomaterials. He is currently working in the Crystal Technology Laboratory of Technical Physics Division, BAR. He is involved in the development of High Purity Germanium Detector and interested on growth and measurement of electrical properties of semiconductor single crystals.</p>

Influence of Gd³⁺ doping on the structural and luminescence properties of SrSnO₃ nano-rods

Dinesh K. Patel^{1,3}, B. Rajeswari², R. M. Kadam² and V. Sudarsan^{1*},

¹Chemistry Division, ²Radio Chemistry Division, Bhabha Atomic Research Centre, Trombay, Mumbai 400085, India

³Human Computer Interaction Institute, Carnegie Mellon University, Pittsburgh, 15213, USA.

E-mail: vsudar@barc.gov.in

Abstract

SrSnO₃ nano-rods doped with Gd³⁺ ions were prepared by thermal decomposition of Gd³⁺ doped SrSn(OH)₆ nano-rods at 700°C. Based on the Rietveld refinement of XRD patterns, it is confirmed that, with incorporation of Gd³⁺ ions up to 4 at % in SrSnO₃ lattice. There are compensating changes in the different Sr-O bond lengths of SrO₁₂ polyhedron, leading to average Sr-O bond length remaining same. Unlike this the average Sn-O bond length systematically decreases with increase in Gd³⁺ concentration. The observed variation in the behaviour of Sr-O and Sn-O bonds can be explained based on the difference in the percentage ionic characters of Sr-O and Sn-O bonds. Above 4 at %, there is formation of Gd₂Sn₂O₇ phase as confirmed by XRD studies. Based on detailed line shape analysis of EPR spectra corresponding to these samples, it is confirmed that, Gd³⁺ ions occupy Sr²⁺ site in the lattice and there is significant distortion in the environment around Gd³⁺ ions, brought about by the cation vacancies generated due to alio-valent substitution. Luminescence observed in the visible region (~490 nm) from these samples has been attributed to the recombination of self trapped excitons which is not affected by Gd³⁺ doping in the lattice.

Introduction:

Alkaline earth stannates (MSnO₃) with perovskite structure have gained substantial importance due to their remarkable electronic and optical properties.¹⁻³ Compounds like SrSnO₃, MgSnO₃, CaSnO₃ and BaSnO₃ belongs to this category and have been extensively investigated for their optical properties.⁴⁻⁷ Many of these hosts are inherently luminescent in the visible region when excited with UV light. For example cubic BaSnO₃ samples give host luminescence around 430 nm⁸ whereas tetragonal and orthorhombic forms of SrSnO₃ give emission around 490 and 425 nm respectively.^{9,10} Emission from the SrSnO₃ lattice is quite sensitive to temperature and it is observed that visible emission from orthorhombic and tetragonal forms of SrSnO₃ lattices is of reasonable intensity only at liquid nitrogen temperatures.^{9,10} From the above studies it is clear that the emission in the visible region from such samples is arising from the recombination self trapped excitons. Doping lanthanide ions (Ln) in these host lattices is an attractive option for making efficient luminescent materials and numbers of reports are available for such materials.¹¹⁻¹⁵ Among the different MSnO₃ hosts/nanomaterials doped with lanthanide ions, CaSnO₃:Ln and SrSnO₃:Ln have got enhanced luminescence properties compared to BaSnO₃:Ln samples.^{11,12} The reason, for weak emission from BaSnO₃:Ln³⁺ sample, is due to its cubic nature and symmetric crystal field around Ba²⁺/Ln³⁺

ions. CaSnO₃:Ln and SrSnO₃:Ln samples have enhanced emission due to orthorhombic structure.

Our group has previously carried out detailed structural and luminescence investigations on SrSnO₃ nanomaterials doped with europium ions.^{9,16} Based on these studies it is established that up to 2 at % Eu³⁺ ions, SrSnO₃ lattice is unaffected, as revealed by the compensating changes in the different Sr-O bond lengths leading to lattice parameters remaining unaffected. In the same study it was also observed that part of the Eu³⁺ ions exists as Eu²⁺ species which can significantly affect the luminescence and solubility limits of Eu³⁺ ions. Hence results obtained on Eu³⁺ doped samples can not be extended to other lanthanide ions like La³⁺, Gd³⁺, etc., which do not change its oxidation states. Further it is also interesting to understand the effect of lanthanide ions doping on the host luminescence from the above stannates. Keeping this in mind, in the present study, another representative lanthanide ion like Gd³⁺, which exists only in +3 oxidation state under the experimental conditions has been chosen as a dopant in SrSnO₃ and detailed structural and luminescence investigations have been carried out at variable temperatures. As Gd³⁺ is paramagnetic in nature, electron paramagnetic resonance (EPR) technique can be very effectively used to find out its environment. The present studies also address the role of partial ionic character of Sr-O and Sn-O bonds, on the nature of SrO₁₂

and SnO_6 polyhedra in SrSnO_3 lattices. Such studies are quite relevant for understanding the structural changes associated with lanthanide ions doping in technologically important perovskite materials.

Experimental

Preparation of SrSnO_3 and Gd^{3+} doped SrSnO_3 ($\text{SrSnO}_3:\text{Gd}$)

Around 0.41g of $\text{SrCl}_2 \cdot 6\text{H}_2\text{O}$ was dissolved in 10 ml distilled water and to this solution 5ml of aqueous solution containing around 0.3g of sodium stannate was added drop wise while stirring. The precipitate obtained was washed twice with methanol followed by acetone and dried under ambient conditions. The resulting hydroxide ($\text{SrSn}(\text{OH})_6$)¹⁷ was heated to 700°C for 5 hrs to obtain SrSnO_3 phase. Similar procedure was used for preparing Gd^{3+} doped SrSnO_3 samples except that the required amount of $(\text{CH}_3\text{COO})_3\text{Gd} \cdot x\text{H}_2\text{O}$ was added to the solution containing Sr^{2+} ions prior to the addition of Na_2SnO_3 .

Characterization

X-ray diffraction (XRD) studies were carried out using a Philips powder X-ray diffractometer (model PW 1071) with Ni filtered Cu-K α radiation. The lattice parameters were obtained from the Rietveld refinement of the XRD patterns using the GSAS software.¹⁸ For account of Gd doping in the refinement of XRD patterns of Gd doped samples, it is assumed that Gd is in the Sr site of SrSnO_3 lattice. Cosine Fourier series function has been chosen for background shape and Type-2 function of GSAS software has been chosen for peak profile during refinement. All steady state luminescence and lifetime measurements were carried out by using an Edinburgh Instruments FLSP 920 system, having 450W Xe lamp and micro second flash lamps as excitation sources. Around 20 mg sample was mixed with 1 ml methanol, made into a slurry and spread over a glass plate and dried under ambient conditions and the same is used for luminescence measurements. All emission spectra were corrected for the detector response and all excitation spectra for the lamp profile. All emission measurements were carried out with a resolution of 5 nm. The EPR spectra were recorded on a Bruker ESP-300 spectrometer operating at X-band frequency (9.5 GHz) equipped with 100 kHz field modulation and phase sensitive detection to obtain the first derivative signal. Diphenyl picrylhydrazyl (DPPH) was used for the calibration of g-values of paramagnetic species. The EPR parameters have been precisely determined from the calculated spectra, obtained by using BRUKER SIMFONIA program. The simulations were carried out assuming mixed line shape (Lorentzian / Gaussian = 0.5) with a peak to peak line width of 0.01 T.

Results and discussion

Representative SEM image of the as prepared sample after heat treatment at 700°C is shown in Fig. 1. The image consists of nano-rods having length around 2-2.5 μm and width less than 100 nm. Energy dispersive X-ray analysis (EDXA) performed on the sample (not shown) confirmed the presence of both Sr and Sn ions in the desired ratio.

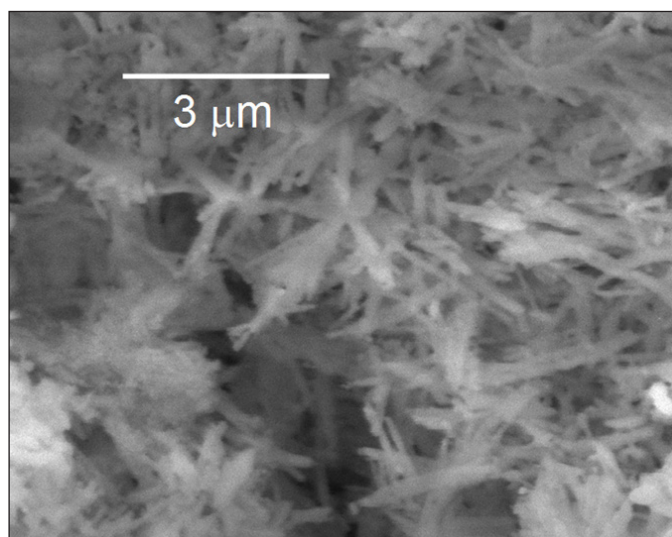


Figure 1. Representative SEM image of SrSnO_3 sample.

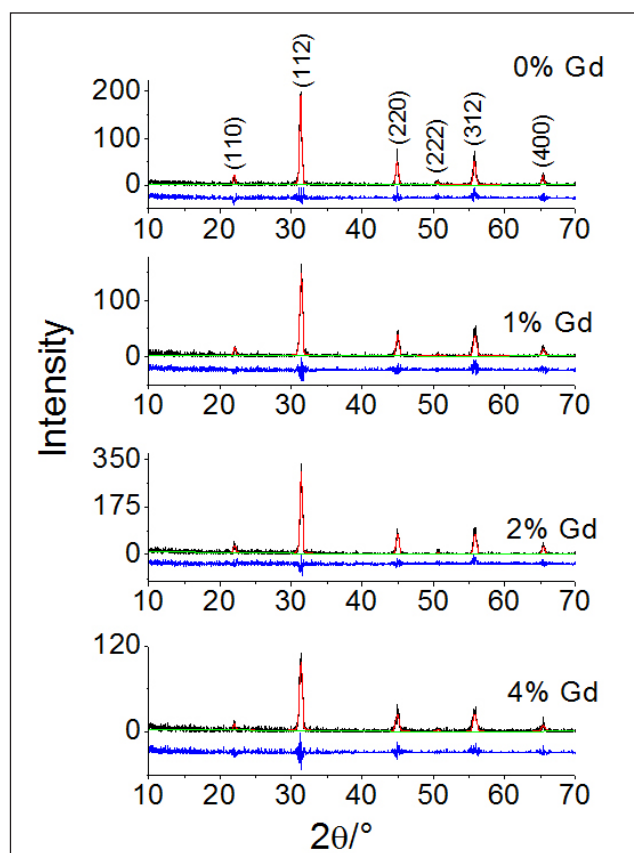


Figure 2. XRD patterns of SrSnO_3 nano-rods containing different amounts of Gd^{3+} ions

Figure 2 shows the XRD patterns of SrSnO₃ samples doped with different amounts of Gd³⁺ ions. Beyond 4 at % Gd³⁺ doping, there is separate phase of Gd₂Sn₂O₇ as can be seen from the XRD pattern corresponding to 6 at % Gd³⁺ doped sample is shown in Fig. 3.

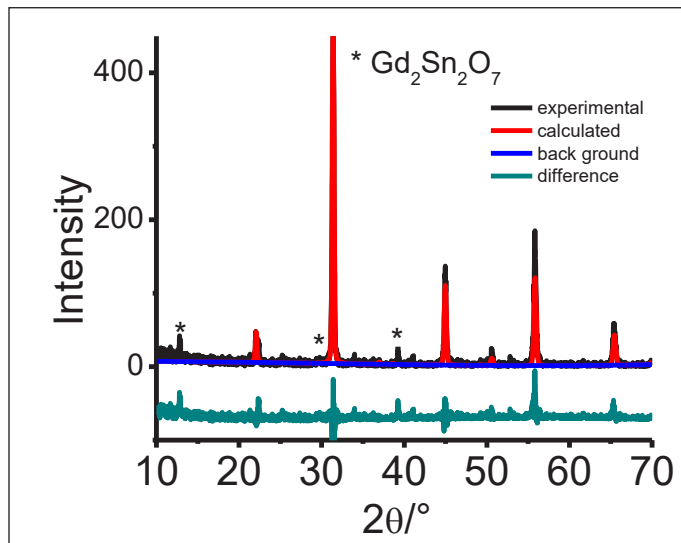


Figure 2. XRD pattern of SrSnO₃ nano-rods doped with 6 at % Gd³⁺ ions

Undoped SrSnO₃ is known to exist in hettotype and aristotype phases depending up on the temperature at which it is annealed. Generally, hettotype phase is observed for SrSnO₃ sample annealed at temperatures less than 900°C and aristotype phase is observed for samples annealed at

Table 1. The values of lattice parameters and unit cell volumes of SrSnO₃ samples containing different amounts of Gd³⁺

SrSnO ₃	a (Å)	b (Å)	c (Å)	Volume (Å ³)
0% Gd	5.704(2)	5.704(2)	8.066(6)	262.48
1% Gd	5.706(5)	5.706(5)	8.062(6)	262.55
2 % Gd	5.712(1)	5.712(1)	8.046(3)	262.54
4% Gd	5.715(5)	5.715(5)	8.036(5)	262.52

Table 2. Bond length values of different Sr-O and Sn-O bonds in SrSnO₃ lattice containing different amounts of Gd³⁺ ions

SrSnO ₃	Sr-O1 (Å)	Sr-O2 (Å)	Sr-O3 (Å)	Sr-O _{avg} (Å)	Sn-O1 (Two bonds)	Sn-O2 (four bonds)	Sn-O _{avg} (Å)
0% Gd	2.8521(4)	2.7143(3)	2.9969(4)	2.8544(3)	2.0166(2)	2.0267(2)	2.0216(2)
1% Gd	2.8533(3)	2.7140(1)	2.9968(2)	2.8547(1)	2.0156(1)	2.0275(1)	2.0215(1)
2 % Gd	2.8561(3)	2.7122(2)	2.9957(3)	2.8546(1)	2.0120(1)	2.0294(2)	2.0207(1)
4% Gd	2.8580(4)	2.7114(4)	2.9954(4)	2.8546(2)	2.0090(3)	2.0306(2)	2.0198(2)

900°C and above. Glerup et al.¹⁹, have carried out detailed investigations on different forms of SrSnO₃ phases based on the Rietveld refinement of the XRD patterns. From these studies it is inferred that SrSnO₃ samples heated at 300, 700 and 900°C, correspond to the space groups Pm₃n, Incn and I4/mcm respectively. The first two space groups are characteristic of the orthorhombic form of SrSnO₃ and the third one corresponds to body centered tetragonal form of SrSnO₃. In the present study Rietveld refinement was attempted for the XRD pattern of SrSnO₃ with all the three above mentioned space groups. It is observed that acceptable quality refinement was observed only when the space group chosen was I4/mcm, which corresponds to tetragonal form of SrSnO₃. Lattice parameters along with unit cell volumes obtained from the refinement of the XRD patterns are shown in Table 1. Unit cell volumes are found to be unaffected by Gd³⁺ doping in SrSnO₃ lattice.

Based on the position coordinates obtained from the Rietveld refinement of the XRD pattern, the SrO₁₂ and SnO₆ polyhedra were constructed and are shown in Fig. 4 (a and b). The SrO₁₂ polyhedron (Fig. 4(a)) is characterized by three different types of Sr-O bond lengths namely the medium (Sr-O1), shorter (Sr-O2) and the longer (Sr-O3) whereas the SnO₆ polyhedron (Fig. 4(b)) is characterized by two shorter and four longer axial and equatorial Sn-O bonds respectively. The different bond length values are shown in Table 2.

With increase in Gd³⁺ concentration, medium Sr-O1 bond length increases systematically whereas shorter Sr-O2 bond length decreases (beyond 1 at % doping). The longer Sr-O3 bond lengths and average Sr-O bond lengths are not affected by Gd³⁺ doping (within error limits). In the case of Sn-O bond lengths, with increase in Gd³⁺ concentration, axial Sn-O bond (Sn-O1) decreases its length and the equatorial Sn-O bond (Sn-O2) increase its length. The average Sn-O bond lengths decrease with increase in Gd³⁺ doping concentrations (Table 2). Observed difference in the variation of average Sr-O and Sn-O bond lengths can be explained based on the difference in the percentage

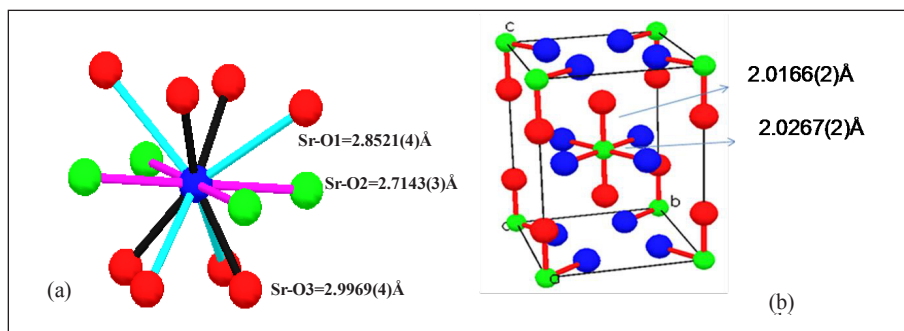


Figure 4. Schematic representation of (a) SrO_{12} and (b) SnO_6 polyhedron present in undoped $SrSnO_3$ nano-rods. Three different Sr-O and two different Sn-O bond length values obtained from Rietveld refinement are also shown in the figure. The colour codes in Fig. 4(a) are Sr atom: blue, O1 and O3 atoms: red and O2 atoms: green. Four equidistant and shorter Sr-O2 bonds are shown in magenta colour, four medium length Sr-O1 bonds in cyan colour and the larger Sr-O3 bonds in black colour. The corresponding codes in Fig. 4(b) are: Sn atom: green, O atoms at longer distance from Sn: blue and O atoms at shorter distance from Sn: red.

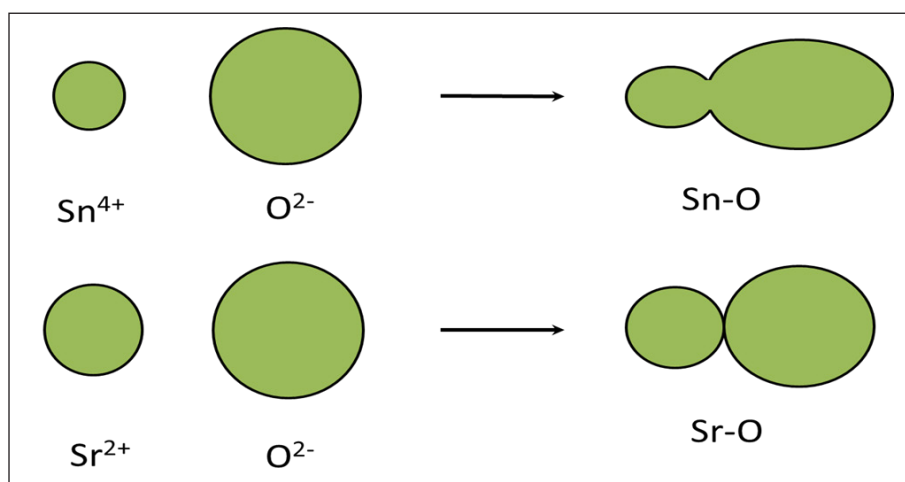


Figure 5. Schematic representation of difference in the partial ionic (partial covalent) nature of Sr-O and Sn-O bonds

ionic characters of Sr-O and Sn-O bonds. Percentage ionic character of a bond can be calculated based on the Pauling's equation (equation 1)²⁰,

$$\text{Percentage ionic character} = 1 - e^{-0.25(\chi_A - \chi_B)} \dots \dots \dots (1)$$

Where χ_A and χ_B represent electro-negativity values for oxygen and metal cation respectively. The values of percentage ionic character of Sr-O, Sn-O and Gd-O bonds have been calculated based on the above equation and found to be approximately 42, 31 and 46% respectively. In other words covalent character is more with Sn-O bonds compared to Sr-O and Gd-O bonds. As the ionic radius of Sn^{4+} (0.69 Å) is significantly smaller compared to Sr^{2+} (1.44Å) or Gd^{3+} (1.1Å),²¹ extent of polarisability of electron cloud of oxygen ions brought about by Sn^{4+} is more compared to Sr^{2+} or Gd^{3+} in the corresponding Sn-O, Gd-O and Sr-O bonds as can be seen from Fig. 5.

This leads to higher extent of orbital overlapping between Sn^{4+} and oxide ions and thereby increasing the covalent nature of the Sn-O bonds compared to Sr-O/Gd-O bonds. In other words Sr-O and Gd-O bonds are more ionic and columbic forces (non-directional) are the major force of interaction between cations and anions. Unlike this covalent interactions, which are more directional in nature, are predominant with Sn-O bonds. Hence with Gd^{3+} doping in $SrSnO_3$ lattice, SrO_{12} polyhedra get itself adjusted (due to the ionic nature of Sr-O bonds) keeping the average Sr-O bond length same.

Due to the directional nature of Sn-O bonds, such an adjustment is not that effective with SnO_6 polyhedra. As the extent of polarization on oxide ion by Gd^{3+} is more than that made by Sr^{2+} on oxide ions, average Sn-O bond length is expected to decrease as Gd replaces Sr in the $SrSnO_3$ lattice and this is in conformity with the variation in average Sn-O bond length values observed in Table 2. Further the unit cell volume remains same with increase in Gd^{3+} concentration as can be seen from Table 1. It is quite interesting to see that even though the ionic radius of Gd^{3+} (1.1Å under a coordination number of 9) is much smaller than Sr^{2+} (1.44Å under 12 coordination)²¹, the unit cell

volume is found to be same for $SrSnO_3$ samples containing different Gd^{3+} concentration. This can be explained based on the improved covalent character of Gd-O linkages compared to Sr-O linkages. It is worth mentioning here that in related study dealing with $Ga_{1-x}Al_xPO_4$ samples, the lattice parameter has been found to increase as smaller ionic radii Al^{3+} replaces larger ionic radius Ga^{3+} in the lattice.²² Increased covalent character of Al-O bond compared to Ga-O bond has been attributed as the reason for this.²² A similar explanation is also valid here. In order to further confirm that Gd^{3+} ions are occupying Sr^{2+} site in $SrSnO_3$ lattice EPR studies have been carried out on the samples and are discussed in the following section.

Figure 6(a) shows the representative X-band EPR spectrum of $SrSnO_3$ sample containing 2 at % gadolinium ions measured at 100K. It can be seen that resonance occurs over a wide range of magnetic field namely

0-0.7T. The pattern consists of an intense signal at 0.348 T corresponding to a “g” value of 1.98 and six weak shoulders symmetrically placed with respect to the intense signal. The relative intensity of the shoulders decreases as they move away from the central line. The spacing between the shoulders is quite large which is about 25 times larger than the reported hyperfine coupling constants for gadolinium. Therefore the respective shoulders are assigned to the zero field splitting and not due to hyperfine splitting of Gd³⁺ species. The observed zero field splitting is attributed to electron-electron dipole interaction due to electron spin quantum number 7/2 in non cubic sites. The energies after taking into account the second order interactions can be expressed as equation 2²³

$$M(M_s) = GM_s + 1/2[M_s^2 - 1/3S(S+1)]\{D[3\cos^2\theta - 1] + 3E\sin^2\theta\cos 2\varphi\} + 2M_s\{2M_s^2 + 1/4 - S(S+1)\}\{(D - E\cos 2\varphi)^2\sin^2\theta\cos^2\theta + (E\sin 2\varphi)^2\sin^2\theta\}/G_0 + M_s\{2S(S+1) - 2M_s^2 - 1\}\{D\sin^2\theta + E\cos 2\varphi(1 + \cos^2\theta)^2 + 4(E\cos\theta\sin 2\varphi)^2\}/8G_0 \dots\dots\dots(2)$$

Where G and G₀ correspond to gβH and hν₀, where β is the Bohr magneton, H is the applied magnetic field, h is Planck’s constant and ν₀ is the microwave frequency. M_s is the spin magnetic quantum number, D and E are axial and rhombic zero field splitting parameters, respectively. The symbols θ and φ represent Euler angles. Simulated EPR spectrum was obtained by using Spin Hamiltonian parameters for Gd³⁺ (S=7/2), g = 1.98, D = 270 G, E = 90 G, E/D~1/3 and the values are listed in Table 3 along with data reported for Gd³⁺ in other matrices. Simulated pattern matches well with that of experimentally observed (Fig. 6(b)), establishing the zero field splitting of the Gd³⁺ spins in a 12 coordinated low symmetric environment. Similar EPR spectrum was observed for 1 at % Gd³⁺ doped samples. However for more than 2 at % Gd³⁺ doped sample, significant broadening occurred as can be seen from EPR spectrum of 6 and 8 at % Gd³⁺ doped sample shown in Fig. 6 (c and d)

Based on EPR studies it is confirmed that Gd³⁺ ions occupy the Sr²⁺ site in the SrSnO₃ lattice. The well resolved EPR spectra consisting of a central intense peak along with six symmetrically placed shoulders (distortion parameter, λ=E/D~0.3) suggests that in Gd³⁺ doped SrSnO₃, Gd³⁺ ion is located at a low symmetry site. It may be noted that low symmetry of Eu²⁺ and Gd³⁺ ions in alkaline earth aluminates hosts has been investigated by using high frequency EPR technique.²⁴⁻²⁶ Compared to the host lattice, the environment around Gd³⁺ ions gets further distorted due to the difference in their ionic radii (Gd³⁺(1.1Å) and Sr²⁺ (1.44Å))²¹. When higher concentration of Gd³⁺ ions is substituted at Sr²⁺ sites, then the extra positive charges are to be compensated by the presence of Sr²⁺ vacancies. This

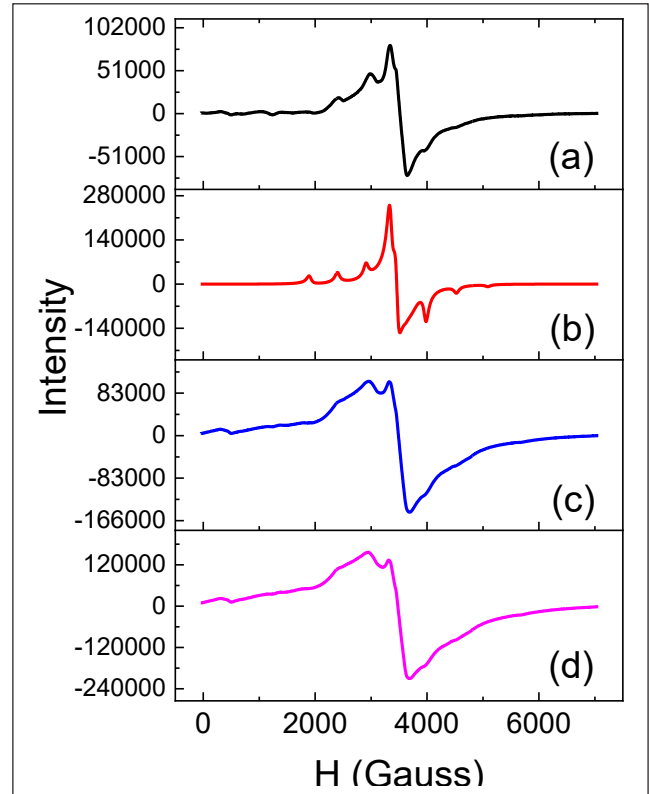


Figure 6. EPR spectrum at 100 K for SrSnO₃ nano-rods containing (a) 2 at % Gd³⁺ ions. Corresponding simulated spectrum is shown in Fig. 6 (b). Parameters used for simulation are Gd³⁺, S=7/2, g = 1.98, D = 270 G, E = 90 G, E/D~1/3. Line shape parameters used are L/G=0, line widths Δ_{x,y}=60 G; Δ_z=250 G. EPR patterns corresponding to 6 and 8 at. % Gd³⁺ doped samples are given in Fig. 6 (c and d)

mechanism of charge compensation leads to lowering of the symmetry around Gd³⁺ ions. Generally, it is expected that distortion in local environments in lattices can influence their luminescence characteristics. To check this aspect both steady state and lifetime measurements were carried out on the samples and are described below.

No emission characteristic of Gd³⁺ has been observed from these samples even after exciting the sample over wavelength values upto 200 nm. Further, at room temperature no emission was observed from undoped SrSnO₃ upon UV excitation. However after cooling to liquid nitrogen temperatures, strong emission is observed from the sample with a maximum around 490 nm as can be seen from Fig. 7. Corresponding excitation spectrum showed a peak maximum around 280 nm. Significant Stokes shift in the excitation and emission maximum confirms that the emission is arising due to the recombination of self trapped excitons (STE). Similar STE recombination has been observed for the orthorhombic form of SrSnO₃ by Zhang et al. [10]. However, the emission maximum

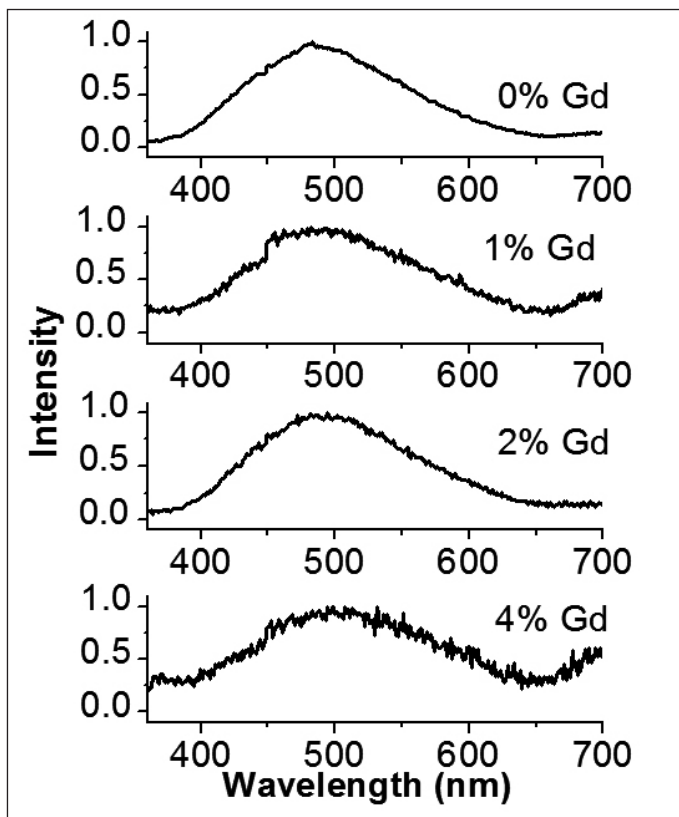


Figure 7. Emission spectra at 77K from SrSnO₃ nano-rods doped with 0, 1, 2 and 4 at% Gd³⁺ ions. Excitation wavelength was 283 nm.

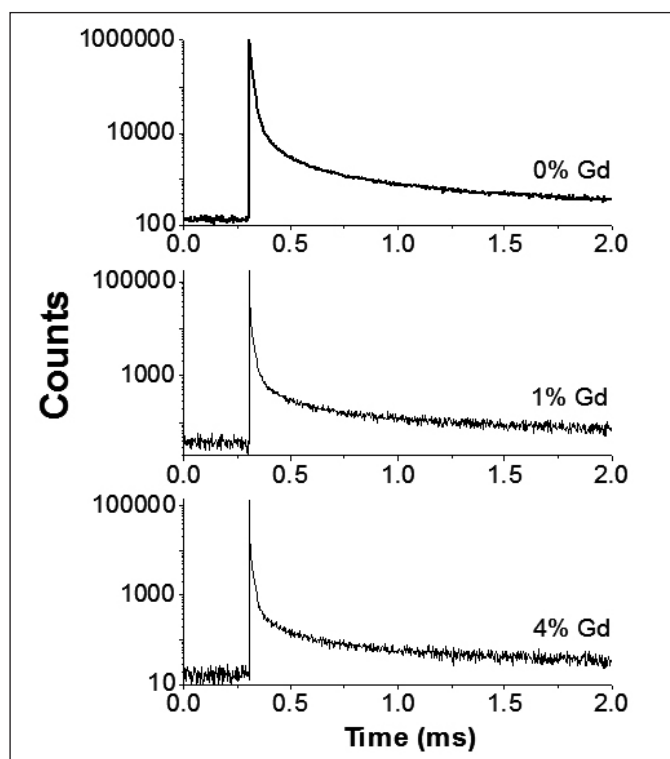


Figure 8. Decay curves corresponding to visible emission from SrSnO₃ nano-rods doped with 0, 1 and 4 at% Gd³⁺ ion recorded at 77K. Excitation and emission wavelengths are 283 and 492 nm respectively.

Table 3. EPR parameters obtained at X band frequency in SrSnO₃:Gd³⁺ and that reported previously in SrSnO₃:Eu²⁺, BaSnO₃:Eu²⁺ matrices and at W band frequency in SrAl₂O₄:Gd³⁺ and SrAl₂O₄:Eu²⁺ matrices

	g- value	D (cm ⁻¹)	E (cm ⁻¹)	I	A (cm ⁻¹)
^a SrSnO ₃ :Eu ²⁺	1.9600	0.0435	0.0150	1/3	----
^a SrSnO ₃ :Gd ³⁺	1.9800	0.0270	0.0090	1/3	----
^b BaSnO ₃ :Eu ²⁺	1.9600	----	----	----	0.0030 (¹⁵¹ Eu)
					0.0015 (¹⁵³ Eu)
^c SrAl ₂ O ₄ :Gd ³⁺					
Site I	1.986	0.138		1/3	----
Site II	1.986	0.091		1/3	----
^c SrAl ₂ O ₄ :Eu ²⁺					
Site I	1.989	0.140		0.258	----
Site II	1.989	0.112		0.306	----

a, b, c and d are references with numbers 8, 9, 24 and 26 respectively in the reference list

* Current study

Table 4. The lifetime values corresponding to visible emission from SrSnO₃ nano-rods containing different amounts of Gd³⁺ ions

SrSnO ₃	τ ₁ (μs)	τ ₂ (μs)	τ ₃ (μs)	τ ₄ (μs)	τ _{avg.} (μs)
0% Gd	4.04 (28.57%)	11.49 (52.07%)	58.94 (10.53%)	358.95 (8.81%)	44.97
1% Gd	3.61 (39.65%)	17.07 (35.76%)	243.71 (24.59%)	-	67.46
4% Gd	3.26 (34.89)	14.90 (40.55%)	238.95 (24.56%)	-	65.86

is found to be around 425 nm in their studies. In the present study emission maximum is around 490 nm and this difference in emission maximum can be attributed to difference in structure of the two forms of SrSnO₃. With increase in Gd³⁺ concentration in the lattice, the emission spectrum is found to remain unaffected as can be seen from Fig. 7. Decay curves corresponding to this emission from different samples are shown in Fig. 8. The decay is found to be multi exponential. The individual lifetime components along with the average lifetime values are shown in Table 4. The values are found to be same (within error limits) for different samples. This is because the energy levels corresponding to excitonic emission and absorption do

not match with that of different 4f levels of Gd³⁺ species. Due to this there is no energy transfer between host SrSnO₃ and Gd³⁺ ions.

From the XRD and EPR studies it is confirmed that Gd³⁺ up to 4 at %, occupies Sr²⁺ site in the SrSnO₃ lattice. The environment around Gd³⁺ is significantly distorted as revealed by the distortion parameter obtained from the simulation of the EPR spectrum. There is no interaction between self trapped excitons and Gd³⁺ ions in these samples as revealed by the steady state emission spectrum and the lifetime of the self trapped excitonic states.

Conclusions

Based on XRD and EPR studies it is confirmed that Gd³⁺ occupies Sr²⁺ site in SrSnO₃ lattice up to 4 at% and beyond which Gd₂Sn₂O₇ phase is formed. Lattice parameters and unit cell volumes of SrSnO₃ nano-rods are not affected by Gd³⁺ doping in the lattice and this has been explained based on the different extent of partial ionic character of Sr-O, Gd-O and Sn-O bonds in SrSnO₃ lattice. Both undoped and Gd³⁺ doped samples show luminescence in the visible region at low temperatures due to recombination of self trapped excitons in tetragonal SrSnO₃ lattice and this is unaffected by Gd³⁺ concentration in the lattice.

References

1. T. Ishihara, K. Kometani, M. Hashida, Y. Takita, *J. Electrochem. Soc.* **1991**, *138*, 173- 176.
2. A.M. Azad, L.L. W. Shyan, P.T. Yen, N.C. Hon, *Ceram. Int.*, **2000**, *26*, 685-692.
3. U. Lumpe, J. Gerblinger, H. Meixner, *Sens. Actuators B*, **1995**, *26&27*, 97-98.
4. J. Bohnemann, R. Libanori, M. L. Moreira, E. Longo, *J. Chem. Eng.*, **2009**, *155*, 905-909.
5. W. Zhang, J. Tang, J. Ye, *J. Mater. Res.*, **2007**, *22*, 1859-1871.
6. S. Omeiri, B. Hadjarab, A. Bouguelia, M. Trari, *J. Alloys Compds.*, **2010**, *505*, 592-597.
7. B. Lei, Bin Li, H. Zhang, L. Zhang, Y. Cong, W. Li, *J. Electrochem. Soc.*, **2007**, *154*, H623-H630.
8. D. K. Patel, A. Sengupta, B. Vishwanadh, V. Sudarsan, R. K. Vatsa, R. M. Kadam, S. K. Kulshreshtha, *Eur. J. Inorg. Chem.*, **2012**, 1609-1619.
9. D.K. Patel, B. Rajeswari, V. Sudarsan, R.K. Vatsa, R.M. Kadam, S.K. Kulshreshtha, *Dalton Trans.*, **2012**, *41*, 12023-12030.
10. W.F. Zhang, J. Tang, J. Ye, *Chem. Phys. Lett.*, **2006**, *418*, 174-178.
11. Z. Lu, L. Chen, Y. Tang, Y. Li, *J. Alloys Compd.*, **2005**, *387*, L1-L4.
12. X. Pang, Y. Zhang, L. Ding, Z. Su, W. F. Zhang, *J. Nanosci. Nanotechnol.*, **2010**, *10*, 1860-1864.
13. S. Wang, M. Lu, G. Zhou, H. Zhang, Z. Yang, *J. Alloys Compd.*, **2008**, *452*, 432-434.
14. K. Ueda, T. Yamashita, K. Nakayashiki, K. Goto, T. Maeda, K. Furui, K. Ozaki, Y. Nakachi, S. Nakamura, M. Fujisawa, T. Miyazaki, *Jpn. J. Appl. Phys.*, **2006**, *45*, 6981-6983.
15. D. K. Patel, B. Vishwanadh, V. Sudarsan, and S K. Kulshreshtha, *J. Am. Ceram. Soc.*, **2013**, *96*, 3857-3861.
16. S. Basu, D. K. Patel, J. Nuwad, V. Sudarsan, S. N. Jha, D. Bhattacharyya, R. K. Vatsa, S. K. Kulshreshtha, *Chem. Phys. Lett.*, **2013**, *561&562*, 82-86.
17. D. K. Patel, J. Nuwad, B. Rajeswari, B. Vishwanadh, V. Sudarsan, R. K. Vatsa, R. M. Kadam, C. G. S. Pillai, S. K. Kulshreshtha. *Mater. Res. Bull.*, **2013**, *48*, 566-573.
18. A.C. Larson, R.B. Von Dreele, Report No. LAUR 86-748, Los Alamos National Laboratory, **2004**.
19. M. Glerup, K.S. Knight, F. W. Poulsen, *Mater. Res. Bull.*, **2005**, *40*, 507-520.
20. B.R. Puri, L.R. Sharma, K.C. Kalia, Principles of Inorganic Chemistry, Shoban Lal Nagin Chand & Co, Jalandhar, India, **1998**, p114.
21. R. D. Shanon, *Acta Cryst. A*, **1976**, *32*, 751-767.
22. S.K. Kulshreshtha, O.D. Jayakumar, V. Sudarsan, *J. Solid State Chem.*, **2010**, *183*, 1071-1074
23. J.R. Pilbrow, in Transition Ion Electron Paramagnetic Resonance, Clarendon Press, Oxford, **1990**.
24. T. Nakamura, K. Kaiya, N. Takahashi, T. Matsuzawa, M. Ohta, C.C. Rowlands, G.M. Smith, P.C. Riedi, *Phys. Chem. Chem. Phys.*, **2001**, *3*, 1721-1723.
25. T. Nakamura, K. Kaiya, N. Takahashi, T. Matsuzawa, C.C. Rowlands, V. Beltran-Lopez, G.M. Smith, P. C. Riedi, *J. Mater. Chem.*, **2000**, *10*, 2566-2569.
26. T. Nakamura, T. Matsuzawa, C. C. Rowlands, V. Beltran-Lopez, G.M. Smith, P.C. Riedi, *J. Chem. Soc. Faraday Trans.* **1998**, *94*, 3009-3012.

	<p>Dinesh K. Patel received his B.S. and M. S. degrees in Chemistry from University of Mumbai, India. He received a Ph.D. degree in Chemistry from the Bhabha Atomic Research Centre-University of Mumbai, India in 2014. Currently, he is a Postdoctoral Researcher at Carnegie Mellon University. Prior joining to Carnegie Mellon, he worked as Postdoctoral Fellow at The Hebrew University of Jerusalem, Israel (2014-2018). He has co-authored over 30 refereed journal and conference publications along with 1 book chapter. His research interests are functional 3D printing at micron and mm-scale, soft robotics, actuators, printed electronics, and mechano-luminescent devices.</p>
	<p>B. Rajeswari did his B. Sc in Chemistry discipline from Mumbai University and joined Radio Chemistry Division of BARC in the year 1985 as a Scientific Assistant. She obtained her M. Sc degree in Chemistry by Research from Mumbai University and presently working as a Senior Scientific Officer in the Actinide Spectroscopy section. Her field of work mainly involves Analytical Spectroscopic techniques for trace metallic assay of nuclear materials while on the basic research front, she has carried out synthesis of lanthanide doped inorganic compounds for their characterisation using different spectroscopic techniques. She has published about 50 research papers in peer reviewed journals. She is a recipient of Department of Atomic Energy (DAE) Group Achievement Award (2010 and 2017).</p>
	<p>R.M. Kadam obtained his M. Sc degree in Chemistry discipline from Mumbai University and joined Radiochemistry Division of BARC in the year 1984 after graduating from 27th batch of BARC Training School. He received his Ph. D degree in Chemistry from Mumbai University and subsequently worked as a post-doctoral fellow at the at Linköping Universitet, Linköping, Sweden, in the area of ENDOR and pulsed EPR studies to investigate weaker hyperfine interaction specially in aromatic radical cations. He has extensively worked on Electron Paramagnetic Resonance (EPR) spectroscopy at X band frequency for characterization of structure of radiation induced defects, EPR dosimetry, structural phase transition in solids, EPR of transition metal complexes, ferromagnetism in nano materials, superconductivity, EPR and Thermally Stimulated Luminescence (TSL) co relation studies in solids, Photoluminescence investigations in lanthanides and actinide doped solids, molecular dynamics and auto-radiolysis effects in pure actinide compounds and actinide doped compounds. In addition, he was also involved in the Chemical Quality Control of nuclear materials using emission spectroscopic techniques. He has published about 240 research papers in peer reviewed journals and 2 book chapters. He is a recipient of Special Contribution Award of Department of Atomic Energy (2018) and Department of Atomic Energy (DAE) Group Achievement Award (2010).</p>
	<p>V. Sudarsan, joined Chemistry Division of BARC in the year 1994 after graduating from 37th batch of BARC Training School. He received his Ph. D degree in Chemistry from Mumbai University and subsequently worked as a post-doctoral fellow at the University of Victoria, British Columbia, Canada in the area of structural aspects and luminescence properties of inorganic nanoparticles. He is a recipient of several awards including Young Achiever Award for the year 2010 (DAE Solid State Physics Symposium (2010)), Scientific & Technical Excellence Award of Department of Atomic Energy (2010), Department of Atomic Energy (DAE) Group Achievement Award (2018), Homi Bhabha Science & Technology Award (2019). He is an elected fellow of the National Academy of Sciences, India (NASI).</p>

Chemistry and Prospects of Some Nanocrystalline Multiferroic Materials

Tokeer Ahmad^{1*} and Irfan H. Lone^{1,2}

¹Nanochemistry Laboratory, Department of Chemistry, Jamia Millia Islamia, New Delhi-110025, India

²Department of Chemistry, University of Kashmir, Hazratbal, Srinagar-190006, Jammu & Kashmir, India

**Address for Correspondence:*

E-mail: tahmad3@jmi.ac.in; Phone: 91-11-26981717, Extn: 3261

Abstract

Nanomaterials are among the most challenging areas of current scientific and technological research because of the variety of interesting changes in their properties at nano-dimension. The preparation of nanoparticles with well defined size and morphology is an important challenge for various industrial applications. Multifunctional materials exhibit ferromagnetic and ferroelectric properties which may lead to number of applications for future computer memory concepts, multiple state memory devices, sensors, spin valves, actuators and transducers etc and play an important role in solid oxide fuel cells, catalysts materials for electrodes and chemical sensors. Multiferroics could be prepared successfully by using various chemical methods such as hydrothermal, reverse micelles, polymeric citrate precursor methods etc. with high specific surface areas. The temperature and frequency dependences of electrical properties including dielectric constant, dielectric loss and conductivity properties could be investigated. The room temperature ferroelectric properties and normal ferromagnetic loop with well defined saturation magnetization (M_s), remanent magnetization (M_r) and coercive field led to multiferroic characteristics. Few multiferroics also act as photocatalysis for hydrogen evolution and other sensing applications.

Keywords: Nanoparticles; Multiferroic; Ferroelectricity; Ferromagnetism.

Introduction:

In the recent years, scientists are more interested in materials exhibiting more than one phases of ferroic order e.g, ferromagnetism, ferroelectricity and even anti-ferromagnetism etc [1]. To understand the basic interaction between the magnetic and electric coupling has become important for the emerging field of multiferroics and the potential use of such materials in electronic devices. Surely, one could think the shifting of magnetic condition by applying an electric field or vice versa. These applications give rise to magneto electronic devices [2]. Not only silicon based electronic devices greatly reduced the scale to its limit but also has inspired for the search of new materials which combines several required properties in a single phase. In this regard, transition metal oxides offer great potential, because they have most of the materials with fascinating properties that are known to mankind [3-9]. These properties range from insulators, superconductors, metals, semiconductors, ferroelectricity, dielectrics, magnetism and colossal magnetoresistance etc. [5, 8, 9]. There are small group of materials which possess more than one classical physical properties pointed out above e.g. multiferroics and in general most of the complex oxides have either of the like ferroelectricity or ferromagnetism. During the last 10 years, the new field of research which

has become a popular subject of investigation in chemistry and solid state physics known as multiferroics, which possess both the ferroelectricity and ferromagnetism [10, 11]. The term multiferroic was first used by H. Schmid in 1994. His definition referred to multiferroics as single phase materials which simultaneously possess two or more primary ferroic properties [10]. Since it is difficult to have co-existence of several types of order, so there are relatively few compounds which shows multiferroic properties [12]. The perovskite transition metal compounds which shows multiferroic properties that includes for example $TbMnO_3$, $Tb_2Mn_2O_5$, $BiFeO_3$, $BiMnO_3$, $YMnO_3$, $YFeO_3$, $HoMn_2O_5$, $LuFe_2O_4$, etc [13-14]. There are two types of multiferroics; the first type is proper (or type 1) where electric and magnetic properties occur for different reasons, but both are coupled together e.g. $BiFeO_3$; however the second type is improper (or type 2) multiferroics where both properties are deeply coupled e.g. $TbMnO_3$. The second type is of fundamental interest but not of practical use today due to their low critical parameters and the first type of multiferroics represent the main area for future applications. There is active research to understand both classes of multiferroics [15]. Today the term multiferroic has been expanded to the materials which exhibit any type of long range magnetic ordering, spontaneous electric polarization and


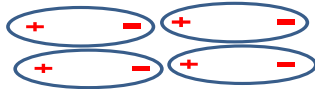


Time \ Space	Invariant	Change
Invariant	Ferroelastic 	Ferroelectric 
Change	Ferromagnetic 	Ferrotoroidic 

Figure 1. Multiferroic possess multiple type of ordering, including magnetism, ferroelectricity, ferroelasticity, ferrotoroidicity, and often have strong coupling between order parameters.

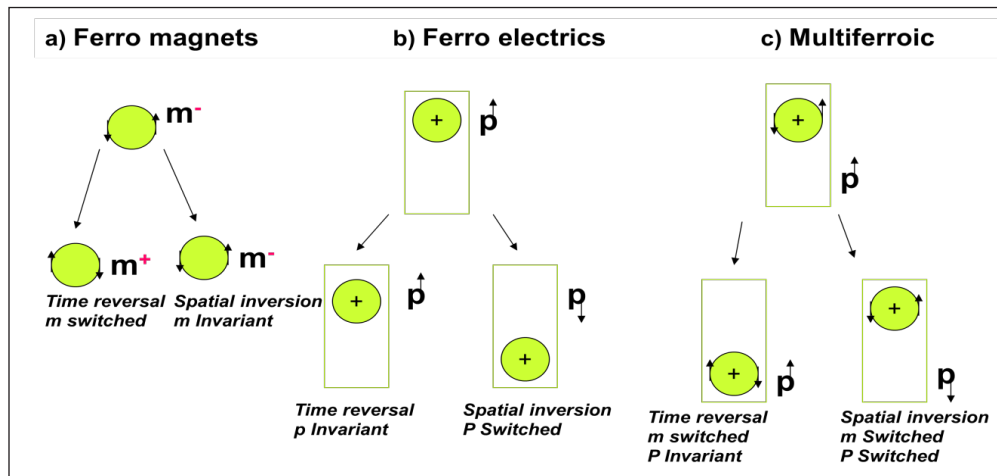


Figure 2. a) *Ferromagnets*: The local magnetic moment m may be represented classically by a charge that dynamically traces an orbit, as indicated by the arrow heads. A spatial inversion produces no change, but time reversal switches the orbit and thus m . b) *Ferroelectrics*: The local dipole moment p may be represented by a positive point charge that lies asymmetrically within a crystallographic unit cell that has no net charge. There is no net time dependence, but spatial inversion reverses p . c) *Multiferroics*: that are both ferromagnetic and ferroelectric possess neither symmetry.

ferroelasticity. Working under this expanded definition the history of magnetoelectric multiferroics can be traced back to the 1960s [16]. In the most general sense the field of multiferroics was born from studies of magnetoelectric systems [17]. After an initial burst of interest, research remained static until early 2000. In 2003, the discovery of large ferroelectric polarization in epitaxially grown in thin films of BiFeO_3 and the discovery of strong magnetic and electric coupling in orthorhombic TbMnO_3 and TbMn_2O_3 re-stimulated in the field of multiferroics [13, 14, 18]. Each multiferroic property is closely linked to symmetry. The primary ferroic properties can be characterized by their behavior under space and time inversion. Space inversion will reverse the direction of polarization P while

leaving the magnetization M invariant. Time reversal, in turn, will change the sign of M , while the sign of P remains invariant. Recently, the idea of ferrotoroidic materials has been added into consideration (Figure 1). These are materials that possess a stable and spontaneous order that is taken to be the curl of the magnetization or polarization. The curl of the vector is the amount of rotation or the angular momentum of the contents of a given region of space as shown in figure 1.

The coupling between magnetism and ferroelectricity in the microscopic conditions for different degrees of freedom can be explained using the symmetry requirements. The magnetic moment within a ferromagnetic material depicted as a charge tracing an orbit, is unchanged under spatial inversion. The opposite is true for a ferroelectric material. Considering a ferroelectric material as a positive point charge lying asymmetrically in a crystal unit cell, spatial inversion reverses the polarization while time inversion has no effect. A multiferroic shows no spatial or time invariance as shown in figure 2 [19].

The major problem to create a new multiferroic material is that multiferroics do not follow one specific theory [20]. The microscopic nature of magnetic ordering is well understood and generally follows the same principles as all insulating magnetic materials [21]. A material will possess a magnetic moment if it contains transition metal or rare earth ions with partially filled d or f electron shells. Ions with full shells are nonmagnetic as the spins of the electrons add to zero, so do not participate in the magnetic ordering. Long-range magnetic ordering within the material occurs as a result of exchange interactions (virtual hopping of electrons) between the partially filled d shells of different ions [22]. The type of ordering (i.e.

ferromagnetic, antiferromagnetic) is dependent on the form of the exchange [23]. The theory of ferroelectricity on the other hand is not as well defined; a number of different mechanisms and types of ferroelectric order exist, many of which are not fully understood [21]. Most ferroelectrics are transition metal oxides containing transition metal ions with empty d electron shells. Traditionally, these materials become ferroelectric when the positively charged metal ions form covalent bonds with neighboring negatively charged oxygen ions through the virtual hopping of electrons from the filled oxygen shells to the empty d shells. An electric polarization is then induced within these materials as a result of a relative displacement of cations and anions within the periodic crystal. Although magnetism and ferroelectricity share the same mechanism of electron exchange, it is the contrast of empty and partially filled d or f electron shells that make the properties mutually exclusive [22]. Consequently, nearly every multiferroic material has to be studied in its own right. The theories defining the mechanisms within one multiferroic can ultimately be very different from the next [20]. Coupling between magnetic and electric degrees of freedom is not a new phenomenon. The induction of magnetisation by an electric field or polarisation by a magnetic field has long been studied under the name 'magnetoelectric effect' [21]. The linear magnetoelectric coupling term α linking the magnetic and electric degrees of freedom is shown in the relation (Equation 1) for the free energy of a material in an electric and/or a magnetic field, [24].

$$F(\mathbf{E}, \mathbf{H}) = F_0 - P_i^s E_i - M_i^s H_i - \frac{1}{2} \epsilon_{ij} E_i E_j - \frac{1}{2} \mu_{ij} H_i H_j - a_{ij} E_i H_j - \frac{1}{2} \beta_{ijk} E_i H_j H_k - \frac{1}{2} \gamma_{ijk} H_i E_j E_k - \dots \text{Eq.1}$$

A small group of multiferroics display this type of coupling (i.e. $\alpha \neq 0$). This overlap between the magnetoelectric effect and multiferroicity is not surprising as large magnetoelectric responses are expected within the materials

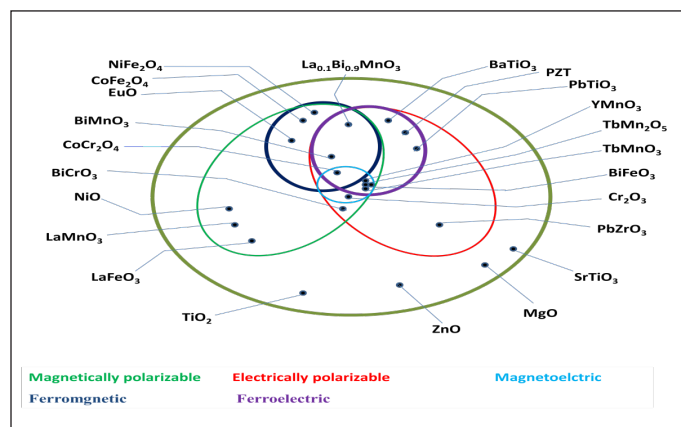


Figure 3. Classification of Insulating Oxides [19].

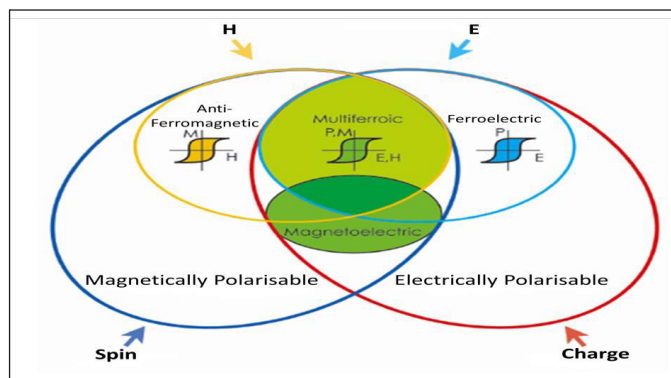


Figure 4. Relationship between multiferroics and magnetoelectrics [19].

that display strong internal electromagnetic fields, often found within ferromagnets and ferroelectrics which display the largest magnetic susceptibilities and dielectric constants, respectively. Not all materials displaying the magnetoelectric effect are multiferroic, (Figures 3 and 4) the material must break both spatial and time inversion symmetry in order to give a non-zero value for the magnetoelectric susceptibility tensor [24].

Contra-Indication between Magnetism and Ferroelectricity:

There are relatively few compounds which show multiferroic behavior is because of the contra-indication between the conventional mechanism for ferroelectrics (which requires formally empty d orbitals) and the formation of magnetic moments (which usually results from partially filled d orbitals [1] . In order to achieve the co existence of ferroelectricity and magnetism in a single phase, therefore, the atoms that move off centre to form the electric dipole moment should be different from those that carry the magnetic moment. This could be achieved through either an alternative (non d- electron) mechanism for magnetism or through alternative mechanism for ferroelectricity; but only the latter route has been followed. For the magnetic perovskite-structure oxides and related materials, multiferroism is most commonly achieved by making the use of stereochemical activity of the lone pair on the large (A- site) cation to provide the ferroelectricity, while keeping the small (B-site) cation magnetic as is well known example for Bi-based compounds like BiFeO₃ [14] (Note that BiFeO₃ acquires the perovskite, not the 'ferrite' structure, despite of its nomenclature). In case of the antiferromagnetic ferroelectrics YMnO₃ compounds, the way to explain the multiferroism is provided by 'geometrically driven' ferroelectricity, which is compatible with the co existence of magnetism [26]. A new attracting mechanism identified occurs in TbMnO₃; in which ferroelectricity is induced by the formation of a symmetry-

lowering magnetic ground state that lacks inversion symmetry [13]. Even if the resulting polarization is small, but because it is caused directly by the magnetic ordering, strongly and possibly new magnetoelectric interactions should be expected. Magnetoelectric multiferroics require simultaneous violation of space and time inversion symmetry. In BiFeO_3 , for example, off-centering of ions gives rise to an electric polarization, while at a lower temperature additional magnetic ordering breaks time-reversal symmetry.

Literature for Some Multiferroic Materials:

Briefly review the most commonly studied multiferroic materials like BiFeO_3 , BiMnO_3 , RMnO_3 , TbMnO_3 etc.

Bismuth Ferrite (BiFeO_3):

The most promising and most studied material for multiferroic devices is bismuth ferrite (BiFeO_3 or BFO), which shows room temperature ferroelectricity ($T_c \approx 1100$ K) and antiferromagnetism ($T_N \approx 640$). The material (BiFeO_3) has a rhombohedral structure and shows a large ferroelectric polarization [14]. Owing to its large spontaneous polarization, possibly the largest among all known perovskite and non perovskite multiferroic oxides, coupled with its lead free nature, BFO is also a prospective candidate for next generation ferroelectric memory applications. However, the major challenge BFO faces, in this context are its poor leakage characteristics, tendency fatigue [27] and thermal decomposition near coercive field [28]. The multiferroic properties and potential applications of BiFeO_3 were strongly diminished by its leakage current arising from impurities, defects or non stoichiometry [29-31]. Therefore, many efforts were tried for the synthesis of pure-phase of BiFeO_3 . The conventional solid state (ceramic) synthesis requires prolonged treatment at considerably high calcination temperature causing the loss of bismuth due to its high volatility and easily leads to the formation of impurity phases, such as $\text{Bi}_2\text{Fe}_4\text{O}_9$ and $\text{Bi}_{25}\text{FeO}_{40}$ [32]. Now researchers have developed wet chemistry based routes to synthesize nanosized multiferroic powders [33-35]. The soft chemistry methods have also been used to prepare BiFeO_3 nanostructures, such as co-precipitation [36], sonochemical and microemulsion techniques [37], sol-gel [38-41], molten salt synthesis [42] and hydro-/solvothermal synthesis [43-45]. Further, the major thrust towards the research of BFO is driven by their prospective applications in magnetoelectric and spintronic devices. Moreover, the key advantage of BFO-based memory devices are their electrical writing and magnetic reading operations, which can further utilize the advantages of solid-state circuits that is, their low energy consumption, scalability, nondestructive read operations etc. [46].

Bismuth Manganate (BiMnO_3):

Bismuth manganite perovskite ABO_3 -structured compound is another interesting multiferroic material with low-temperature ferromagnetic and room-temperature ferroelectric characteristics. The material shows ferromagnetic ordering below 105 K attributed to the orbital ordering of B-site ions that is, Mn^{3+} ions and a magnetization of $3.6 \mu_B$ per formula unit [47]. The material has perovskite triclinic structure which hangs to monoclinic structure, at 450 K and then to a nonferroelectric orthorhombic phase at 770 K [48]. In BiMnO_3 (BMO), as in BiFeO_3 , the $6s^2$ lone pair on the Bi leads to the displacement of that ion from the centro symmetric position at the A-site of a perovskite unit cell. The resultant distortion leads to a ferromagnetic interaction between the Mn ions at the B-site in BMO [49-50]. In bulk form, BMO has been observed to be both ferromagnetic and ferroelectric [51]. While preparation in the bulk form requires use of high pressures, thin resistive films of these materials can be prepared with much ease [52].

Hexagonal Magnates (RMnO_3):

Hexagonal magnates are another interesting class of magnates of general formula RMnO_3 ; Where R is typically a rare earth ion such as Y and Ho. These compounds simultaneously exhibit ferroelectricity and anti ferromagnetic ordering of magnetic Mn ions. In general, rare earth elements having a small ionic radii tend to stabilize hexagonal phase, RMnO_3 (R=Sc, Y, Ho, Er, Tm, Yb, Lu,) with space group $\text{P6}_3\text{cm}$ [53, 54]. Despite of having an ABO_3 -type formula, similar to perovskite, hexagonal magnates have altogether different crystal structure and electronic structure. In compare to conventional perovskite, hexagonal magnates have their Mn^{3+} ions with 5-fold coordination, located at the centre of an MnO_5 trigonal bipyramid. R ions on the other hand have 7-fold coordination. The MnO_5 bi-prisms are arranged in space and are separated by a layer of R^{3+} ions. Crystal field level scheme of Mn^{3+} ions in hexagonal RMnO_3 is also different from that of Mn^{3+} ions with octahedral coordination. Here, the d levels are split into two doublets and an upper singlet. As a result, four d electrons of Mn^{3+} ion occupy two lowest lying doublets and unlike Mn^{3+} ion in octahedral coordination, there is no degeneracy present. Consequently, Mn^{3+} ions in these compounds are not Jahn-Teller ions [55].

Strongly Coupled Multiferroics:

Multiferroic materials belonging to this class show ferroelectricity in their magnetically ordered state and too of a particular type. Moreover, very strong coupling between ferroelectric and magnetic-order parameters has

also been observed. In 2003, Kimura et al. reported presence of spontaneous polarization in the magnetized state of the TbMnO_3 . This compound has various magnetic structures: it is disproportionate anti-ferromagnet between 27 and 42 K and a proportionate state antiferromagnetic between 7 and 27 K. So the proportionate state between 7 and 27 K that the material shows ferroelectricity [13]. This discovery was followed by an observation of similar effects in TbMn_2O_5 [18]. Later on a variety of other materials have also been investigated such as $\text{Ni}_3\text{V}_2\text{O}_8$, MnWO_6 and $\text{Ca}_3\text{CoMnO}_6$ showing this effect [56-58].

Short- Comings and Scope for Research Work:

1. For single phase multiferroic nanopowders, wet chemical routes (sol-gel and co-precipitation methods, polymeric precursors from organometallic complexes, hydrothermal/solvothermal and microemulsion synthesis, self-combustion), molten salt procedures, will be used. To synthesis the pure phase of nanocrystalline multiferroic compounds by low temperature methods is itself a challenging topic as these compounds have been generally synthesized by solid state methods which require high temperature and high pressure conditions, even the impurities are still prevailing with the main phase.
2. Development of innovative synthesis methods and appropriate processing routes to produce high purity defect-free single phase nanosized ferroic structures with controlled size and shape. The most simple and cost effective methods for the synthesis of multiferroic nanocrystalline compounds are: Reverse micellar method, Polymeric citrate precursor method, hydrothermal and sonochemical methods.
3. For the single phase multiferroics, methods will be focused towards: (i) increasing purity of phases and reducing the tendency to agglomerate (for nanopowders); (ii) tailoring the degree of crystallinity, structural parameters and morphological features (dimensional characteristics, shape and size distribution) of particles and grains in order to obtain controlled surface and bulk (cross-section) microstructures leading to suitable functional properties required by certain applications.
4. Identification of correlations between synthesis, processing/shaping methods, nanoscale characteristics, functional properties and possible applications for ferroic/multiferroic nanostructures and to detect novel properties of the samples, characterizing by sophisticated instruments.
5. Although expected to produce an applications breakthrough, single-phase multiferroics show poor properties at room temperature. Thus, an important task is to elucidate the origin of their conductivity and losses, and to develop valuable strategies to improve their properties.
6. Synthesis and processing of a range of single-phase multiferroics nanopowders, BiFeO_3 , BiCrO_3 , BiMnO_3 , YMnO_3 , EuTiO_3 , RMn_2O_5 (R=Tb, Y, Eu, Gd), $(\text{Sr,Mn})\text{TiO}_3$, LuFe_2O_4 , GdMnO_3 , GdFeO_3 , TbMnO_3 , YFeO_3 , MnWO_4 , PbVO_3 etc.

In this review, we outline some of the progressive milestones in this stimulating field, especially for those single-phase multiferroics where magnetism and ferroelectricity coexist. First, we highlight the physical concepts of multiferroicity and the current challenges to integrate the magnetism and ferroelectricity into a single-phase system and then categories the compounds into different types on the basis of showing the strange properties. Thus the main objectives and target for the planning of the research work on multiferroics may ranges on the following points:

1. To synthesis the multiferroic compounds in the nano dimension is a world challenging problem and many efforts have been devoted to synthesis the pure phase of oxide type multiferroic compounds in the nano dimension. For the most multiferroic perovskite oxides, a high temperature and high pressure is required to get a single phase. Not only is the equipment for the synthesis complicated but also the nanostructure of the sample cannot be controlled well and it is very hard to separate out the impurity like oxides and predominating secondary phases. In spite of an intense study, a fundamental understanding of the structure-property correlations in multiferroic compounds is still missing. Specially, the fundamental dependence of its magnetic behavior on the particle size is an issue of deep interest. It is well known, the properties of the sample strongly depend on their morphologies, sizes, and defect densities.
2. The main objective is to synthesis the monophasic nanopowders with zero impurity level of nanocrystalline multiferroic compounds by low temperature synthesis methods via Reverse micellar route, Hydrothermal method, Polymeric citrate precursor method and Sonochemical method.
3. To characterize the synthesized multiferroic compound by various techniques viz. X-ray diffraction (XRD), Transmission electron microscope (TEM), Scanning

electron microscope (SEM), Thermogravimetry and Differential thermogravimetry analysis (TGA/DTA), BET surface analyzer etc. and to study the dielectric and magnetic properties.

- The field of multiferroics, besides promising important applications, contains rich and interesting physics. It is now a very active and fruitful field. A lot is already known, many basic principles are established. Thus, what is next? One can think of several promising directions, some of which have already been pursued. First, the search for new multiferroics is still proceeding at a rapid pace, and one should expect that many new examples and even new classes will be discovered. Each new multiferroic is a challenge in itself; every substance has its own material-specific aspects, which one has to explore.

Acknowledgement:

TA thanks the SERB-DST Govt. of India research scheme (EMR/2016/001668) for financial support. IHL thanks to UGC New Delhi for research fellowship.

References:

- Spaldin, A. N.; Fiebig, M., *The renaissance of magnetoelectric multiferroic*, Science, 309, **2005**, 391-392.
- Bibes, Manual; Barthelemy, Agnes, *Multiferroics: Towards a magnetoelectric memory*, Nature Mater. **7**, **2008**, 425-426.
- Galasso, F. S., *Perovskite and high-Tc Superconductors*; Gordon and Breach Science Publishers: Paris, **1990**.
- Ogale, S. B.; *Thin films and Heterostructures for oxide electronics*, Springer Verlag Publication: New York, **2005**.
- Bednorz, J. G.; Muller K. A., *Possible High T_c Superconductivity in the Ba-La-Cu-O System*, Z. Phys. B- Condensed Matter, **64**, **1986**, 189-193.
- Herman, M.A.; Sitter, H., *Molecular Beam Epitaxy*; Springer Verlag Publishers: New York, **1989**.
- Paine, C. D.; Bravman J. C.; Eds., *Laser Ablation for Materials Synthesis*, Mater. Res. Soc. Symp. Proc., **191**, **1990**, 191-205.
- Helmolt, von, R.; Wecker, J.; Holzapfel, B.; Schultz, L.; Samwer, K., *Giant negative magnetoresistance in perovskite like La_{2/3}Ba_{1/3}MnO_x ferromagnetic films*, Phys. Rev. Lett., **71**, **1993**, 2331-2333.
- Jin, S.; Tiefel, H.; McCormack, M.; Fastnacht, R. A.; Ramesh, R.; Chen L. H., *Thousandfold change in resistivity magnetoresistive La-Ca-Mn-O films*, Science, **264**, **1994**, 413-415.
- Schmid, Hans, *Multiferroic Magnetolectrics*, Ferroelectrics, **162**, **1994**, 317-338.
- Schmid, Hans, *On the possibility of ferromagnetic, antiferromagnetic, ferroelectric and ferroelastic domain reorientations in magnetic and electric fields*, Ferroelectrics, **221**, **1999**, 9-17
- Khomskii, D., *Classifying multiferroics: Mechanism and effects*, Physics, **2**, **20(2009)**.
- Kimura, T.; Goto, T.; Shintani, H.; Ishizaka, K.; Arima, T.; Tokura, Y., *Magnetic control of ferroelectric polarisation*, Nature, **426**, **2003**, 55-58.
- Wang, J.; Neaton, B. J.; Zheng, H.; Nagarajan, V.; Ogale, S. B.; Liu, B.; Viehland, D.; Vaithyanathan, V.; Schlom, D. G.; Waghmare, U. V.; Spaldin, N. A.; Rabe, K. M.; Wuttig, M.; Ramesh, R., *Epitaxial BiFeO₃ multiferroic thin film heterostructures*, Science, **299(5613)**, **2003**, 1719-1722.
- Martin, L. W.; Crane, S. P.; Chu, Y. H.; Holcomb, M. B.; Gajek, M.; Huijben, M.; Yang, C. H.; Balke, N.; Ramesh, R., *Multiferroics and magnetolectrics: thin films and nanostructures*, J. Phys. Condens. Matter, **20**, **2008**, 434220(1-13).
- Ascher E; Rieder, H.; Schmid, H.; Stossel, H., *Some properties of Ferromagnetolectric Nickel-Iodine Boracite, Ni₃B₇O₁₃I*, J. Appl. Phys., **37**, **1966**, 1404-1405
- Smolenskii, G.; Iscrov, A. V.; Agranovskaya, I. A., *New ferroelectrics of complex composition of the type A₂²⁺(B₁³⁺B_{II}⁵⁺)O₆*, Sov. Phys. Solid State, **1**, **1959**, 150-151.
- Hur N.; Park S.; Sharma P. A.; Ahna J. S.; Guha S.; Cheong W., *Effect polarization reversal and memory in a multiferroic materials induced by magnetic field*, Nature, **429**, **2004**, 392-395.
- Eerenstein W.; Mathur N. D.; Scott J. F., *Multiferroic and magnetolectric materials*, Nature, **442**, **2006**, 759-765.
- Picozzi S.; Ederer C., *First principles studies of multiferroic materials*, J. Phys.: Condens. Matter, **21**, **2009**, 303201(1-18).
- Khomskii D. I., *Multiferroics: Different ways to combine magnetism and ferroelectricity*, J. Magn. Magn. Mater., **306**, **2006**, 1-8.
- Cheong, S. W.; Mostovoy, M., *Multiferroics: a magnetic twist for ferroelectricity*, Nature Mater., **6**, **2007**, 13-20.
- Blundell, S., *Magnetism in Condensed Matter*, Oxford Master Series in Condensed Matter Physics., **2001**.
- O'Flynn D., *Ph.D thesis*, University of Warwick, **2010**.
- Van Aken, B. B.; Palstra, M. T. T.; Filippetti, A.; Spaldin, A. N., *The origin of ferroelectricity in magnetoelectric YMnO₃*, Nature Mater, **3**, **2004**, 164-170.
- Jang, H. W.; Baek S. H.; Ortiz D.; Folkman, C. M.; Eom, C. B.; Chu, Y. H.; Shafer, P.; Ramesh, R.; Vaithyanathan, V.; Schlom, D. G., *Epitaxial (001) BiFeO₃ membranes with substantially reduced fatigue and leakage*, Appl. Phys. Lett., **92**, **2008**, 062910(1-3).
- Lou, X. J.; Yang, A. T. Tang; Lin, Y. Y.; Zhang, M.; Scott, F. J., *Formation of magnetite in bismuth ferrite under voltage stressing*, Appl. Phys. Lett., **90**, **2007**, 262908(1-3).
- Wang, Y.; Zhou, L.; Zhang, M.; Chen, X.; Liu, Z., *Room temperature saturated ferroelectric polarization in BiFeO₃ ceramics synthesized by rapid liquid phase sintering*, Appl. Phys. Lett., **84**, **2004**, 1731-1733.
- Park, T.; Papaefthymiou, G.; Viescas, A.; Moodenbaugh, A.; Wong, S., *Size-dependent magnetic properties of single-crystalline multiferroic BiFeO₃ nanoparticles*, Nano. Lett., **7**, **2007**, 766-772.
- Mazumder, R.; Ghosh, S.; Mondal, P.; Bhattacharya, D.; Dasgupta, S.; Das, N.; Sen, A.; Tyagi, A.; Sivakumar, M.; Takami, T.; Ikuta, H., *Particle size dependence of magnetization and phase transition near T_N in multiferroic BiFeO₃*, J. Am. Ceram. Soc., **100**, **2006**, 033908-033916.
- Kothari, D.; Reddy, R. V.; Sathe, G. V.; Gupta, A.; Banerjee, A.; Awasthi, M. A., *Raman scattering study of polycrystalline*

- magnetolectric BiFeO₃, J. Magn. Magn. Mater. 320, **2008**, 548-552.
32. Selback, Sverre, M.; Tybell, Thomas; Einarsrud, Mari-Ann; Grande, Tor, *Size-Dependent Properties of Multiferroic BiFeO₃ Nanoparticles*, Chem. Mater., 19, **2007**, 6478-6484.
 33. Mazumder, R.; Devi, S. P.; Choudhury, P.; Sen, A.; Raja, M., *Ferromagnetism in nanoscale BiFeO₃*, Appl. Phys. Lett., 91, **2007**, 062510(1-3).
 34. Fruth, V.; Tenea, E.; Gartner, M.; Anastasescu, M.; Berger, D.; Ramer, R.; Zaharescu, M., *Preparation of BiFeO₃ films by wet chemical method and their characterization*, J. Eur. Ceram. Soc., 27, **2007**, 937-940.
 35. Shetty, S.; Palkar, V.; Pinto, R., *Size effect study in magnetoelctric BiFeO₃ system*, Pramana, 58, **2002**, 1027-1030.
 36. Das N.; Majumdar, R.; Sen, A.; Maiti, H., *Nanosized bismuth ferrite powder prepared through sonochemical and microemulsion techniques*, Mater. Lett., 61, **2007**, 2100-2104.
 37. Wei, J.; Xue, D.; Xu, Y., *Photoabsorption characterization and magnetic property of multiferroic BiFeO₃ nanotubes synthesized by facile sol-gel template process*, Scripta Mater, 58, **2008**, 45-48.
 38. Gao, F.; Yuan, Y.; Wang, K.; Chem, F.; Liu, J.; Ren, Z., *Preparation and photoabsorption characterization of BiFeO₃ nanowires*, Appl. Phys Lett., 89, **2006**, 102506-102508.
 39. Liu, H.; Wang, X., *Large electric polaisation in BiFeO₃ flim prepared via a simple sol gel process*. J. Sol-Gel Sci. Technol, 47, **2008**, 154-157.
 40. Wang, X.; Zhang, Y.; Wu, Z., *Magnetic and optical properties of multiferroic bismuth ferrite nanoparticles by tartaric acid-assited sol-gel strategy*, Mater. Lett., 64, **2010**, 486-488.
 41. Chen, J.; Xing, X.; Watson, W.; Yu, R.; Deng, J.; Yan, L.; Sun, C.; Chen, X., *Rapid synthesis of multiferroic BiFeO₃ single crystalline nanostructures*, Chem. Mater., 19, **2007**, 3598-3600.
 42. Han, J.; Huang, Y.; Wu, X.; Wu, C.; Peng, B.; Haung, W.; Goodenough, J., *Tunable synthesis of bismuth ferrite with various morphologies*, Adv. Mater., 18, **2006**, 2145-2148.
 43. Wang, Y.; Xu, G.; Ren, Z.; Wei, X.; Weng, W.; Du, P.; Shen, G.; Han, G., *Mineralizer-assisted hydrothermal synthesis and characterization of BiFeO₃ nanoparticles*, J. Am. Ceram., 90, **2007**, 2615-2617.
 44. Chen, C.; Cheng, J.; Yu, S.; Chen, L.; Meng, Z., *Hydrothermal synthesis of perovskite bismuth ferrite crystalline*. J. Cryst. Growth, 291, **2006**, 135-139.
 45. Catalan, G.; Scott, J. F., *"Physics and applications of bismuth ferrite,"* Adv. Mater. 21, **2009**, 2463-2485.
 46. Kimura, T.; Kawamoto, I. Yamada, Azuma, M.; Takano, M.; Tokura, Y., *"Magnetocapacitance effect in multiferroic BiMnO₃"*, Physical Review B, 67, **2003**, Article ID 180401(1-4).
 47. Atou, T.; Chiba, H.; Ohoyama, K.; Yamaguchi, Y.; Syono, Y., *Structure Determination of Ferromagnetic Perovskite BiMnO₃*, J. Solid State Chem., 145, **1999**, 639-642.
 48. Santos, dos, A. M.; Cheetham, A. K.' Atou, T.; Syono, Y.; Yamaguchi, Y.; Ohoyama, K. Chiba, H.; Rao, C. N. R., *Orbital ordering as the determinant for ferromagnetism in biferroic BiMnO₃*, Phys. Res. B, 66, **2002**, 064425(1-4).
 49. Santos, dos, A. M.; Parashar, S.; Raju, R. A.; Zhao, Y. S.; Cheetham, A. K; Rao, C. N. R., *Evidence for the likely occurrence of magnetoferroelectricity in the simple perovskite, BiMnO₃*, Solid State Commun., 122, **2002**, 49-52.
 50. Eerenstein, W., *"Growth of highly resistive BiMnO₃ films,"* Appl. Phys. Lett., 87, **2005**, 1-3.
 51. Lee, S.; Pirogov, A.; Kang, Misun; Jang, Kwang-Hyun; Yonemura, M.; Kamiyama, T.; Cheong, S. W.; Gozzo, F.; Shin, Namsoo; Kimura, H.; Noda, Y.; Park, J. G., *Giant magneto-elastic coupling in multiferroic hexagonal mangnetes*, Nature, 451, **2008**, 805-808.[
 52. Yakel, H. L. J.; Koehler, W. C.; Bertaut, E. F.; Forrat, E. F., *On the crystal structure of the manganese (111) trioxides of the heavy lanthanides and yttrium*, Acta Cryst., 16, **1963**, 957-962.
 53. Khomskii, D. I., *"Multiferroic: different ways to combine magnetism and ferrelectricity,"* J. Magn. Magn. Mater., 306, **2006**, 1-8.
 54. Lawes, G.; Harris, A. B.; Kimura, T.; Rogado, N.; Cava, R. J.; Aharony, A.; Enten-Wohlman, O.; Yildirim, T.; Kenzelmann, M.; Broholm, C.; Ramirez, A. P., *Magnetically Driven Ferroelectric Order in Ni₃V₂O₈*, Phys. Rev. Lett., 97, **2005**, 087205(1-4).
 55. Taniguchi, K.; Abe, N.; Takenobu, T.; Iwasa, Y.; Arima, T., *Ferroelectric polarization Flop in a Frustrated Magnet MnWO₄ Induced by a Magnetic Field*, Phys. Rev. Lett., 97, **2006**, 097203(1-4).
 56. Choi, Y. J.; Yi, H. T.; Lee, S.; Huang, Q.; Kiryukhin, V.; Cheong, S. W., *Ferroelectricity in an Ising Chain Magnet*, Phys. Rev. Lett., 100, **2008**, 267602(1-4).

SOCIETY FOR MATERIALS CHEMISTRY (SMC)
(Reg. No. - Maharashtra, Mumbai/1229/2008/GBBSD)
c/o Chemistry Division
Bhabha Atomic Research Centre, Mumbai 400 085

APPLICATION FOR MEMBERSHIP

Please enroll me as a Life member of the *Society for Materials Chemistry (SMC)*. My particulars are as follows:

Name : _____

Educational Qualifications : _____

Field of Specialization : _____

Official Address : _____

Telephone No. (Off.) : _____

Residential Address : _____

Telephone No. (Res.) : _____

Address for Correspondence : Home/Office (Please tick one of the options)

E-mail Address : _____

Subscription Details

Mode of Payment : Cheque/DD/Cash
(Cheque/DD should be drawn in favor of "*Society for Materials Chemistry*" for Rs. 1000/- payable at Mumbai. For out-station *non-multi-city* cheques, please include Rs.50/- as additional charge for bank clearance.

Number : _____

Dated : _____

Drawn on Bank & Branch : _____

Amount : _____

Place: _____

Date: _____

Signature

Registration Number: _____ (To be allotted by SMC office)

Printed by:

Ebenezer Printing House

Unit No. 5 & 11, 2nd Floor, Hind Service Industries

Veer Savarkar Marg, Shivaji Park Sea-Face, Dadar (W), Mumbai - 400 028

Tel.: 2446 2632 / 2446 3872 Tel Fax: 2444 9765 E-mail: outworkeph@gmail.com

In this issue

Sr. No	Feature Articles	Page No.
1	Non-oxide Ceramics in Nuclear Technology: Potential and Challenges <i>Sourav Majumder, Dheeraj Jain and V. Sudarsan</i>	63
2	Recent advances in iron phosphate glass as vitrification matrix for nuclear waste <i>Dimple P. Dutta</i>	73
3	Transparent ceramics for radiation detection <i>Shashwati Sen, S G Singh, G D Patra, S Pitale, M Ghosh</i>	79
4	Influence of Gd³⁺ doping on the structural and luminescence properties of SrSnO₃ nano-rods <i>Dinesh K. Patel, B. Rajeswari, R. M. Kadam and V. Sudarsan</i>	88
5	Chemistry and Prospects of Some Nanocrystalline Multiferroic Materials <i>Tokeer Ahmad and Irfan H. Lone</i>	96

Published by
Society for Materials Chemistry
C/o. Chemistry Division
Bhabha Atomic Research Centre, Trombay, Mumbai 40085
e-mail: socmatchem@gmail.com, Tel: 91-22-25592001